THE
PHYSICAL REVIEW
A journal of experimental and theoretical physics established by E. L. Nichols in 1893

VOL. 62, NOS. 1 AND 2 JULY 1 AND 15, 1942 SECOND SERIES

The Characteristic Radiations of Co^{60}

MARTIN E. NELSON,* M. L. POOL, AND J. D. KURBATOV
The Ohio State University, Columbus, Ohio

(Received April 4, 1942)

The 10.7-minute period previously obtained from Co(n, γ) and Ni(n, p) reactions was produced by a Co(d, p) reaction. The increased activity from this latter reaction made energy measurements possible. The beta-rays were measured with a magnetic spectrometer. In spite of the difficulties caused by the rapid decay of the activity, the best interpretation of the data is that the beta-rays are a continuous spectrum. The end point was evaluated at 1.35±0.1 Mev. Absorption measurements indicated that each beta-ray is accompanied by approximately one gamma-ray of 1.5±0.2-Mev energy. The 5.3-year period radiations previously studied were also investigated and found to consist of a 1.7±0.2-Mev gamma-ray and a 220±20-Kev beta-ray spectrum. These data suggest that Co^{60} may consist of isomeric nuclei in which the two activities decay independently, as an alternative to the previously reported scheme of disintegration.

INTRODUCTION

A RECENT mass spectrographic investigation of cobalt has shown that this element consists of a single stable isotope of mass number 59.[1] It is therefore necessary to consider the slow neutron induced activities, 5.3 years and 10.7 minutes, as isomers with mass number 60. The radiations from the 5.3-year period were first studied by Risser[2] who found a 1.5–2.0-Mev gamma-ray, a beta-ray spectrum with an absorption end point in aluminum at 30 mg/cm², and another weak beta-ray group with an end point at about 650 mg/cm². Later measurements by Livingood and Seaborg,[3] however, indicated that the gamma-ray energy was 1.3 Mev, that the soft beta-rays had a somewhat greater range of 30 mg/cm² to 60 mg/cm², and that the weaker beta-ray group had a range of about 300 mg/cm².

A description of the characteristic radiations of the 10.7-minute period has not been previously reported, probably because of the low yield obtained in Co(n, γ) and Ni(n, p) reactions. It has been suggested,[4] however, that the radiations consist largely of conversion electrons resulting from an isomeric transition from an upper level (10.7 minutes) to a lower level (5.3 years) in Co^{60}. Since it was found possible to produce this activity by a Co(d, p) reaction with an intensity several thousand times that obtained from Co(n, γ) and Ni(n, p) reactions, a further investigation of the radiations was made. The radiations from the 5.3-year activity were also studied in order to determine whether the two periods were genetically related.

* Now at Princeton University.

[1] J. J. Mitchell, H. S. Brown, and R. D. Fowler, Phys. Rev. **60**, 359 (1941).

[2] J. R. Risser, Phys. Rev. **52**, 768 (1937).

[3] J. J. Livingood and G. T. Seaborg, Phys. Rev. **53**, 847 (1938).

[4] J. J. Livingood and G. T. Seaborg, Phys. Rev. **60**, 913 (1941).

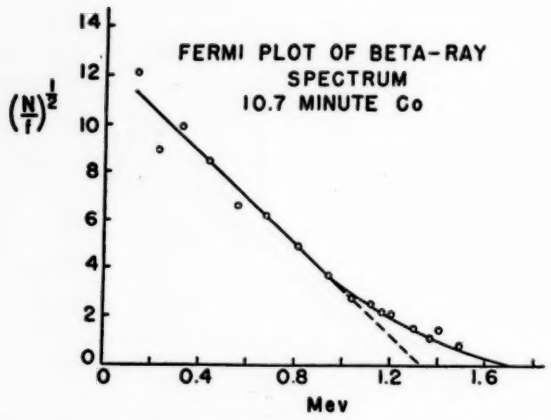

FIG. 1. Fermi plot of 10.7-minute Co^{60} beta-ray spectrum.

THE 10.7-MINUTE PERIOD

The 10.7-minute activity was produced by deuteron bombardment of Hilger No. 11045 V.P.S. cobalt metal. Spectroscopic analysis indicates that the impurities in this metal are nickel in a concentration less than 0.1 percent and traces of copper, chromium, zinc, lead, silver, iron, and calcium totaling about 0.1 percent. The short-lived activities produced from these impurities were present in a very low intensity and did not affect the measurement of the Co^{60} activity, which was verified to decay with a half-life of 10.7 minutes. Hence, no chemical separations were made previous to the energy measurements of the short-lived radiations.

The ratio of the beta-ray and gamma-ray activities as measured with an ionization chamber and Wulf electrometer indicated that approximately one gamma-ray was emitted for each beta-ray. The lead absorption coefficient of the gamma-ray activity was 0.58 cm^{-1}, corresponding to an energy of 1.5 ± 0.2 Mev.

The beta-rays emitted were measured with a magnetic beta-ray spectrometer, which is described elsewhere.[5] It appears from this spectrum that the 10.7-minute beta-rays are continuous. There is some indication of a tail due to recoils from the 1.5-Mev gamma-ray which accompanied the beta-emission. If one allows for this tail the end point is found near $5800H\rho$ or about 1.3 Mev. A beta-emitter of this energy and half-life gives a point on the first Sargent curve, and therefore the 10.7-minute transition, Co^{60} to Ni^{60}, is probably an allowed transition. The Fermi plot of this spectrum, as shown in Fig. 1, also had a slight tail indicating the presence of gamma-ray recoils. From the momentum distribution and the Fermi plot the end-point energy is evaluated at 1.35 ± 0.1 Mev.

THE 5.3-YEAR PERIOD

The 5.3-year period was also produced by deuteron bombardment of Hilger cobalt. The long-lived activities, which might be produced from the previously mentioned impurities are 250-day zinc, 310-day manganese, 47-day iron, 180-day calcium, and 85-day scandium. These and other elements were chemically separated so that their activities would not mask the soft cobalt radiations. These separations were complicated by the fact that it was necessary to keep the total bulk to a minimum so that thin samples could be prepared.

The activated metal was dissolved in aqua regia with the addition of a few milligrams of tin. The solution was evaporated several times with nitric acid and filtered off to remove any volatile radioactive substances. During this process no carriers were added so that minute concentrations of di- and tri-valent elements were adsorbed by the meta-stannic acid. Since cobalt was present in a weighable quantity (300 milligrams), its loss due to adsorption was negligible.

Carriers of about 50 milligrams each of sodium, calcium, strontium, and barium were added and cobalt was precipitated after oxidation as cobaltic hydroxide by potassium hydroxide. The precipitate was filtered off, washed, and dissolved in nitric acid. One hundred milligrams of the rare earth elements were added and were precipitated as the oxalate and filtered off. The filtrate was evaporated, ignited, and converted into the chloride.

Carriers of 50 milligrams each of the trivalent elements iron and chromium were then introduced and the solution was added to ammonium hydroxide. The precipitate was filtered off and reprecipitated by the same process to avoid any loss of cobalt. Finally carriers of phosphate ions, nickel, zinc, manganese, and other elements which did not interfere with the precipitation of cobalt were added. Cobalt was then precipitated with

[5] John W. DeWire, M. L. Pool, and J. D. Kurbatov, Phys. Rev. **61**, 564 (1942).

α-nitroso-β-naphthol and was converted into Co_3O_4 for measurement. All active impurities separated from cobalt were measured with a G-M immersion tube. When the activities were found to be considerable the chemical separations were repeated.

The lead absorption coefficient of the gamma-ray activity was 0.54 cm^{-1}, corresponding to an energy of 1.7 ± 0.2 Mev. Lower energy gamma-rays were looked for but not observed. Beta-ray ranges in aluminum varied from 44 mg/cm² to 55 mg/cm², corresponding to an energy of 220 ± 20 kev. As previously reported,[3] the shape of the absorption curve indicated that the beta-rays were probably continuous. The presence of beta-rays with an absorption limit at 300 mg/cm² to 400 mg/cm² was observed only in samples in which no chemical separations had been made. Hence, it is probable that this group of beta-rays does not belong to Co^{60}.

In order to estimate the relative activities due to the beta- and gamma-rays an ionization chamber filled with Freon at atmospheric pressure and having a 3 mg/cm² paper window was used. From the absorption curve taken with this chamber it was estimated that approximately one gamma-ray was emitted for each beta-ray.

The ratio of the activities (5.3-year : 10.7-minute) which would have been produced by an infinitely long deuteron bombardment was greater than 200 : 1. The ratio of the slow neutron cross sections for the two periods[6] (5.3-year : 10.7-minute), when corrected to account for their production from the same stable isotope, is about 40 : 1.

Isomeric decay of the 5.3-year period into the 10.7-minute period is excluded by the fact that no 1.35-Mev electrons are observed in the 5.3-year activity. Isomeric decay of the 10.7-minute period into the 5.3-year period is improbable since this level decays by continuous beta-emission. An interpretation consistent with the data is that Co^{60} consists of isomeric nuclei in which the two activities decay independently.

ACKNOWLEDGMENTS

We wish to express our appreciation to Dr. John W. DeWire for making the spectrometer measurements on the 10.7-minute period. It is a pleasure to acknowledge the support received from Mr. Julius F. Stone, the University Development Fund, and the American Association for the Advancement of Science. Valuable assistance through the W.P.A. cyclotron project No. 65-1-42-89 is also acknowledged.

[6] K. Sinma and F. Yamasaki, Phys. Rev. **59**, 402 (1941)

JULY 1 AND 15, 1942 PHYSICAL REVIEW VOLUME 62

Disintegration Schemes of Radioactive Substances. IV. Fe^{59}

M. DEUTSCH, J. R. DOWNING, L. G. ELLIOTT, J. W. IRVINE, JR., AND A. ROBERTS
Department of Physics, Massachusetts Institute of Technology, Cambridge, Massachusetts

(Received May 8, 1942)

The mode of disintegration of the 47-day isotope of iron Fe^{59} has been investigated by spectrometer and coincidence techniques. The beta-ray spectrum is complex, consisting of two components of approximately equal intensity with end points 0.257 ± 0.008 Mev and 0.460 ± 0.007 Mev. The low energy group is accompanied by gamma-rays of energy 1.30 ± 0.02 Mev, and the high energy group by gamma-rays of energy 1.10 ± 0.02 Mev. No beta-rays of energy greater than 0.460 Mev are present to as much as 0.25 percent of the main group. The yield of Fe^{59} from an iron target bombarded by 12-Mev deuterons is 0.05 microcurie per microampere hour. Methods of purification and preparation are described.

INTRODUCTION

THE 47-day activity induced in iron by deuteron bombardment is uniquely assigned to Fe^{59}.[1] The use of this isotope in biological work has been widespread, although it has been considered a difficult substance to use because of the low energy of the beta-radiation. The widely used dipping counter[2] has recently

[1] J. J. Livingood and G. T. Seaborg, Phys. Rev. **54**, 51 (1938).

[2] W. F. Bale, F. L. Haven, and M. L. Le Fevre, Rev. Sci. Inst. **10**, 193 (1939).

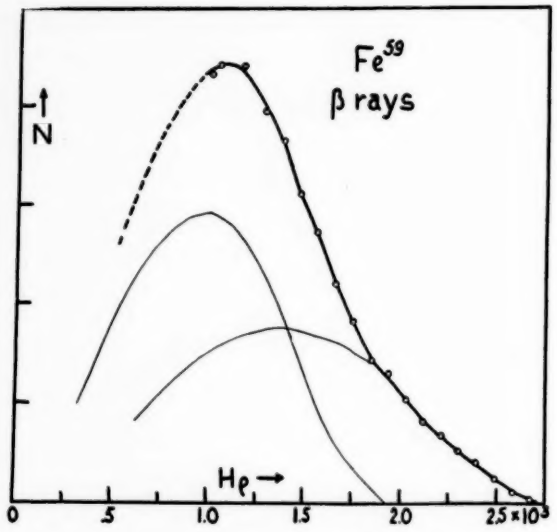

FIG. 1. The beta-ray spectrum of Fe^{59}, showing the two-component spectra. The high energy tail due to secondary electrons from the gamma-rays has been subtracted. The source was mounted on 0.001" Al and had a surface density of 1.5 mg/cm².

been shown to detect less than 5 percent as many disintegrations from a given sample as a properly constructed thin window counter.[3] In view of the metabolic importance of this isotope, its radiations have appeared worth investigation in detail. Livingood and Seaborg[1] reported that 97 percent of the beta-rays constituted a spectrum with an end point at 0.4 Mev, with 3 percent extending to 0.9 Mev, from observations on the absorption of the beta-rays in Al. They also found that gamma-radiation was present, the absorption of which in lead corresponded to an energy of 1.0 Mev.

RADIOCHEMICAL PREPARATION OF Fe^{59}

It is difficult to obtain high specific activities of Fe^{59}, since it is usually made by a (d,p) reaction and is thus isotopic with the target material; furthermore, the isotope Fe^{58} from which it is made constitutes only 0.3 percent of stable iron. Fortunately, during the course of this work it was necessary to prepare radioactive iron of high specific activity for biological work, and bombardments of up to 6500 microampere hours were made on the M.I.T. cyclotron. Specific activities as great as 1.3 microcuries per milligram were obtained, and sufficiently thin sources for good beta-ray spectroscopy were prepared by electroplating the iron upon a suitable backing material.

After activation, 100 mg/cm² were removed from the iron target face with an end mill. The coarse powder thus obtained was dissolved in 6 *M* nitric acid, 10 mg of phosphorus added as phosphoric acid and the phosphate precipitated as ammonium phosphomolybdate. The precipitate was filtered off, 10 mg more phosphorus added, and the precipitation repeated. After removal of excess molybdenum with hydrogen sulphide the iron was precipitated three times with pyridine.[4] Each time 1 mg of manganese and 1 mg of cobalt were added as chlorides for carriers and the ferric hydroxide precipitate was dissolved in hydrochloric acid. The final precipitate was ignited and weighed as ferric oxide.

Upper limits of radioactive impurities of iron thus obtained were: radiophosphorus <0.01 percent of the total activity; radiocobalt plus radiomanganese <0.04 percent. A decay curve of this iron corresponded to $_{26}Fe^{59}$ with no long lived $_{26}Fe^{55}$ detectable in $4\frac{1}{2}$ half-periods of $_{26}Fe^{59}$. The observed half-period was 46 days.

Beta-ray sources of metallic iron were prepared by electrodeposition from an acid oxalate solution by a method similar to that of Ross and Chapin.[3]

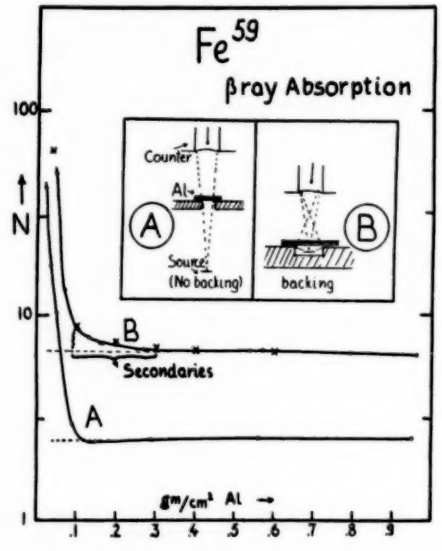

FIG. 2. The origin of the spurious beta-ray tail. The appearance of the high energy tail is a function of the geometry of the apparatus. The crosses represent the data of Livingood and Seaborg (reference 1).

[3] J. F. Ross and M. F. Chapin, Rev. Sci. Inst. **13**, 77 (1942).

[4] Ray, J. Lab. Clin. Med. **25**, 745 (1940).

An electrolyte consisting of 10 percent saturated oxalic acid solution and 90 percent saturated ammonium oxalate solution was added to one to ten milligrams of radio-iron in the form of ferric chloride. A rotating platinum anode stirred the solution in a cylindrical cell. Cathodes of thin aluminum or brass foil formed the bottom of the cell making it possible to deposit the iron in a circular area of any desired size. A current density of 0.3 amp./cm² over 3 cm² or less for 75 minutes leaves approximately 0.005 mg of iron in solution. One to ten milligrams of iron are usually plated out.

Gamma-ray sources were prepared by sealing ferric oxide into small thin wall glass capsules of approximately 0.2-ml volume. Secondary electron radiators were fastened to a flattened end of the capsule with wax.

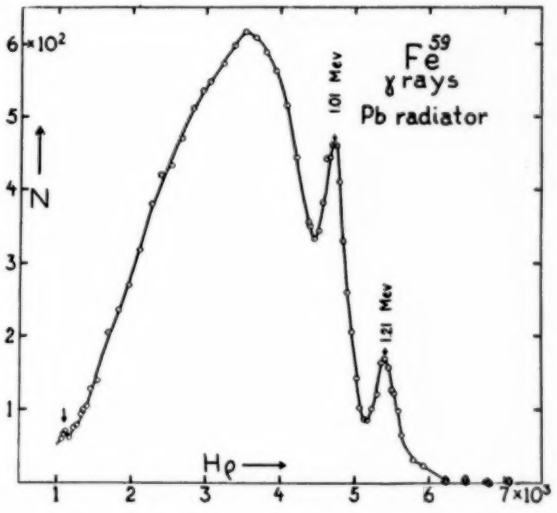

FIG. 4. Spectrum of secondary electrons from a lead radiator due to the gamma-rays of Fe^{59}. The energies of the gamma-rays corresponding to the photoelectron lines are 1.10 ± 0.02 and 1.30 ± 0.02 Mev. The arrow shows a line due to a 2-percent radiocobalt contamination, at $Hp=1010$.

RESULTS

1. The Beta-Ray Spectrum

The beta-ray spectrum obtained with the magnetic lens beta-ray spectrometer by the use of a counter with a mica window of 7 microns thickness is shown in Fig. 1. It is seen that the main group of beta-rays has a maximum energy of 0.460 ± 0.007 Mev. There is also a very much less abundant group (about 1 percent with maximum energy about 1.1 Mev, not shown in Fig. 1). Experiments with sources of different thicknesses and different backing materials showed varying relative intensity of the high energy group. It was further noted that the end point of the high energy electrons corresponded to the maximum energy of the Compton recoils from the highest energy gamma-ray present. Therefore, on the supposition that the high energy group might be gamma-ray secondaries and not a primary beta-ray spectrum at all, the source was covered with 500 mg/cm² of Cu, sufficient to stop all these electrons if they were primary beta-rays, and again placed in the spectrometer. The high energy group remained unaltered with the copper absorber in place. We conclude that the high energy group is not due to primary beta-rays but to secondaries from the gamma-rays.

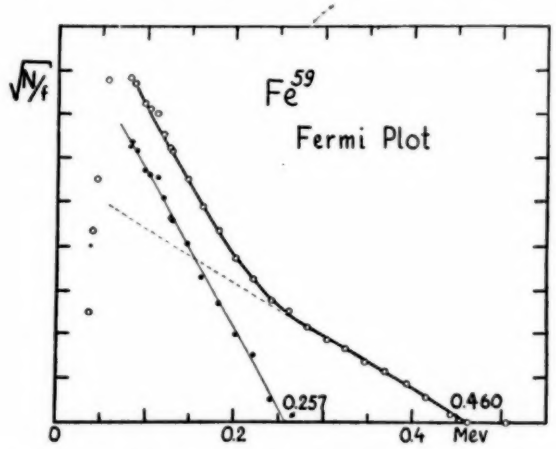

FIG. 3. Fermi plot, (for $Z=26$) of the beta-spectrum of Fe^{59}. The secondary electron tail has been subtracted.

In addition, absorption measurements were taken with two arrangements shown in Fig. 2. Arrangement *A*, in which the source was suspended by strings, was considered satisfactory as to collimation and absence of scattering material. With this arrangement the high energy group is completely absent, while other arrangements, such as *B*, show high energy tails similar to that observed by Livingood and Seaborg.[1] We conclude that if any high energy spectrum exists at all, its intensity must be less than 0.25 percent of the main spectrum.

The Fermi plot of the beta-spectrum after correction for the gamma-ray secondaries is shown in Fig. 3. It is seen to break into two

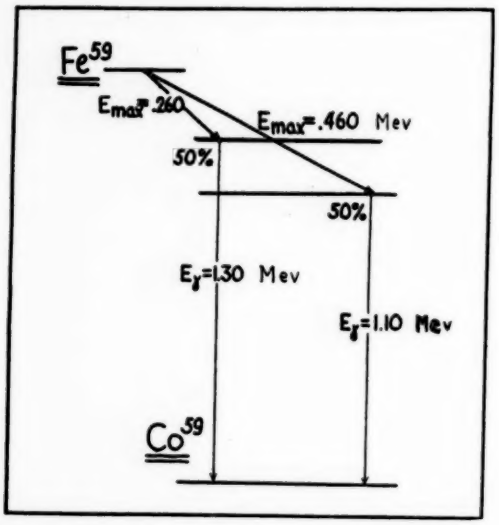

FIG. 5. Probable mode of disintegration of Fe^{59}.

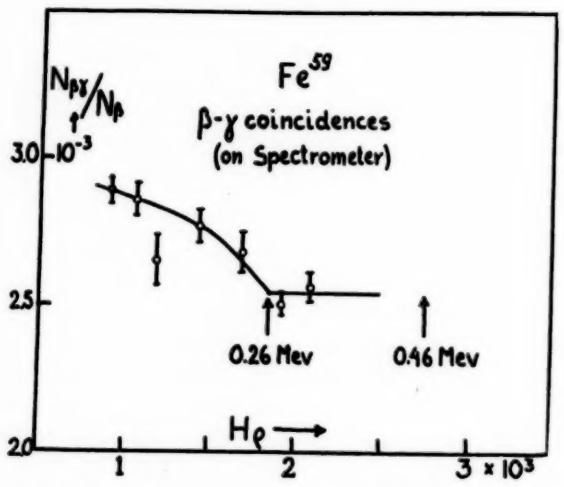

FIG. 6. Coincidence spectrum of Fe^{59}. The full line shows the shape of the curve to be expected from the energy level scheme of Fig. 5, and the known shape of the efficiency curve of the gamma-ray counter. The curve is normalized to the experimental points for the higher energy spectrum (above 0.26 Mev).

straight lines corresponding to partial spectra whose end points are 0.257 and 0.460 Mev.

The beta-decay of Fe^{59} is no doubt forbidden, and thus the significance of the breaking of the Fermi plot of the beta-ray spectrum into two linear components is not to be given too much significance, especially in view of the tentative character of current theory. In the usual interpretation, each component represents a branch to a different level in the product Co^{59} nucleus. The verification of this interpretation in the present case is thus of considerable interest.

The spectrum of secondary electrons excited in a 35 mg/cm² lead radiator by the gamma-rays is shown in Fig. 4. As previously reported[5] there are 2 gamma-rays of energies 1.10 and 1.30.

2. Coincidence Measurements

The number of beta-gamma coincidences per beta-ray showed immediately that the two gamma-rays are not in cascade, since the coincidence rate observed with a gamma-ray counter of known efficiency was characteristic of only one gamma-ray of about 1.2 Mev per beta-ray, and half what it would have been had the two gamma-rays been in cascade. An attempt to disclose the complexity of the beta-spectrum by finding a variation in the beta-gamma coincidence rate* as absorber was interposed before the beta-counter was unsuccessful, as a rise at low energies could not be unequivocally established. It was also found, with the "poor" geometry necessary in coincidence experiments, that as absorber was interposed the coincidence rate fell off, gradually approaching zero at the 0.460-Mev end point, since the secondary electrons constituting the high energy tail do not coincide with gamma-radiation. This observation is of no use in determining the origin of the tail, however, since these electrons would not coincide with gamma-rays if they were either a high energy branch to the ground state of Co^{59} or secondaries from a gamma-ray not coinciding with other gamma-rays.

Since the gamma-rays apparently do not coincide with each other, one might suppose that they represent transitions directly to the ground state from excited levels, respectively, 1.10 and 1.30 Mev above the ground state. The beta-ray transitions would end upon these levels, as in Fig. 5, the difference between their end points corresponding to the difference between the gamma-ray energies within the experimental error. This scheme does predict, however, a somewhat higher beta-gamma coincidence rate for the low energy beta-ray spectrum since the efficiency of the gamma-ray counter is higher for the higher

[5] M. Deutsch, A. Roberts, and L. G. Elliott, Phys. Rev. **61**, 389A (1942).

* Throughout this section beta-gamma coincidence rates are taken per recorded beta-ray and gamma-gamma rates are taken per recorded gamma-ray.

energy gamma-ray. The failure to observe this rise in the absorption experiment is not conclusive, since the number of electrons in the low energy spectrum counted is less than half of the total even with zero absorber, because of source thickness and counter window absorption. A much better chance of observing the rise at low energies will be obtained by measuring the beta-gamma coincidence rate on the spectrometer, where the relative number of electrons from each spectrum at low energies is much more favorable. The beta-gamma coincidence spectrum so taken is shown in Fig. 6, and the predicted rise at low energies verified.

A considerable number of attempts to detect gamma-gamma coincidences were made. According to the disintegration scheme of Fig. 5 none is to be expected. Careful repeated measurements gave a weighted mean value of $(0.050\pm0.033)\times10^{-3}$ gamma-gamma coincidence in the standard gamma-gamma set-up. Careful search of the gamma-ray spectrum for a 200-kev gamma-ray due to an occasional transition between the excited levels shows that such a gamma-ray cannot be present to more than five percent of the intensity of the competing 1.30-Mev gamma-ray. In fact Fig. 4 shows a peak in this neighborhood due to the L conversion in lead of the 131-kev gamma-ray of a 2-percent radiocobalt contamination which was subsequently removed. If one attempts to attribute the observed gamma-gamma coincidences to such a transition, the known efficiencies of the gamma-ray counters for gamma-rays of the energies involved predict a gamma-gamma coincidence rate of not more than 0.015×10^{-3}. We do not think our apparatus capable of greater accuracy than that already obtained in measuring so small a number of true coincidences (less than 1 percent of the coincidence background). We are therefore inclined to question the significance of the observed gamma-gamma coincidence rate.

DISCUSSION

The reasonably certain establishment of the disintegration scheme of Fig. 5 shows that the splitting of the Fermi plot may be of significance in establishing complexity of the beta-ray emission, even in cases of such low energy and highly forbidden disintegrations as this.

A word or two as to the angular momentum of the levels involved is in order. The ground state of Co^{59} is known to have a total angular momentum of 7/2.[6] The two beta-ray spectra have approximately equal probabilities, and since they do not differ greatly in total disintegration energy (0.77 and 0.97 Mev) it seems reasonable to suppose that they are about equally forbidden. On the other hand, beta-decay directly to the ground state is highly forbidden, and from the considerably greater energy available for such a transition it would seem that it must be forbidden at least twice more than the observed transitions. Unique angular momentum or parity assignments from these data are not possible. The indicated value for the angular momentum of the ground state of Fe^{59} is different from that of Co^{59} by at least two units, and thus may perhaps be satisfied by the values $\frac{1}{2}$ or $\frac{3}{2}$.

Yield of Fe^{59}

Since knowledge of the gamma-ray counter efficiency and the disintegration scheme permit the determination of the number of disintegrations per minute without comparison with curie standards an estimate of the total yield of Fe^{59} with 12-Mev deuterons was made. The principal errors are those of deuteron beam current measurement during the bombardment. At 12 Mev the yield is at least 0.05 microcurie per microampere hour. This is greater than the reported Berkeley yield of 0.03 microcurie per microampere hour[7] at 16 Mev.

ACKNOWLEDGMENTS

We are glad to acknowledge the cooperation of the M.I.T. cyclotron crew under Professor M. S. Livingston, and the continued interest and support of Professor R. D. Evans.

[6] K. R. More, Phys. Rev. **46**, 470 (1934); Kopfermann and Rasmussen, Zeits. f. Physik **49**, 58 (1935).
[7] J. G. Hamilton, J. App. Phys. **12**, 440 (1941).

On the Excited States of Nuclei Beyond Oxygen

A. GUTHRIE AND R. G. SACHS
Purdue University, Lafayette, Indiana
(Received April 2, 1942)

If spin-orbit coupling and the difference between neutron-neutron, neutron-proton, and proton-proton forces are neglected, the energies of the ground states of the nuclei beyond oxygen can be expressed in terms of the symmetry character of the wave functions and a smoothly varying function of atomic weight. With the same assumptions, the energies of the excited states of these nuclei can be expressed in similar terms. Thus the difference in energy of the ground states and the excited states of the same symmetry would be expected to vary smoothly as a function of mass number. Since each state is a supermultiplet of states which will be split under the influence of spin-orbit coupling, it will not in general be possible to observe this behavior of the energy levels. However, in the case of the alpha-particle nuclei, the low-lying excited states are singlets so the regularity should be observable. Unfortunately there are insufficient experimental data on the excited states of these nuclei to make a positive statement as to agreement, but those data which are available do not disagree with the suggested behavior.

IT has been shown by Wigner[1] that the energies of the ground states of the nuclei beyond oxygen can be calculated by means of a simple expression involving the symmetry character of the wave function in the ground state and a smoothly varying function of atomic weight. This result is obtained by neglecting the spin-orbit coupling and the difference between neutron-neutron, neutron-proton, and proton-proton forces except for the average effect of the Coulomb interaction. Barkas[2] has compared the theoretical masses of the nuclei obtained in this way with the experimental masses and has found reasonably good agreement between them.

If the energies of the excited states are calculated with the same approximations, they are expressions of the same type as those for the ground states. Thus the difference in energy of the ground states and the excited states of the same symmetry character would be expected to vary smoothly as a function of the mass number of the nuclei. However, each state is a supermultiplet[3] of states which will be split into its many components under the influence of the spin-orbit coupling. In addition it is likely that states belonging to different multiplets will be mixed. Therefore, it will in general be very difficult to make any correlation between the experimentally observed excited states and those predicted in first approximation by the Wigner theory. The only type of state for which it seems feasible to make this correlation is that belonging to a singlet supermultiplet[3] of the (0,0,0) type. Even these states may give trouble if the influence of the tensor spin-orbit coupling is important[4] since this interaction mixes the (0,0,0) state with other multiplets. However, the general success of the Wigner theory in giving the masses of the nuclei seems to indicate that the influence of the tensor interaction on the ground states is not very great. Therefore, it may not be a factor of great importance in determining the energies of the low excited states.

The low states of the alpha-particle nuclei are expected to be (0,0,0) multiplets, so the difference in energy between these states and the ground states would be expected to behave as a smoothly varying function of atomic number if the influence of the tensor force is small. An evaluation of this smooth function for these nuclei would make it possible to determine what the energies of the excited states of other nuclei in the same region of the periodic table would be if spin-orbit coupling were negligible. Comparison with the actual experimental energies of these excited states would then lead to information concerning the spin-orbit coupling.

[1] E. Wigner, Phys. Rev. **51**, 947 (1937).
[2] W. H. Barkas, Phys. Rev. **55**, 691 (1939).
[3] E. Wigner, Phys. Rev. **51**, 106 (1937).
[4] A rough calculation by E. Gerjuoy and J. Schwinger [Phys. Rev. **61**, 138 (1942)] indicates that the influence of the tensor interaction on the energy of the ground state of He^4 may not be negligible. The influence on the energy of an excited state would probably be even more important.

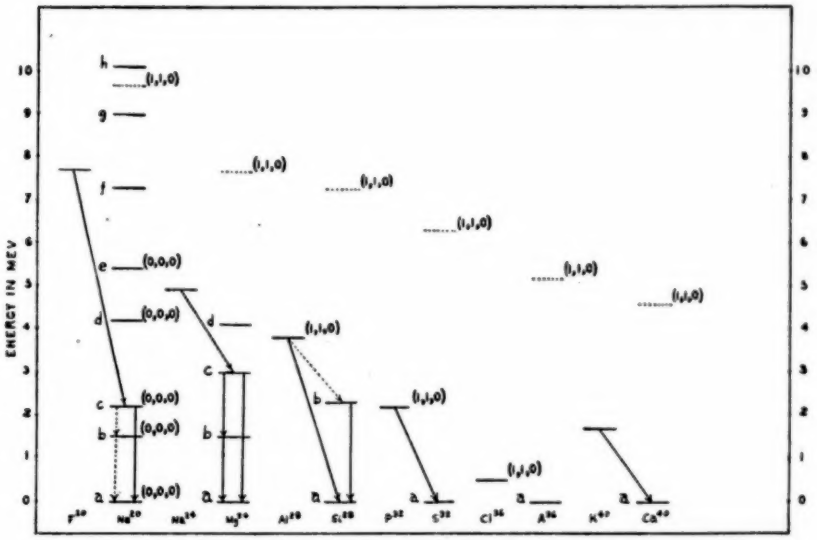

FIG. 1. The solid lines indicate experimentally observed energy levels and transitions. The transitions associated with the broken lines are predicted but not yet observed. The horizontal broken lines are the positions of the lowest (110) levels of the corresponding nuclei as calculated by means of a formula given by Barkas (reference 2).

The purpose of the present note is to point out that the known data on the excited states of the nuclei[5] Ne^{20}, Mg^{24}, Si^{28}, S^{32}, A^{36}, and Ca^{40} do not disagree with the suggested behavior. Unfortunately there are insufficient data to make any positive statement as to agreement, but it is to be hoped that calling attention to these facts will stimulate experimental work which will complete the picture.

The observed energy levels of Ne^{20}, Mg^{24}, Si^{28}, S^{32}, A^{36}, Ca^{40}, and the beta- and gamma-transitions leading to them are indicated in Fig. 1 by the solid lines. The levels *b*, *d*, *e*, *f*, *g*, *h* of Ne^{20} have been obtained by Bonner[6] by measuring the neutron energies in the $F^{19}(d,n)Ne^{20}$ reaction. His high energy maxima are too broad to allow a separation of the levels *b* and *c*. The beta- and gamma-assignments are taken from Curran and Strothers.[7] The $b \rightarrow a$ and $c \rightarrow b$ transitions have not been observed.

The beta- and gamma-ray spectra assigned to Na^{24} are somewhat different from the latest given by Curran, Dee, and Strothers.[8] They assume that the 3-Mev and 1.5-Mev gammas are in cascade. However, such an arrangement of levels would lead to a mass for Na^{24} which would be much higher than expected on the basis of present ideas about nuclei. The best evidence for the level scheme given in Fig. 1 is that the levels *b* and *c* are in excellent agreement with those found by Wilkins[9] who measured the energies of protons which had been inelastically scattered from Mg. He assigned the level *d* to Mg^{26}, but it may be a level of Mg^{24} corresponding to a gamma-ray of approximately 4.5 Mev tentatively reported by Curran, Dee, and Strothers[8] for the reaction $Na^{23}(p,\gamma)Mg^{24}$.

The data on Al^{28}-Si^{28} are taken from Livingston and Bethe.[10] According to them, the beta-transi-

[5] Only these nuclei have been considered because the nuclei at either end of this series involve a change from one closed shell to another.

[6] T. W. Bonner, Proc. Roy. Soc. **A174**, 339 (1940).

[7] S. C. Curran and J. E. Strothers, Proc. Camb. Phil. Soc. **36**, 252 (1940).

[8] S. C. Curran, P. I. Dee, and J. E. Strothers, Proc. Roy. Soc. **A174**, 546 (1940).

[9] T. R. Wilkins, Phys. Rev. **60**, 365 (1941).

[10] M. S. Livingston and H. A. Bethe, Rev. Mod. Phys. **9**, 245 (1937). This assignment has recently been contradicted by the coincidence experiments of Watase [Proc. Physico-Math. Soc. Jap. **23**, 618 (1941)]. He found no evidence for a complex beta-spectrum and therefore assumes that the 3.3-Mev beta-transition is followed by the 2.3-Mev gamma-transition, thus increasing the mass of Al^{28} by 2.3 Mev. This mass is in complete disagreement with the theoretical value obtained by Barkas and may indicate that the tensor force is particularly important in determining the mass of Al^{28}. It is hoped that this coincidence experiment will be repeated within a short time.

tion to state *b* must be weak since the beta-spectrum of Al^{28} appears to be simple. The maximum energy of the beta-spectrum of P^{32} is taken from the results of Lawson.[11] No gamma-radiation has been observed. The levels of Cl^{36} and A^{36} are those given by Barkas.[2] The beta-transition appears to be energetically forbidden. The energy difference K^{40}-Ca^{40} has been taken from the results of Henderson.[12]

Evidently there is a correspondence between those levels in Fig. 1 which carry the same label. Thus it would be assumed that the energies of the levels of type *b* are a smooth function of atomic weight. Apparently the level *c* continues to rise so that it is above the ground state of Al^{28} and P^{32}, thereby causing the beta-transition to follow a different path. Similarly the level *b* is rising rather rapidly at S^{32} so it is above the ground state of P^{32} and the only possible beta-transition is that to the ground state of S^{32}. Direct energy level determinations for Si^{28}, S^{32}, A^{36}, and Ca^{40} are essential for a verification of this behavior.

All of the lower levels of the alpha-particle nuclei are (0,0,0) states. However, the ground states of F^{20}, Na^{24}, etc. are (1,1,0) states and there are corresponding states of the same multiplet for the alpha-particle nuclei. The positions of these levels have been estimated by means of formulae given by Barkas[2] on the basis of the Wigner theory. They are indicated by the horizontal broken lines in Fig. 1. Apparently levels *g* and *h* and possibly *f* belong to the (110) multiplet.

Information concerning the angular momenta and parity of the states can be obtained by considering the product of the lifetime *t* for the beta-transition and a function, $I(E_{max})$, of the maximum beta-energy which gives the dependence of the lifetime on this energy. For an allowed transition this product should be of the order of magnitude of[13] 10^3 and increases roughly by a factor of 100 for each order in which the transition is forbidden. The values of $It/\log 2$ are given in Table I under the assumption that the observed beta-spectra are essentially simple. The fact that all values are at least of the order of 10^5 agrees with the fact that a (110)→(000) transition is forbidden at least in first order for either Fermi or Gamow-Teller selection rules.[13] Apparently the P^{32}→S^{32} transition is even more strongly forbidden, as one would expect if the symmetry of the ground state of P^{32} is the same as that of F^{20} and Na^{24}. The data on the decay of K^{40} were not included since this nucleus has one neutron outside of a closed shell so that no correlation between its ground state and those of the other beta-active nuclei can be expected.

TABLE I. Values of $It/\log 2$ for the given radioactive elements.

Element	F	Na	Al	P
$10^{-5}It/\log 2$	8.00	8.62	1.44	672

No attempt has been made to assign the angular momenta of the levels because there are many possibilities depending on the parity, the spin in the lowest state of the (110) multiplet of the radioactive nuclei, and the particular type of selection rule (Fermi or Gamow-Teller) assumed. We can say that there is no contradiction if one assumes that corresponding levels have the same parity and orbital angular momenta. The apparent contradiction in the case of Al^{28}→Si^{28} may be due to an inversion of the (110) multiplet in Al^{28}.

[11] J. L. Lawson, Phys. Rev. **56**, 131 (1939).
[12] W. J. Henderson, Phys. Rev. **55**, 238 (1939).
[13] E. Wigner, Phys. Rev. **56**, 519 (1939).

Proton Production by Electron Collisions in Molecular Hydrogen

HERBERT F. NEWHALL
Cornell University, Ithaca, New York

(Received April 11, 1942)

The collision processes leading to the production of protons by single electron collisions with molecular hydrogen were investigated. A mass spectrometer was used for the analysis. The electron beam, along which ions were produced, was coaxial with a cylindrical conductor, and the radial field within this conductor due to the electron space charge was used as an energy selector for the ions. The ions measured were those moving initially at right angles to the electron beam. The "fast" protons (ions having several electron volts of energy) found by Bleakney were observed, and a rough measurement of the cross section for their production was made. The cross section was found to reach a maximum of about 0.015 cm^2/cm^3 for 110-volt electrons. No evidence was found for the slow protons observed by Bleakney. It is believed that these were formed by secondary collision processes. From the theory developed by Smith, it is possible to compute roughly the initial energy distribution of the ions. The distributions are in accord with the potential energy curves of the hydrogen molecule..

INTRODUCTION

THE mechanism of proton production by electron collisions in molecular hydrogen has been the subject of many investigations.[1–6] Of particular interest is the work of Bleakney.[4] Analyzing the results of electron collisions in hydrogen with a mass spectrometer, Bleakney found evidence for two groups of protons, one group having kinetic energies of the order of several electron volts and the other group having essentially thermal energies. The ion clearing field was used as an energy selector to separate these groups of ions.

The protons having relatively large energies ("fast" protons) were readily understandable in terms of an excitation of the molecule from the ground state to state *f* (see Fig. 1) in the electronic diagram. Upon application of the Franck-Condon principle[7] to this excitation, it is necessary that the dissociating atom and proton share from 10 to 15 electron volts between them. The collision process giving rise to the slow protons is not so clear, however. Bleakney attributed them to excitations to the electronic state for the molecular ion (state *e*, Fig. 1), indicating that a portion of the potential energy curve for this state, lying within the Franck-Condon region, was above the dissociation level. Curve *e* in Fig. 1, which was taken from the work of Burrau,[8] indicates that this process is not very probable.

The slower protons observed by Bleakney might arise from secondary collision processes. A possible process is the dissociation of the

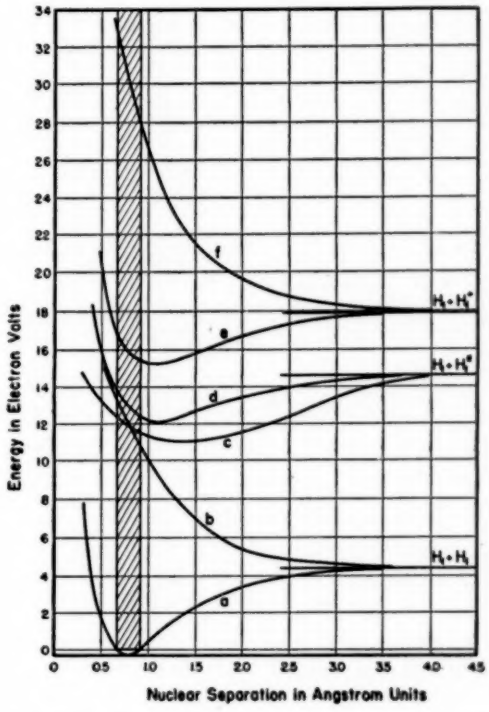

FIG. 1. Potential energy curves for the electronic states of the hydrogen molecule.

[1] A. J. Dempster, Phil. Mag. **31**, 438 (1916).
[2] H. D. Smyth, Phys. Rev. **25**, 452 (1925).
[3] H. D. Smyth and E. U. Condon, Proc. Nat. Acad. **14**, 871 (1928).
[4] W. Bleakney, Phys. Rev. **35**, 1180 (1930).
[5] W. Bleakney, Phys. Rev. **38**, 496 (1932).
[6] J. W. Hiby, Ann. d. Physik **34**, 5, 473 (1939).
[7] E. U. Condon, Phys. Rev. **32**, 858 (1928).
[8] Burrau, Kgl. Danske Vid. Selskal. Math-fys. Med. **7**, 14 (1927).

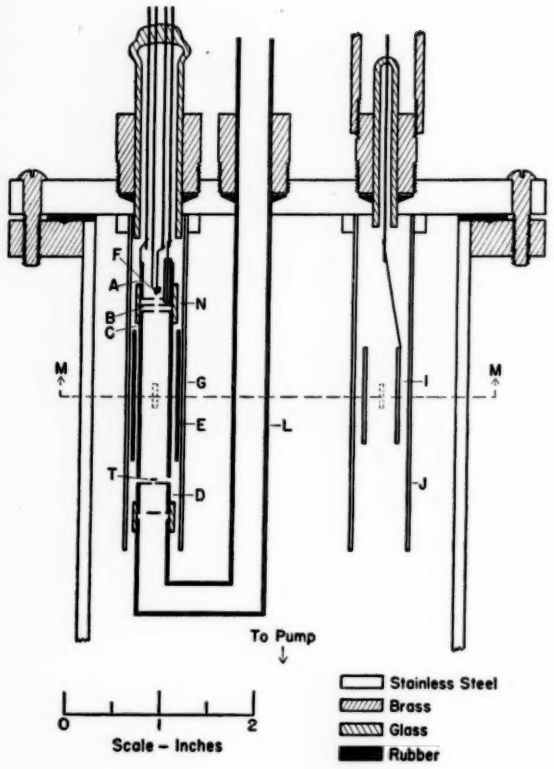

FIG. 2. Sectional view of the experimental apparatus.

molecule into two atoms, with subsequent ionization of one of the atoms, as indicated:

$$\begin{aligned} H_2+e &\rightarrow H_1+H_1+e \\ H_1+e &\rightarrow H_1^++2e. \end{aligned} \qquad (1)$$

The collision cross section for the first step in this process has been computed by Massey and Mohr,[9] and they find it to be quite large for low electron energies (around 15 volts). However, the cross section decreases rapidly for higher energies. This dissociation process (excitation to state *b*, Fig. 1) gives the atoms a considerable amount of kinetic energy, and they would be expected to go to the walls of the apparatus. They may, however, return and form an appreciable atomic concentration, depending on the rate of recombination at the walls. Another process giving rise to slow atomic ions involves molecule-molecular ion collisions:

$$\begin{aligned} H_2+H_2^+ &\rightarrow H_3^++H_1 \\ H_3^+ &\rightarrow H_1^++H_2. \end{aligned} \qquad (2)$$

[9] N. Massey and F. Mohr, Proc. Roy. Soc. **A135**, 258 (1932).

The unstable ion H_3^+ and the products resulting from it have been observed by several investigators.[2,10,11] In order for this process to occur, the molecular ion must acquire enough energy to dissociate the molecule.[12]

In view of the results of Bleakney, it seemed worthwhile to investigate again the collision processes in hydrogen, in order to see if the production of slow protons was the result of a direct collision process. Furthermore, it was thought worthwhile to attempt to make a rough measurement of the collision cross section for the production of the fast protons (excitation to state *f*, Fig. 1). This process is somewhat similar to the simple dissociation process (excitation to state *b*), and the two cross sections might be expected to be comparable and to vary similarly with electron energy.

EXPERIMENTAL METHOD

The experimental apparatus is shown in cross section in Fig. 2. Electrons are emitted by

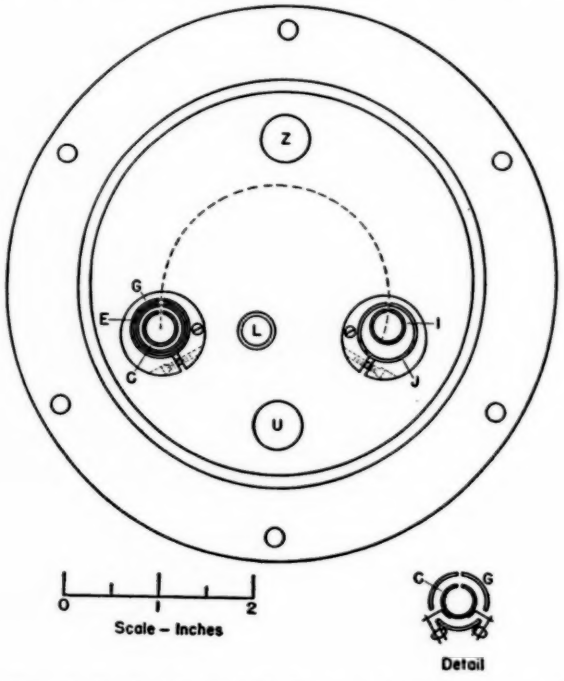

FIG. 3. Sectional view of the experimental apparatus (section through *MM* of Fig. 2). *U*, port for electrical connections. *Z*, port for ionization gauge.

[10] H. D. Smyth, J. Frank. Inst. **198**, 795 (1924).
[11] T. R. Hogness and E. G. Lunn, Phys. Rev. **26**, 44 (1925).
[12] K. E. Dorsch and H. Kallmann, Zeits. f. Physik **53**, 80 (1929).

the filament F and are accelerated and collimated by the electrodes A and B. The electron beam is coaxial with the cylindrical electrode C. The electron current is collected at the target T. The electrode D was used in adjusting the collimation and direction of the electron beam.

Hydrogen was introduced into the vacuum system through the tube L, and ions were formed by electron collision along the electron beam. Some of the ions go toward the slit in C (indicated by broken lines in Fig. 2). They are accelerated by the electrodes E and G, concentric with C. Under the action of the magnetic field parallel to the electron beam, the ions move in a circular path and are collected at the electrode I, which is surrounded by the guard J. The ion path is indicated by the broken line in Fig. 3, a sectional view through MM of Fig. 2. The magnetic field also serves to confine the electron beam.

The distinction between the collision processes leading to proton production is accomplished by the separation of the protons according to their kinetic energies. The field within the cylinder C due to the space charge of the electron beam is used as the energy selector. The radial variation of potential across the interior of a cylindrical conductor, in which there is an axial electron beam, has been computed by Smith.[13] The potential distribution is shown in Fig. 4, where V represents the potential (with respect to the electron source) at a point r from the axis of the cylinder. The space charge potential V_R will, of course, increase with increasing electron current and decrease with increasing electron energy. Ions produced by electron collisions in the beam will be able to reach the walls of the cylinder C (and the slit) only if they have at least an energy eV_R, where V_R is the potential difference between the center of the beam and the wall. The potential variation across the beam is neglected.

This experimental arrangement also serves to suppress proton production by molecule-molecular ion interactions. As was mentioned above, the molecular ion must acquire some energy to make this process possible. Molecular ions produced in the beam are effectively trapped there by the space charge field, unless their thermal energies are enough for them to reach the wall. In any case, they can acquire no energy from the radial field. There is, of course, a potential gradient along the beam, but this must be small.

As indicated in Fig. 2, the vacuum system was constructed almost entirely of stainless steel, U.S. 18–8 non-magnetic steel being used throughout. The electron gun was carried on

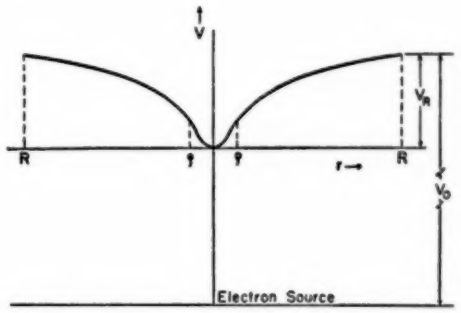

FIG. 4. Radial potential distribution across the cylinder C. V_0 = potential difference between electron source and cylinder C. V_R = potential difference between middle of electron beam and wall. R = inner radius of cylinder C. ρ = radius of electron beam.

one press seal, and it was centered with respect to C by the glass sleeve N. The filament was spiral of 5-mil tungsten wire. The aperture in B had a diameter of 1 mm and that in the cap on C a diameter of 2 mm. Electrodes B and C were held at fixed potentials, and the potential corresponding to the desired electron energy applied between the filament and C. Beam currents as large as 900 microamperes could be obtained with electron energies of 40 volts or more, though it was found desirable to limit the current to about 500 microamperes. From the size of the discolored spot found on the target T, it was concluded that the beam divergence was not appreciable.

The electrodes C, E, and D were mounted from the cylinder G by the Pyrex bead construction shown in the detail drawing in Fig. 3. The slits in C, E, and G were 1 mm wide and 6 mm long. A small fixed ion accelerating potential was applied between C and E, and the rest of the accelerating potential between E and G. The ion collector I was mounted from J by the same method used for C. The ion current

[13] L. P. Smith and P. L. Hartman, J. App. Phys. **11**, 220 (1940).

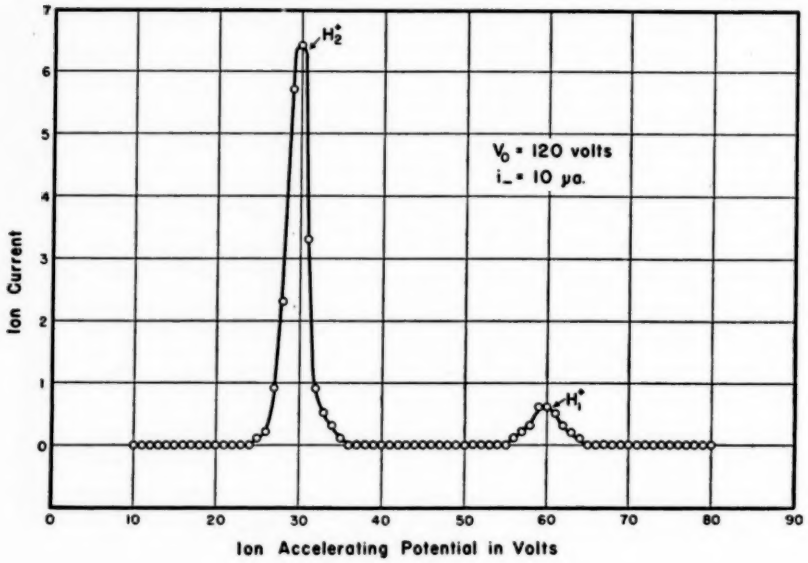

FIG. 5. Mass spectrum of hydrogen ions.

was measured with an electrometer tube circuit of the modified Barth type,[14,15] with the Western Electric D96475 tube. A maximum sensitivity of about 10,000 mm per volt was available, when a grid resistance of about 10^{10} ohms was used.

The system was evacuated by an oil diffusion pump of the type described by Malter and Marcuvitz.[16] A Cenco Megavac provided the fore vacuum. The hydrogen gas leaked into the system through a Hoke high vacuum valve. Commercial tank hydrogen was regarded as sufficiently pure for this work, as a mass-spectrometric analysis was being made. The operating pressure was about 5×10^{-5} mm Hg.

The magnetic field for the mass analysis was provided by a pair of Helmholtz coils. These coils gave a field of about 370 gauss at their center, with 7 amperes in the coils. The coils were mounted so their axis could be aligned with the desired direction of the electron beam.

EXPERIMENTAL RESULTS

A representative mass spectrum of the hydrogen ions is shown in Fig. 5. The magnetic field is held constant during such a series of measurements. The identification of the ion peaks is indicated in Fig. 5. At relatively high gas pressures, there was some background in the mass spectrum. This was attributed to the results of ion-molecule collisions in the ion-accelerating or in the analyzing region.

In order to observe the energy selection effect of the electron space charge, it is desirable to measure the variation in ion current with electron current, for a fixed value of the electron energy (V_0 in Fig. 4). By setting the apparatus to record the peak value of the ion current (for the atomic ions, say), this variation can be measured directly. Such a curve for protons at $V_0=60$ volts is shown in Fig. 6. It is seen that, for small electron currents, the ion current

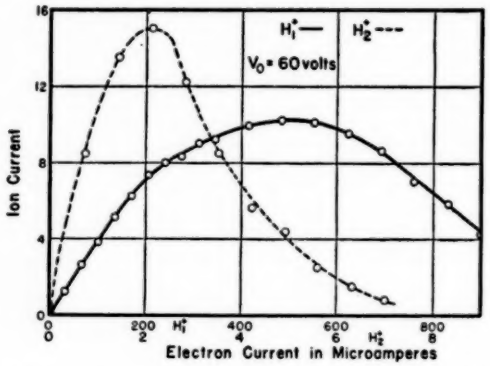

FIG. 6. Proton current and molecular ion current *vs.* electron beam current for 60-volt electrons.

[14] G. Barth, Zeits. f. Physik **87**, 399 (1934).
[15] D. B. Penick, Rev. Sci. Inst. **6**, 115 (1935).
[16] L. Malter and N. Marcuvitz, Rev. Sci. Inst. **9**, 92 (1938).

increases linearly with electron current. For larger electron currents, the energy selection effect becomes important, and, finally, the ion current decreases with increasing electron current. The corresponding curve for the molecular ions at $V_0=60$ volts is also shown in Fig. 6. It is important to notice that the electron current ranges are very different in the two cases. For the atomic ions, the ion current reaches a maximum for about 500-microamperes beam current, whereas the molecular ion current is a maximum for only two-microamperes beam current. Since the molecular ions acquire very little kinetic energy in the electron collision, the energy distribution of these ions should be essentially a Maxwellian one, corresponding to the gas temperature. The average energy of the molecular ions is therefore of the order of hundredths of electron volts with the gas at room temperature, and an electron current of only two microamperes is sufficient to produce a value of the space charge potential V_R in this range. In the case of the protons, however, an electron current of about 500 microamperes is necessary to increase V_R to the average energy of the ions. These protons clearly have much more than thermal energies, and it is reasonable to conclude that they arise from the excitation of the molecule from the ground state to state f (see Fig. 1).

Curves of proton current *vs.* electron current for various values of V_0 are shown in Fig. 7. The experimental points have been omitted from these graphs, for clarity. The fit for all the curves is about as good as in Fig. 6. The electron current for these data was limited to about 400 microamperes, because of difficulties with filament failure at higher currents. There is a regular variation in the slope of the linear portion of these curves with changing V_0, showing a variation of the cross section with electron energy (see below). The departure from linearity occurs at smaller electron currents for smaller values of V_0. This is reasonable, inasmuch as the electron current necessary to produce a given space charge potential V_R is smaller for smaller values of V_0. In the curves for large values of V_0, there seems to be a slight upward curvature, though this effect does not seem large enough to be significant.

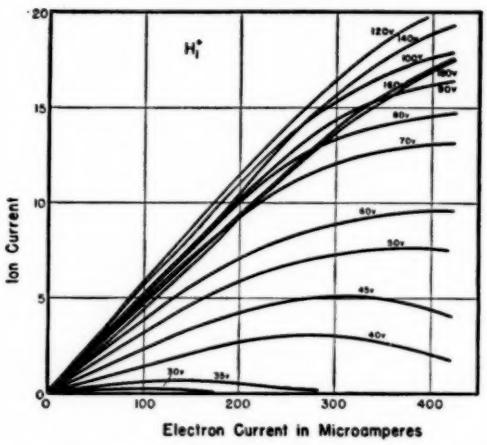

FIG. 7. Proton current *vs.* electron beam current for various electron energies.

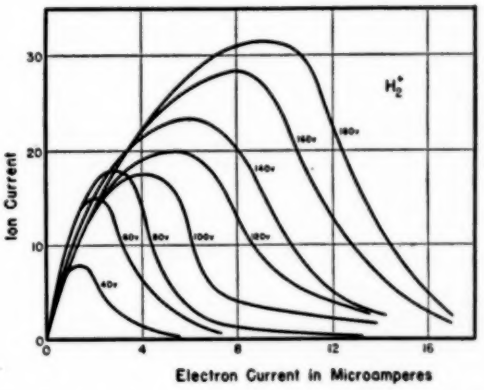

FIG. 8. Molecular ion current *vs.* electron beam current for various electron energies.

The corresponding curves for the molecular ions for various values of V_0 are shown in Fig. 8. Here again the experimental points are omitted, the fit being as good as that in Fig. 6. There is some variation in the slope of these curves near the origin, indicating a change in the ionization cross section with energy (see below). The variation of the beam current required to produce a given value of V_R as V_0 is changed, is shown more strikingly in these curves, as the maxima occur at smaller electron currents for smaller values of V_0.

If there are any slow protons (i.e., having energies in the thermal range) produced by single electron collisions, these protons should appear as a deviation from linearity in the curves of Fig. 7 for small electron currents. To

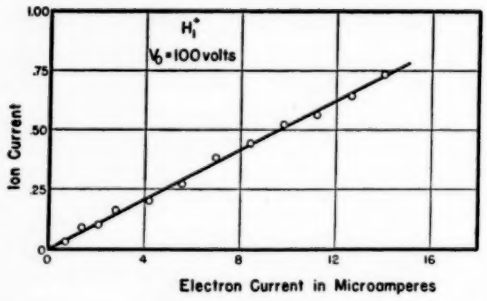

FIG. 9. Proton current *vs.* electron beam current for 100-volt electrons (small electron currents).

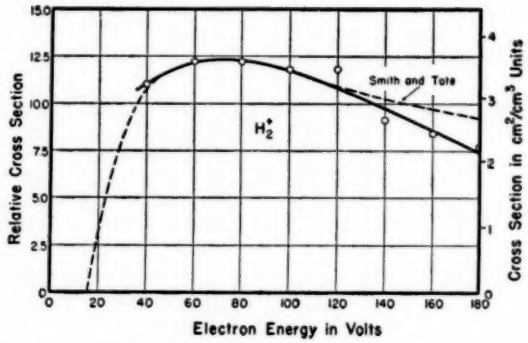

FIG. 10. Ionization cross section for molecular ions.

investigate this, the proton current was measured for the electron current range of Fig. 8, for various values of V_0. A typical curve for $V_0 = 100$ volts is shown in Fig. 9. There seems no reason to describe the variation as anything but linear. Similar curves were obtained for other values of V_0 in the range investigated.

INTERPRETATION

A. Cross Section for Molecular Ions

The slopes of the linear portions of the ion current *vs.* electron current curves are a measure of the collision cross section for the process involved. The relative molecular ionization cross section, as measured this way, is shown by the solid curve in Fig. 10. This result is not very accurate, since the curves of Fig. 8 depart from linearity for very small values of the electron current. The ionization cross section for hydrogen molecular ions has been measured absolutely by Smith and Tate,[17] and their result is shown by the broken line in Fig. 10. The two curves were matched at the maximum at 70 volts. The scale on the right is the ionization cross section for Smith and Tate's curve in cm^2/cm^3 units. When the uncertainty in the present results is considered, the agreement in trend is satisfactory.

B. Cross Section for Atomic Ions

The cross-section curve for the atomic ions (Fig. 11) was obtained in the same way as that for the molecular ions. The right-hand scale in Fig. 11 (in cm^2/cm^3 units) was obtained from the correspondence between the two scales in Fig. 10. The cross section for fast proton production is seen to be roughly 1/200 that for molecular ions, for the electron energy range investigated. This result does not agree with the work of Bleakney,[4] who found the ratio to be about 1/15. It was mentioned above that Bleakney measured the fast ions by reversing the ion collecting field across the collision region. In order to make the measurements on fast ions comparable with those on slow ions, Bleakney measured the fast ion current as this retarding field was reduced. By extrapolating to zero field, he obtained a value for the fast ion current which was presumably comparable with the slow ion currents measured. However, Hagstrum and Tate[18] have shown that the efficiency of collection of ions under such circumstances is a sensitive function of the ion energy. It is not certain, therefore, that the comparison is accurate.

C. Energy Distribution of the Ions

Since the ion current *vs.* electron current curves represent the result of an energy selection process, it is possible to derive the initial energy distribution of the ions from them. In order to compute the distribution, it is necessary to obtain an analytic expression connecting V_R, V_0 and the electron current i_-. From the theory developed by Smith,[13] it can be shown that, if V_R is not too large compared to V_0, the following relation holds:

$$V_R = \{1.52 \times 10^4 i_- (1 + 2 \log R/\rho)\}/V_0^{\frac{1}{2}}. \quad (3)$$

In this expression, i_- is measured in amperes

[17] P. T. Smith and J. T. Tate, Phys. Rev. **39**, 270 (1932).

[18] H. D. Hagstrum and J. T. Tate, Phys. Rev. **59**, 354 (1941).

and V_R and V_0 in volts. R and ρ are the radii indicated in Fig. 4. In the computation of the energy distributions, it is assumed that the ions measured are those which start out initially at right angles to the electron beam. Since the angular aperture of the collector slit, as seen from the accelerating slits (around the ion path), is quite small, this assumption is reasonable. It is quite accurate in the case of the fast protons, since these ions must have a very small original velocity component parallel to the electron beam if they are to be collected. Since the magnetic field supplies no energy to the ions, its effect on the motion of the ions within the cylinder C is neglected.

Let $f(E)dE$ be the fraction of the total number of ions produced per unit electron current per unit gas pressure, which have an energy between E and $E+dE$. $f(E)$ is, then, the desired energy distribution function. Let n_+ be the rate at which ions reach the wall per unit beam length. It is assumed that the measured ion current is proportional to n_+. Ions will reach the wall only if they have an energy greater than eV_R. The total rate at which they reach the wall is

$$n_+ = i_- \sigma p \int_{eV_R}^{\infty} f(E)dE, \tag{4}$$

where σ is the collision cross section and p the gas pressure. V_R can be expressed in terms of i_-, by use of Eq. (3). For the apparatus used, R is 3.9 mm and ρ is estimated to be 0.5 mm. Equation (3) reduces to:

$$V_R = \{7.8\times 10^4 i_-\}/V_0^{\frac{1}{2}} = \lambda i_-. \tag{5}$$

Equation (4) then becomes:

$$n_+ = i_- \sigma p \int_{e\lambda i_-}^{\infty} f(E)dE. \tag{6}$$

Let δ be the ratio of n_+ to i_-.

$$\delta = \sigma p \int_{e\lambda i_-}^{\infty} f(E)dE. \tag{7}$$

Differentiating δ with respect to i_-, one obtains:

$$d\delta/di_- = -e\sigma\lambda p f(E), \tag{8}$$

where E is the energy corresponding to the potential difference $V_R = \lambda i_-$.

The energy distribution of the ions is found from the experimental curves for a particular value of V_0 by first dividing each ion current value by the corresponding electron current. This ratio (δ) is plotted as a function of the electron current and the slope measured for various values of the electron current. The slope is plotted against λi_-, where λ is evaluated for the value of V_0 involved. This analysis has been carried through for the fast protons for several values of V_0. Figure 12 shows the resulting energy distribution curves, with the computed points indicated. The ordinates of these curves have been corrected for the change in cross section with V_0. These computations have been carried through only for rather small values of V_0, since the location of the maximum of the energy distribution requires that the ion current *vs.* electron current curves be measured well beyond the maxima. The method is not very accurate for finding the shape of the energy

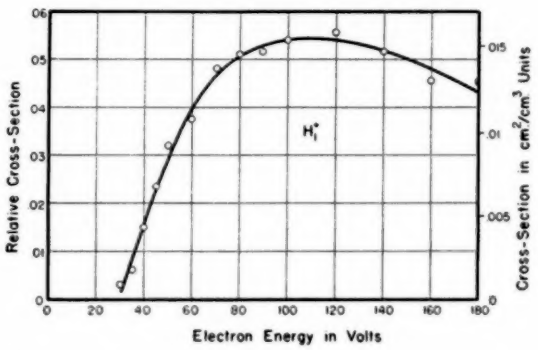

FIG. 11. Collision cross section for proton production.

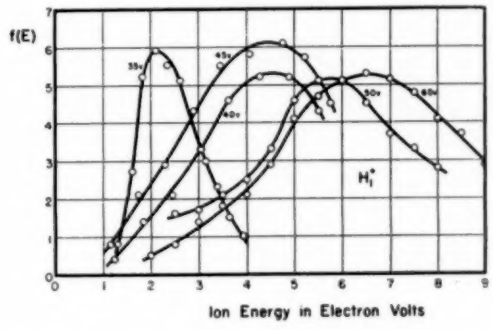

FIG. 12. Energy distributions of protons for various electron energies.

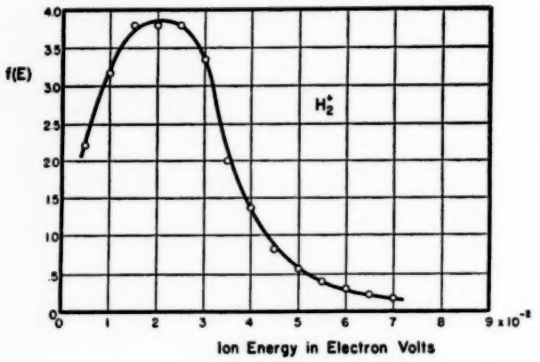

FIG. 13. Energy distribution of molecular ions for 60-volt electrons.

distribution curve, since it requires a measurement of the slope of the δ *vs.* i_- curves. However, the location of the maximum is probably accurate to half an electron volt. Most of the curves give average energies which are quite reasonable in terms of the potential energy curve for the state f (Fig. 1). There seems to be a significant shift of the maximum of the energy distributions toward lower energies, as the value of V_0 is reduced. This is in agreement with the work of Lozier.[19,20] The curve for $V_0=35$ volts is rather surprising as the maximum at about two electron volts is not compatible with the energy level diagram. However, the ion current for this value of V_0 is quite small, so the derived distribution is not reliable.

For comparison, the energy distribution for the molecular ions at $V_0=60$ volts has been computed. The result is shown in Fig. 13. As was mentioned above, the energy distribution should be Maxwellian. The derived distribution drops off a little too rapidly at high energies to be truly Maxwellian. However, the maximum occurs at about 2×10^{-2} electron volt, which is of the order $1/2kT$ for room temperature. It is not expected, however, that the analysis is as accurate for these ions as for the protons, since the molecular ions may have an appreciable fraction of their initial energy in a direction parallel to the electron beam and still be collected.

[19] W. W. Lozier, Phys. Rev. **36**, 1285 (1930).
[20] W. W. Lozier, Phys. Rev. **44**, 575 (1935).

CONCLUSIONS

From the measurements on the atomic ions, it may be concluded that, within the experimental error, there are no slow atomic ions formed by single electron collisions in molecular hydrogen. The slow ions observed by Bleakney may have come from either process (1) or from process (2). The fact that he observed these slow protons even at high electron energies (up to 500 volts), indicates that process (2), which involves ion-molecule collisions, is more likely.

The cross section for the production of protons was found to be about 1/200 that for molecular ions over the electron energy range investigated. This primary process for proton production cannot, therefore, account for the high proton yields obtained in several ion sources.[21–24] Presumably the secondary processes (1) or (2) are responsible for the majority of the protons obtained. In low voltage ion sources in which the walls have been treated to suppress recombination, process (1), involving dissociation and subsequent ionization, may be important.

It has been shown that the method used allows one to compute the energy distribution of the ions formed. It is possible that this method may be of value in analyses of the ions formed by electron collisions in more complex molecules. The thermochemical data relative to the molecules, as obtained from the appearance potentials of the various types of ions, are always in doubt because of the possible energy of formation of the ion measured.

In conclusion, the author wishes to acknowledge his indebtedness to Professor Lloyd P. Smith, both for suggesting this problem and also for many helpful discussions during the course of this research.

[21] E. S. Lamar, W. W. Buechner, and K. T. Compton, Phys. Rev. **51**, 936 (1937).
[22] G. W. Scott, Phys. Rev. **55**, 954 (1939).
[23] A. T. Finkelstein, Rev. Sci. Inst. **11**, 94 (1940).
[24] E. S. Lamar, W. W. Buechner, and R. J. Van de Graaff, J. App. Phys. **12**, 132 (1941).

New Packing Fractions and the Packing Fraction Curve

H. E. DUCKWORTH*
Ryerson Physical Laboratory, University of Chicago, Chicago, Illinois
(Received May 15, 1942)

Descriptions and data are given of a number of mass comparisons (Ti-O, Cu-O, Cu-Ti, Cr-Ag, Mn-Ag, Fe-Ag, Cu-Zn, Cu-Mo, Cu-Pt-Ir, Cu-Au, Zn-Au, Pt-Au). These, together with other recent data, are critically analyzed in order to obtain values for the packing fraction curve. A curve is shown in which packing fractions are plotted against atomic number (instead of mass number), and the rule is suggested that the packing fraction of an element with odd atomic number is algebraically larger than the average of the two adjacent elements with even atomic number. This implies that elements with even atomic number are more stable than odd-numbered elements and, also, supports the theory that protons in the nucleus are associated together in groups of two.

INTRODUCTION

IN 1935 Professor A. J. Dempster described a double-focusing mass spectrograph[1] in which the ion source consisted of a high frequency spark between metallic electrodes.[1,2] With this type of source, in 1938, he was able to measure the packing fractions of many of the heavier elements[3,4] which had hitherto not been analyzed in a mass spectrograph. The data obtained in these investigations filled in many gaps in Aston's packing fraction curve[5] and suggested the general shape of the whole curve.[4] In 1939, Graves[6] used the same apparatus to examine the mass defects of an additional group of elements. The writer has also employed Dempster's mass spectrograph in further measurements of packing fractions among the heavier isotopes.

EXPERIMENTAL DETAILS

I. The Ion Source

It was discovered by Dempster[1,2] and further demonstrated by Sheng-Lin Ch'u[7] that a high frequency spark between metal electrodes is an abundant source of singly- and multiply-charged ions. It is thus a simple matter to obtain positive ions of any metal provided a rod composed of the desired metallic element is used as one of the electrodes. It will also frequently happen that a non-metallic ion can be obtained from an electrode in which it is present as an impurity. For example, a certain sample of electrolytic calcium has been found to provide a satisfactory source of chlorine. In dealing with other non-metallic elements, the oxide of the desired element has been packed with a suitable reducing agent in a small nickel tube which serves as the electrode. There is also ample evidence that gases present in the spark chamber are ionized by the spark and contribute positive ions to the total ion beam.[3,7] For many elements it has been found that a rod of the pure element is not as satisfactory for electrodes as is an alloy. The noble metals, gold and silver, produce a steady spark with little sputtering and by heating with an oxygen flame can be persuaded to "dissolve" suitable amounts of the desired element. If moderate quantities of another metal are added to gold the alloy spark apparently retains the desirable features of the gold spark.

The electrodes were adjusted by means of sylphons and were arranged so that four different combinations of electrodes could be employed without opening the vacuum system. Since it only took a couple of minutes to adjust the electrodes so that the spark occurred between a different pair, the ion intensity from two alloys containing differing amounts of the desired element could be compared under identical pressure and field conditions.

The ion after emission in the spark passed

* University of Chicago Fellow, 1941–42. On leave of absence from United College, Winnipeg, Manitoba, Canada.

[1] A. J. Dempster, Proc. Am. Phil. Soc. **75**, 762 (1935).
[2] A. J. Dempster, Rev. Sci. Inst. **7**, 46 (1936).
[3] A. J. Dempster, Phys. Rev. **53**, 64 (1938).
[4] A. J. Dempster, Phys. Rev. **53**, 869 (1938).
[5] F. W. Aston, *Mass Spectra and Isotopes* (Longmans, Green and Co., 1933), p. 167.
[6] Alvin C. Graves, Phys. Rev. **55**, 863 (1939).
[7] Sheng-Lin Ch'u, Phys. Rev. **50**, 212 (1936).

through a small aperture in a diaphragm which was at high positive potential. It was then accelerated for a distance of about 3 mm before entering the collimating slit system.

II. The Mass Spectrograph

A complete description of the mass spectrograph has been given by Dempster.[1, 8] In the present investigation the ion beam was collimated by two slits of width 0.14 mm and 0.04 mm, the first being approximately 6 mm from the ion source and the second 20 mm behind the first. After a deflection of 90° in an electrostatic field between quadrant condenser plates, the collimated beam enters a magnetic field where it is bent through 180° and the ions possessing the same values of e/m are brought to a focus. This focusing for a small range of e/m permits mass comparisons of ions whose values of e/m are nearly the same. In some experiments a slit of 1.8 mm was inserted between the electrostatic and magnetic fields in order to select a fairly narrow energy range; in other trials the deflecting field was reduced until most of the ions struck the deflecting condenser plate and only those with least energy passed along the quadrant path. This had the same effect as inserting a slit and worked very well.

III. Current and Voltage Sources

The source of high frequency current needed for the ion source was a simple oscillator with frequency of about 10^6 oscillations per second. The intensity of the spark was controlled by varying the current in the primary side of the transformer. The accelerating potential of 4000–6000 volts was obtained from a transformer and rectified by a kenotron and condenser. The electrostatic deflecting potential of 600–800 volts was supplied by comparatively new B-batteries. The magnetic field of 4000–9000 oersteds required a current of 2–8 amperes which was obtained from lead storage cells.

IV. Sharpness of Lines

Since the accuracy of the measurements depends directly upon the sharpness and symmetry of the mass spectrum lines, it is pertinent to mention the various factors which determine these qualities. Most obvious of these factors is the stability of the electrostatic and magnetic fields. Since the B-batteries were in good condition and the charged plate was connected to one side of a 2-microfarad condenser, the other side being grounded as was the uncharged plate, the electrostatic field due to the batteries was probably quite steady. On the other hand the magnetic current slowly dropped, thereby setting a premium on short exposures. For this reason the magnetic field was generally set at a near-saturation value so that a slight decrement in the field current would produce no appreciable change in the field strength. In order to permit short exposures, as required by the decreasing magnetic field, a fairly large spark current was employed and consequently a strong ion beam obtained. When this beam entered the space between the condenser plates it probably distorted the field somewhat, the distortion depending upon the number of ions constituting the beam. Since the spark current is not altogether steady there is a continual variation in the intensity of the ion beam and hence a continual changing of the distorted electrostatic field. From the point of view of constant electrostatic field, then, the ion current should be kept low, while from magnetic field considerations the ion current should be large: clearly a compromise was necessary. Furthermore, under the impact of positive rays, the deflecting plates may become coated with non-conducting layers and local surface charges collect,[3, 9] while dust particles lodged on the plates may likewise create local field distortions.[3]

Another important factor is the type of plates used for photographing the lines. During the early part of the investigation Eastman I. O. U. V. Sens. plates were used and some of the measurements were made from these. Later, an order from Adam Hilger, Ltd., London, England, for Schumann plates was unexpectedly filled and they were thereafter used exclusively for final measurements. They are undoubtedly finer-grained than the Eastman plates and considerably more sensitive, enabling shorter exposures to be made.

[8] A. J. Dempster, Phys. Rev. **51**, 67 (1937).

[9] R. Lariviere Stewart, Phys. Rev. **45**, 488–90 (1934).

The pressure conditions necessary for satisfactory photographs are happily, not too exacting. As previously reported by Dempster,[3] a pressure of 2×10^{-5} mm of mercury has usually been sufficient to obtain good lines.

The lines were measured with a Gaertner comparator whose accuracy had been checked.[6] The scale on the instrument measured directly to thousandths of a millimeter and could be estimated to ten-thousandths. Since the average result of five measurements of a line was used in the calculations, and settings could generally be reproduced to within 0.001 mm, errors introduced in the measuring process can be considered negligible as compared to other experimental errors.

THEORY OF CALCULATIONS

Dempster has shown[3] that the following relations exist. The position of the mass spectrum line on the photographic plate is given by $M^{\frac{1}{2}}=a+cx$, where M is the mass of the ion divided by the number of charges it carries, x is the distance on the plate measured from some fiducial point, while a and c are constants. In practice the constant c is obtained by using two of the heavier isotopes as a mass scale and assuming that their difference is an integral number of mass units. If one knows the dispersion constant c, other isotopes having approximately the same values of e/m can be compared with the two standards. Thus if M_1 and M_2, isotopes two units apart, be used as the mass scale, an unknown mass M, appearing on the mass spectrum somewhere between M_1 and M_2 or even a short distance outside this space, may be compared with the standards by the relation—

$$\Delta f=\frac{[(I_1)^{\frac{1}{2}}+a]^2-I}{I},$$

where

$$a=\frac{x-x_1}{x_2-x_1}[(I_2)^{\frac{1}{2}}-(I_1)^{\frac{1}{2}}]=\frac{x-x_1}{x_2-x_1}[(I_1+2)^{\frac{1}{2}}-(I_1)^{\frac{1}{2}}],$$

I, I_1, and I_2 being the integers corresponding to M, M_1, and M_2, and Δf being the difference between the packing fraction of M and a suitable average of M_1 and M_2. For example, $\Delta f=f-\frac{1}{2}(f_1+f_2)$, $f-\frac{1}{3}(f_1+2f_2)$, or $f-\frac{1}{4}(f_1+3f_2)$ depending upon whether the unknown line M is one-half, two-thirds, or three-quarters of the distance from M_1 to M_2.

As Dempster has pointed out,[3] the error in the value of f introduced by assuming integral spacing of the heavier isotopes will be much less than 0.1×10^{-4} unless there is a considerable departure from the integral spacing assumption. Since the two isotopes constituting the mass scale will generally be isotopes of the same element it is probable that the mass scale error will be well within the experimental error. Some values of the departure from integral spacing necessary to produce an error of 0.1×10^{-4} in the packing fraction will be given.

DESCRIPTION OF COMPARISONS

Titanium-Oxygen

With two titanium electrodes and also with one titanium and one copper electrode, doublets of O^{16} and triply-charged Ti^{48} were obtained with exposure times of 40–120 seconds. A much shorter exposure time would have been sufficient had it not been necessary to use Ti^{47} and Ti^{49} as the mass scale: Ti^{47}, the more abundant of the pair, is about one-tenth as abundant as Ti^{48}. Altogether thirteen photographs of the doublet were obtained and from this number five were selected as being superior to the remainder. Measurement of these five gave an average value for the packing fraction of Ti^{48} of -7.60 ± 0.07,[10] corresponding to mass 47.9635 ± 0.0004. The average value of the thirteen doublets was -7.71 ± 0.15, in good agreement with the value obtained from the best five. From these same plates it was possible to measure the difference between the packing fraction of oxygen and the average packing fraction of Ti^{47} and Ti^{49}. The five best photographs gave for this pair a value of $\bar{f}=-7.37\pm0.15$.

These results agree well with those obtained last year by T. Okuda and K. Ogata[11] who obtained a discharge through titantetrabromide and measured the weights of the five titanium isotopes with a Bainbridge-Jordan type mass spectrograph. They report packing fractions

[10] Throughout the paper the factor $\times10^{-4}$ will be understood and not written.

[11] T. Okuda and K. Ogata, Phys. Rev. **60**, 690 (1941).

of $Ti^{46} = -7.36 \pm 0.21$, $Ti^{47} = -7.50 \pm 0.20$, $Ti^{48} = -7.64 \pm 0.10$, $Ti^{49} = -7.19 \pm 0.11$, and $Ti^{50} = -7.54 \pm 0.08$, from which we can calculate $\bar{f}$ of Ti^{47} and Ti^{49} as -7.34 ± 0.16.

The assumption that Ti^{47} and Ti^{49} are two mass units apart is here clearly justified: it would require a departure of 0.025 mass unit from this supposition to introduce an error of 0.1×10^{-4} in the packing fraction while the divergence from integral spacing is only 0.004 mass unit between Ti^{46} and Ti^{50}!

Copper-Oxygen

This is a very important comparison because copper serves as one of the links between the standard O^{16} and the heavier isotopes. Two copper rods were used as electrodes and photographs obtained in which quadruply-charged copper ions at mass 15.75 and 16.25 bracketed the singly-charged O^{16} atom. For other photographs a copper electrode was used with a titanium electrode. Exposure times varied from 90–240 seconds for the sixteen measurable plates which were obtained. Unfortunately all these photographs were second-rate—either the copper lines were too faint or the oxygen line was over-exposed. Taking the mean of these sixteen we get the average packing fraction of Cu^{63} and Cu^{65} to be $\bar{f} = -7.67 \pm 0.35$: individual values ranged from a high of -6.68 to a low of -8.87. The only previous measurement of copper was made by Dempster,[3] who found $\bar{f} = -6.9 \pm 0.2$ for three photographs.

Unless a very high vacuum is obtained the oxygen line will probably always be more intense than the quadruply-charged copper lines. It is possible that a suitable source of molecular oxygen ions may be found, in which case doubly-charged copper ions can be employed with shorter exposure time. A calcium electrode which had been exposed to air for three weeks, thereby accumulating a layer of CaO on its surface, has proved to be a promising source of molecular oxygen and may make this comparison possible.

Copper-Titanium

With copper and titanium electrodes a comparison was sought between triply-charged titanium ions and quadruply-charged copper ions, the titanium ions appearing at mass 15.67, 16.00, 16.33 and the copper at 15.75 and 16.25. However, the titanium vaporized so rapidly that it soon coated the copper and the spark yielded only titanium ions. In spite of the faintness of the copper ions, the best photograph was measured and it gave $\bar{f}$ of $Ti^{47} - Ti^{48}$ greater than the packing fraction of Cu^{63} by 0.4 and $\bar{f}$ of $Ti^{48} - Ti^{49}$ greater than the packing fraction of Cu^{65} by 0.9. The amounts of these differences are not very significant but it is important to note that according to these results copper lies lower on the packing curve than does titanium. More will be said about this later.

Chromium-Silver

With one electrode of nichrome and the other of silver, with exposures of one hundred seconds, doubly-charged silver ions at mass 53.5 and 54.5 were compared with singly-charged chromium ions at 53 and 54. Here it was possible both to use the chromium isotopes as the mass scale and to regard the silver isotopes as the unknowns, and to employ the separation between the silver lines as the mass scale and calculate the chromium values. From seven photographs, selected from a total of fourteen, the packing fraction of Ag^{107} was calculated to be 2.35 ± 0.10 greater than $\bar{f}$ of $Cr^{53} - Cr^{54}$, and $\bar{f}$ of $Ag^{107} - Ag^{109}$ greater than f of Cr^{54} by 2.38 ± 0.05. Using Dempster's[3] value for silver, $\bar{f} = -4.95 \pm 0.5$, we calculate the packing fraction of Cr^{54} to be -7.33 ± 0.55. Since nichrome contains 20 percent iron and 15 percent chromium, it might be suspected that the line at mass 54 is due to both Cr^{54} and Fe^{54}. However, the faintness of the iron isotope at mass 56, which is fourteen times as abundant as Fe^{54}, indicated that the effect of this latter isotope could be disregarded.

Iron-Silver

With exposures ranging from twenty to one hundred seconds, a spark between one electrode of shim steel and the other of silver yielded satisfactory doubly-charged silver lines at mass 53.5 and 54.5, bracketing an iron isotope at mass 54. Out of 22 photographs the nine best were selected for measurement, giving $\bar{f}$ of

$Ag^{107}-Ag^{109}$ greater than the packing fraction of Fe^{54} by 2.42 ± 0.05. With Dempster's value for silver we find the packing fraction of Fe^{54} is -7.37 ± 0.55. This comparison has been previously made by Dempster[3] who obtained -7.5 ± 0.8 for two photographs.

Manganese-Silver

In the chromium-silver comparison, on a number of plates, the manganese line at mass 55 was sharp enough to measure with respect to the doubly-charged silver lines. Five photographs were measured and an average packing fraction difference of 2.03 ± 0.10 found. Combining this with Dempster's $\bar{f}$ of silver, one finds the packing fraction of Mn^{55} to be -6.98 ± 0.60.

Copper-Zinc

It will be recalled that copper has two isotopes, of mass number 63 and 65, which alternate with two of the more abundant zinc isotopes at 64 and 66. Since both these metals vaporize rapidly, especially the zinc, the ion emission is unsteady and diffuse lines result if the pure metals are used as electrodes. It was found expedient to make alloys of gold, copper, and zinc which were predominantly gold and hence possessed those merits of gold electrodes which have been previously mentioned. With exposures of twenty to fifty seconds, sometimes between two such alloys electrodes and other times between one alloy and platinum, several photographs were secured in which Zn^{64} could be measured in terms of $\bar{f}$ of $Cu^{63}-Cu^{65}$, and Cu^{65} could be measured in terms of $\bar{f}$ of $Zn^{64}-Zn^{66}$. As a rule the copper lines were over-exposed, particularly the more abundant Cu^{63}. Consequently, only one photograph of the $Cu^{63}-Zn^{64}-Cu^{65}$ group was used while four measurements were made of the $Zn^{64}-Cu^{65}-Zn^{66}$ comparison. In the first case the packing fraction of Zn^{64} was 1.01 ± 0.4 smaller than $\bar{f}$ of $Cu^{63}-Cu^{65}$, and in the second case f of Cu^{65} was 1.20 ± 0.15 greater than $\bar{f}$ of $Zn^{64}-Zn^{66}$.

Copper-Molybdenum

An unsuccessful attempt was made to compare singly-charged silicon ions with triply-charged zirconium by using silicon metal in a nickel tube as one electrode and a mixture of zirconium oxide and calcium in a nickel tube as the other. With exposures of two to four minutes, however, triply-charged molybdenum ions appeared at mass 30.67, 31.33, 31.67, 32.0, 32.33, 32.67, and 33.33, and doubly-charged copper ions of similar intensity at mass 31.5 and 32.5. It is probable that the molybdenum was present as an impurity in the zirconium oxide and the copper was an impurity in the nickel tube. Since zirconium and molybdenum both possess isotopes with mass number 92, 94, and 96, the lines corresponding to those mass numbers were attributed to both elements and were not used for measurement. With three photographs Cu^{63} was compared to $\bar{f}$ of $Mo^{95}-Mo^{97}$ and on four photographs Cu^{63} was measured in relation to $Mo^{95}-Mo^{98}$. The first set of measurements gave the packing fraction of Cu^{63} as 2.14 ± 0.4 less than $\bar{f}$ of $Mo^{95}-Mo^{97}$, and the second set indicated f of Cu^{63} was 2.31 ± 0.4 less than $\bar{f}$ of $Mo^{95}-Mo^{98}$. These $\bar{f}$'s of molybdenum are clearly not arithmetic means but possess similar values since the divergence from integral spacing is almost certainly small.

Copper-Platinum-Iridium

Platinum electrodes were made by tightly rolling platinum foil and fitting the roll into a nickel tube of small diameter. When two such tubes were used as electrodes, with exposures of forty to ninety seconds, sharp lines were obtained of singly-charged copper and triply-charged platinum and iridium. As can be seen in Plate I of Fig. 1, the more abundant platinum isotopes were more intense than the mass scale copper lines, while the less abundant platinum and the two iridium isotopes were approximately equal in intensity to the copper. The doublet at mass 65 due to Cu^{65} and Pt^{195} was clearly resolved and easily measured. From twelve photographs the packing fraction of Pt^{195} was calculated to be 10.74 ± 0.20 greater than $\bar{f}$ of copper. Other measurements from these plates were: Ir^{191}—$\Delta f=10.55\pm0.05$ (14 photographs), Ir^{193}—$\Delta f=10.58\pm0.05$ (14 photographs), Pt^{192}—$\Delta f=10.53\pm0.15$ (6 photographs), Pt^{194}—$\Delta f=10.49\pm0.15$ (12 photographs), and Pt^{196}—$\Delta f=10.80\pm0.15$ (8 photographs).

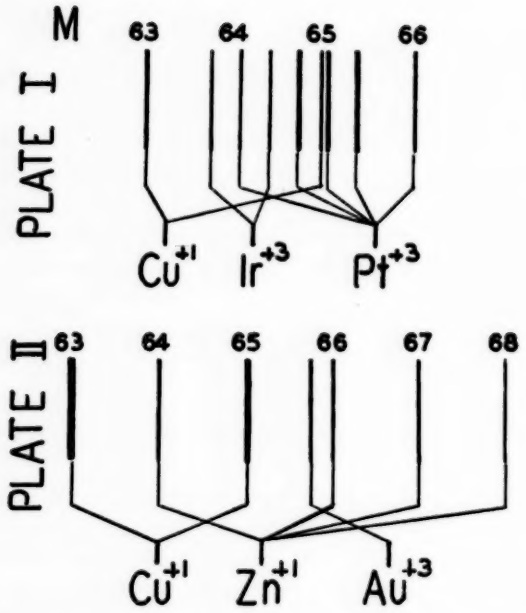

FIG. 1. Plate I shows a typical photograph of the Cu-Pt-Ir comparison. Plate II is a sample plate of the Zn-Au comparison: the two copper lines are present but are too broad to measure.

The previous value of Δf for $Cu^{65}-Pt^{195}$, published by Dempster[3] in 1938, was 8.93 ± 0.1. In his photographs the copper lines are much heavier than the Pt^{195}, the opposite of the situation existing in this comparison. Perhaps an error in measurement, introduced by the extra intensity of the Pt^{195} line, was responsible for the Δf of the $Cu^{65}-Pt^{195}$ comparison being larger than the Δf between copper and the average of the remaining platinum isotopes. Since poor copper lines could invalidate all the measurements, it is important to observe in Plate I that they are perhaps the sharpest of the group.

In order to check these values, Cu^{63} and Cu^{65} were measured individually, by using the separation between Ir^{191} and Ir^{193} as the mass scale. Eight measurements showed f of Cu^{63} to be 10.49 ± 0.1 lower than $\bar{f}$ of $Ir^{191}-Ir^{193}$, and f of Cu^{65} 10.75 ± 0.1 lower than $\bar{f}$ of $Ir^{191}-Ir^{193}$. In addition, Cu^{65} was measured on eight plates, with Pt^{194} and Pt^{196} as the mass scale. It was found that f of Cu^{65} was 10.62 ± 0.1 lower than the average of the packing fractions of those two isotopes. The consistency of these measurements suggested that the copper lines were being accurately located with the measuring instrument, thereby eliminating the most serious possibility of error.

Copper-Gold

Triply-charged gold ions at mass 65.67 appeared with singly-charged copper ions at mass 63 and 65 when the gold-copper-zinc alloy was used with a platinum electrode. Eight photographs, with exposures of forty to sixty seconds, gave f of gold to be 9.82 ± 0.4 greater than $\bar{f}$ of $Cu^{63}-Cu^{65}$. The copper lines were somewhat diffuse and it is for this reason that the probable error has been given a large value.

Zinc-Gold

For this comparison both electrodes were made of the gold-copper-zinc alloy and exposure times ranged from forty to sixty-five seconds. The gold line at 65.67 and the zinc lines at 64, 66, 67, and 68 possessed comparable intensities so that by successively using $Zn^{64}-Zn^{66}$, $Zn^{64}-Zn^{67}$, and $Zn^{64}-Zn^{68}$ as the mass scale it was possible to determine something of the relation between the packing fractions of the zinc isotopes. Eleven good photographs showed the packing fraction of gold was 11.36 ± 0.5 greater than $\bar{f}$ of $Zn^{64}-Zn^{66}$, two photographs gave f of gold 11.50 ± 0.15 greater than $\bar{f}$ of $Zn^{64}-Zn^{67}$, and seven photographs indicated f of gold was 11.34 ± 0.10 greater than $\bar{f}$ of $Zn^{64}-Zn^{68}$. The uniformity of these results is strong evidence that the packing fractions of Zn^{64}, Zn^{66}, Zn^{67}, and Zn^{68} have practically the same values.

Platinum-Gold

In the copper-gold comparison suitable platinum lines appeared on three of the photographs. On these the separation between Pt^{195} and Pt^{196} served as the mass scale and the measurement showed f of gold to be smaller than f of the platinum by 0.23 ± 0.1. This similarity in packing fraction values was to be expected and too much emphasis should not be placed on the small Δf since the results of the copper-platinum comparison assign larger f's to Pt^{195} and Pt^{196} than to the remaining platinum isotopes.

CONCLUSIONS

I. Copper and Zinc Packing Fractions

From Dempster's[3] value for Δf between Au^{197} and $Ti^{49}-Ti^{50}$ of 9.36 ± 0.2, and $\bar{f}$ of $Ti^{49}-Ti^{50}=-7.28\pm0.10$, where Okuda and Ogata's values are averaged in the manner mentioned above, the packing fraction of gold is 2.08 ± 0.30. This value and the packing fraction differences between gold-zinc and zinc-copper enable us to calculate the packing fraction of copper, while the copper-gold comparison gives a second value for copper. A third value for copper can be obtained by employing Graves'[6] values for a gold-molybdenum comparison together with copper-molybdenum values. A fourth value for copper is derived from the less accurate copper-titanium comparison and a fifth is based on the rather unsatisfactory copper-oxygen-copper triplet. The results of these calculations and a mean value for copper based upon them are given in Table I.

The number in brackets following the packing fraction values gives the number of photographs upon which the value is based.

By means of the zinc-gold comparison, the calculated $\bar{f}$ of $Zn^{64}-Zn^{66}=-9.28\pm0.35$. It is surprising to find such a difference between the packing fractions of copper and zinc since they are adjacent in the periodic table and actually overlap each other in their isotopic masses. For this reason it is reassuring to note that the direct copper-zinc comparison yielded a similar result. Using Aston's values for the relative abundance of the zinc isotopes,[12] and assuming that all the zinc isotopes have the same packing fraction of -9.28 ± 0.35, one finds the chemical atomic weight to be 65.36, in reasonable agreement with the value of 65.38 obtained by chemical methods.

II. Discussion of the Packing Fraction Curve

Recent measurements, including those reported in this paper, suggest changes in the packing fraction curve.[3] A critical survey of these measurements will follow.

a. *Titanium*—Previous values of the packing fraction of Ti^{48} were -7.22 ± 0.10 (Dempster[3]), -6.97 ± 0.20 (Aston,[13] recalculated by using $C^{12}=12.003871$[14]), and -7.64 ± 0.10 (Okuda and Ogata[11]). The agreement between the last of these and the present value of -7.60 ± 0.07 is a strong argument for accepting a value of -7.62 ± 0.08. Also, the closeness of the values for $\bar{f}$ of $Ti^{47}-Ti^{49}$, namely, -7.34 ± 0.16 (Okuda and Ogata) and -7.37 ± 0.15 (in this paper), is good justification for adopting the Okuda and Ogata values for the remaining titanium isotopes.

b. *Chromium*—Aston reported a value for the packing fraction of Cr^{52} in 1938[12] of -8.15 ± 0.33 (recalculated by using $C^{12}=12.003871$) which is to be compared with the present value for Cr^{54} of -7.33 ± 0.55. Since this difference is not likely real but due largely to experimental error, a mean value of -7.74 ± 0.45 should be a fair approximation for all chromium isotopes.

c. *Manganese*—The present measurement of the packing fraction of manganese is the only one that has been made.

d. *Iron*—Dempster obtained[3] packing fractions of $Fe^{54}=-7.5\pm0.8$ and $Fe^{56}=-7.0\pm0.4$ while in this paper f of $Fe^{54}=-7.37\pm0.55$. Therefore, for plotting on a packing fraction curve, the iron isotopes may be represented by -7.22 ± 0.3.

e. *Nickel*—The only reported value of a packing fraction for nickel has been given by Aston[13] for $Ni^{58}=-8.35\pm0.35$.

f. *Copper*—The present value of $\bar{f}$ for $Cu^{63}-Cu^{65}$ of -7.92 ± 0.25 is to be preferred to Dempster's previous value[3] of -6.9 ± 0.2 which was based on only two photographs.

g. *Zinc*—Aston has obtained a provisional value for the packing fraction of $Zn^{64}=-9.9\pm3.0$,[12] and Dempster has reported[3] for Zn^{64}

TABLE I.

	f of Cu^{63}	f of Cu^{65}	$\bar{f}$ of Cu
Cu-Zn		-8.07 ± 0.50 (4)	-8.27 ± 0.75 (1)
Cu-Mo	-8.10 ± 0.85 (3) -8.27 ± 0.85 (4)		
Cu-Au			-7.74 ± 0.70 (8)
Cu-O			-7.67 ± 0.35 (16)
Cu-Ti	-7.95 ± 0.55 (1)	-8.30 ± 0.50 (1)	
		Weighted Mean	-7.92 ± 0.25

[12] F. W. Aston, *Mass Spectra and Isotopes* (Longmans, Green, and Co., 1933), p. 120.

[13] F. W. Aston, Nature **141**, 1096 (1938).

[14] K. Ogata, Proc. Phys. Math. Soc. Japan **22**, 486 (1940).

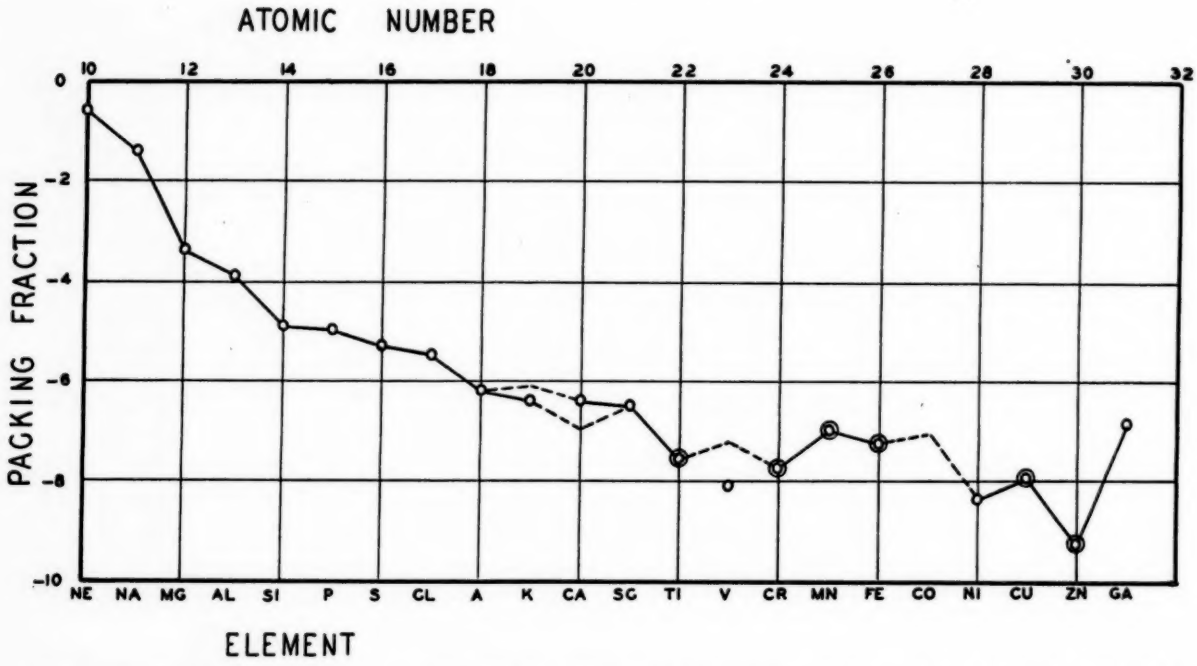

FIG. 2. Curve showing the variation of the packing fraction with increasing atomic number. The values marked by double-circles are reported in this paper, the value for gallium is Dempster's, the value for nickel is Aston's, and the emainder have been obtained from Pollard's list (reference 15).

$f=-6.9\pm0.8$, for Zn^{66} $f=-7.4\pm0.8$, and for $Zn^{68}-Zn^{70}$ $\bar{f}=-6.6\pm0.6$. The present experiments show the packing fractions of all the zinc isotopes (excepting Zn^{70}) to be approximately equal to -9.28 ± 0.35. This value is believed to be fairly reliable.

h. *Gallium*—The only value for gallium has been obtained by Dempster[3] who was able to compare it with palladium and showed that its packing fraction was 1.50 ± 0.20 smaller than that of palladium. This can be used with a palladium-aluminum comparison to calculate the packing fraction of gallium $=-6.85\pm0.9$. Dempster cautions that the palladium-aluminum comparison was not very satisfactory.

When these values, together with values for the lighter elements published by Pollard,[15] were plotted on the usual type of packing fraction curve, it was impossible to draw a reasonable curve which recognized most of the points. To solve this difficulty the packing fraction was plotted against atomic number instead of against mass number. The interesting result is shown in Fig. 2. With two exceptions, plus a possible exception due to the gap at cobalt (atomic number 27), *the packing fraction of an element with odd atomic number is algebraically larger than the average of the two adjacent even-numbered elements.* The two exceptions involve transmutation data which Pollard admits are inaccurate—a slightly smaller packing fraction for calcium and a somewhat larger packing fraction for vanadium would remove these discrepancies. With elements of atomic number less than 10 the adherence to the above rule is very marked and has only been omitted from this graph in order to avoid using too small a scale. Since experimental data above atomic number 32 are incomplete, there has been no attempt to extend this curve to higher elements. However, values for heavier elements published by Aston[13,16] (Br, Kr, Xe), Mattauch[17] (Sr), Dempster[3,4] (Rh, Pd, Ag, etc.), and Graves[6] (Mo, Ru, etc.) seem to follow the same rule although the variations become smaller with increasing atomic number. The fact that the packing fraction of N^{14} is greater than the arithmetic mean of C^{12}

[15] Ernest Pollard, Phys. Rev. **57**, 1186 (1940).

[16] F. W. Aston, Nature **140**, 149 (1937).

[17] J. Mattauch, Naturwiss. **25**, 170 (1937).

and O^{16} has been pointed out by Weizsacker.[18] He suggested in this connection that the packing fraction of an isotope with odd atomic number will be greater than the mean of the neighboring isotopes with the *same* number of neutrons and one proton more or less.

This relation between odd- and even-numbered elements implies that *those with even atomic number are more stable than the odd-numbered elements*. Consequently, elements with an even atomic number should be more abundant in nature—a fact which has long been recognized. In 1917 Harkins[19] pointed out that elements of even atomic number are predominantly abundant both in the earth's crust and in meteors. This rule has been confirmed by x-ray analysis of terrestrial and stellar matter[20,21] and is splendidly illustrated by the relative abundances of the rare earths.[22] A recent estimate states that elements with even atomic number constitute 87 percent of the earth's crust.[23]

Furthermore, since the general form of the packing fraction curve is well-known, it is possible to make a further generalization regarding the relative abundances of the elements. On the whole, elements with algebraically small packing fractions, being very stable, should be more abundant than those with larger packing fractions. This state of affairs is also well-recognized—the elements which comprise most of the earth's crust are those with negative packing fractions, while the very light and the very heavy elements, whose packing fractions are positive, are less abundant.

This rule may be interpreted as confirmation of the theory that protons in the nucleus are associated together in pairs. Starting with an even-numbered element, the addition of one proton produces an odd-numbered element which may or may not be more stable than its predecessor. However, the addition of a second proton results in an even-numbered element and, invariably (excepting the two afore-mentioned cases), in an increase in stability. We might suspect from this that the two protons have united with two neutrons to form the stable He^{++} unit which then forms part of the conveniently pictured "core" of the nucleus.[24] At any rate, whether neutrons are associated with them in the union or not, it appears as if the protons in the nucleus are grouped in pairs, each pair existing in or as a very stable union. In other words, the interaction between two protons in the same or adjacent quantum states adds greatly to the stability.[25] There is also considerable evidence for neutron-neutron interaction in the table of masses of stable nuclei published by Pollard.[15] For example, the packing fractions of Si^{28} (14 neutrons), Si^{29} (15 neutrons), and Si^{30} (16 neutrons) are -4.86, -4.54, -5.79, respectively, and those for S^{32} (16 neutrons), S^{33} (17 neutrons), and S^{34} (18 neutrons) are -5.30, -5.28, and -5.96. In these cases, as well as for the trios $O^{16}-O^{17}-O^{18}$, $Ne^{20}-Ne^{21}-Ne^{22}$, and $Mg^{24}-Mg^{25}-Mg^{26}$, the stability shows a marked increase with the addition of the second neutron. Perhaps neutrons obey a rule similar to the one suggested above for protons.

Using the same ordinates and abscissae as in the shown graph, and extending the range of Z so as to include the elements below $Z=10$, we have drawn two curves, one passing through the points representing the packing fractions of the odd-numbered and the other through the points corresponding to the even-numbered elements. If allowances for the inaccuracy of the data are made, the curves were reasonable, one lying above the other, but it was felt that such curves are of dubious value until the points are located with greater accuracy.

The results of the platinum-gold and copper-platinum-iridium comparisons show that platinum, atomic number 78, has a packing fraction larger than the average of iridium (77) and gold (79). This is in a region where the differences are slight and the apparent contradiction of the

[18] C. F. v. Weizsacker, Zeits. f. Physik **96**, 431 (1935).
[19] W. D. Harkins, J. Am. Chem. Soc. **39**, 856 (1917).
[20] Georg von Hevesy, *Chemical Analysis by X-Rays and Its Application* (McGraw-Hill Book Co., 1932).
[21] V. M. Goldschmidt, *Geochemische Verteilungsgesetze der Elemente*, IX, *Die Mengenverhaltnisse der Elemente und der Atom-Arten* (Oslo, 1939).
[22] V. M. Goldschmidt and L. Thomassen, Videnskaps Skrift. 1, Mat.-Naturv. Kl., No. 5 (1924).
[23] Franco Rasetti, *Elements of Nuclear Physics* (Prentice-Hall, Inc., 1936), p. 160.
[24] W. H. Barkas, Phys. Rev. **55**, 691 (1939).
[25] H. A. Bethe and R. F. Bacher, Rev. Mod. Phys. **8**, 100 ff (1936).

TABLE II. Summary of comparisons.

Mass	Ions	$\Delta f \times 10^4$	Number of Photographs	Assume	Deduce
16	$Ti^{48}-O^{16}$	-7.60 ± 0.07	5	$O^{16}: f=0$	$Ti^{48}: f=-7.60\pm0.07$
16	$Ti^{47}-O^{16}-Ti^{49}$	-7.37 ± 0.15	5	$O^{16}: f=0$	$Ti^{47}-Ti^{49}: \hat{f}=-7.37\pm0.15$
16	$Cu^{63}-O^{16}-Cu^{65}$	-7.67 ± 0.35	16	$O^{16}: f=0$	$Cu^{63}-Cu^{65}: \hat{f}=-7.67\pm0.35$
15.75	$Ti^{47}-Cu^{63}-Ti^{48}$	0.4 ± 0.4	1	$Ti^{47}-Ti^{48}: \hat{f}=-7.55\pm0.15$	$Cu^{63}: f=-7.95\pm0.55$
16.25	$Ti^{48}-Cu^{65}-Ti^{49}$	0.9 ± 0.4	1	$Ti^{48}-Ti^{49}: \hat{f}=-7.40\pm0.10$	$Cu^{65}: f=-8.30\pm0.50$
53.5	$Cr^{53}-Ag^{107}-Cr^{54}$	-2.35 ± 0.10	7		
54	$Ag^{107}-Cr^{54}-Ag^{109}$	2.38 ± 0.05	7	$Ag^{107}-Ag^{109}: \hat{f}=-4.95\pm0.5$	$Cr^{54}: f=-7.33\pm0.55$
54	$Ag^{107}-Fe^{54}-Ag^{109}$	2.42 ± 0.05	9	$Ag^{107}-Ag^{109}: \hat{f}=-4.95\pm0.5$	$Fe^{54}: f=-7.37\pm0.55$
55	$Ag^{107}-Ag^{109}-Mn^{55}$	2.03 ± 0.10	5	$Ag^{107}-Ag^{109}: \hat{f}=-4.95\pm0.5$	$Mn^{55}: f=-6.98\pm0.60$
65.67	$Zn^{64}-Au^{197}-Zn^{66}$	-11.36 ± 0.05	11	$Au^{197}: f=2.08\pm0.3$	$Zn^{64}-Zn^{66}: \hat{f}=-9.28\pm0.35$
65.67	$Zn^{64}-Au^{197}-Zn^{67}$	-11.50 ± 0.15	2		
65.67	$Zn^{64}-Au^{197}-Zn^{68}$	-11.34 ± 0.10	7		
64	$Cu^{63}-Zn^{64}-Cu^{65}$	1.01 ± 0.4	1	$Zn^{64}: f=-9.28\pm0.35$	$Cu^{63}-Cu^{65}: \hat{f}=-8.27\pm0.75$
65	$Zn^{64}-Cu^{65}-Zn^{66}$	-1.20 ± 0.15	4	$Zn^{64}-Zn^{66}: \hat{f}=-9.28\pm0.35$	$Cu^{65}: f=-8.07\pm0.50$
31.5	$Cu^{63}-Mo^{95}-Mo^{97}$	-2.14 ± 0.4	3	$Mo^{95}-Mo^{97}: \hat{f}=-5.96\pm0.45$	$Cu^{63}: f=-8.10\pm0.85$
31.5	$Cu^{63}-Mo^{95}-Mo^{98}$	-2.31 ± 0.4	4	$Mo^{95}-Mo^{98}: \hat{f}=-5.96\pm0.45$	$Cu^{63}: f=-8.27\pm0.85$
63.7	$Cu^{63}-Ir^{191}-Cu^{65}$	-10.55 ± 0.05	14		
64.3	$Cu^{63}-Ir^{193}-Cu^{65}$	-10.58 ± 0.05	14		
64.0	$Cu^{63}-Pt^{192}-Cu^{65}$	-10.53 ± 0.15	6		
64.7	$Cu^{63}-Pt^{194}-Cu^{65}$	-10.49 ± 0.15	12		
65	$Cu^{65}-Pt^{195}$	-10.74 ± 0.20	12		
65.3	$Cu^{63}-Cu^{65}-Pt^{196}$	-10.80 ± 0.15	8		
63	$Cu^{63}-Ir^{191}-Ir^{193}$	-10.49 ± 0.1	8		
65	$Ir^{191}-Ir^{193}-Cu^{65}$	10.75 ± 0.1	8		
65	$Pt^{194}-Cu^{65}-Pt^{196}$	10.62 ± 0.1	8		
65.67	$Cu^{63}-Cu^{65}-Au^{197}$	-9.82 ± 0.4	8	$Au^{197}: f=2.08\pm0.3$	$Cu^{63}-Cu^{65}: \hat{f}=-7.74\pm0.7$
65.67	$Pt^{195}-Pt^{196}-Au^{197}$	0.23 ± 0.10	3	$Au^{197}: f=2.08\pm0.3$	$Pt^{195}-Pt^{196}: \hat{f}=2.31\pm0.40$

rule advanced above may be due to errors. It is believed that the copper-platinum-iridium results are reliable in the main, but the copper-gold plates were not as satisfactory. If the rule is to hold, we must assume that Δf of the copper-gold comparison is too small and that copper possesses an algebraically lower packing fraction than the one which has been assigned (-7.92), possibly about -8.5. On the other hand, an error in Dempster's titanium-gold comparison may have resulted in a packing fraction for gold which is too small. Dempster's plates for this comparison were very good but it should be pointed out that a larger f for Au^{197} would improve the agreement between mass-spectrographic and chemical values for the atomic weight of both gold and zinc (as calculated earlier). The adoption of f of gold $=2.4$, which is the gold packing fraction necessary to bring the zinc values into agreement, would still leave a huge gap of 0.1 mass unit between the gold values.

SUMMARY

In Table II, a summary is given of the comparisons described in this paper. As in the rest of the paper, the factor 10^{-4} must be written with the listed packing fraction values and differences in order to obtain the true packing fractions and differences. The errors are expressed in the form of probable errors.

ACKNOWLEDGMENTS

The author is deeply sensible of the privilege of carrying out this research under the direction of Professor A. J. Dempster. He is grateful not only for permission to use Professor Dempster's mass spectrograph, and for his advice and encouragement so readily given, but also for the opportunity of associating with a man who is at once so excellent a scientist and so considerate a mentor. Appreciation is expressed to Dr. Hans Beutler and Dr. A. E. Shaw for several helpful suggestions, and to the other members of the University of Chicago Physics Department for their interest and help.

The Energy of Gamma-Rays Accompanying the Decay of Be^7

IGNACE ZLOTOWSKI AND JOHN H. WILLIAMS
University of Minnesota, Minneapolis, Minnesota

(Received April 21, 1942)

Coincidence counter measurements have been made on the absorption of secondary electrons produced by the gamma-rays accompanying the decay of Be^7. The gamma-rays from the annihilation of N^{13} positrons were used for calibration of the absorbing system. The maximum ranges in aluminum are respectively 0.86 ± 0.04 mm for the annihilation radiation and 0.77 ± 0.03 mm for that due to Be^7. The energy of the latter was found to be 0.485 ± 0.005 Mev by assuming gamma-rays of 0.510 Mev from N^{13}. The agreement between the experimental result and the low excited level of Li^7 (0.475 Mev) deduced from other reactions confirms the suggestions of previous authors that the observed gamma-rays from Be^7 originate from this excited state of Li^7 which is created by electron capture.

INTRODUCTION

THE 43-day half-life radioactivity observed in lithium targets bombarded with deuterons has been assigned[1] to Be^7 from the reaction $Li^6(d,n)Be^7$. Since no charged particle emission could be detected the radioactivity was explained by the capture of an orbital electron by the nucleus of Be^7 following the equation: $Be^7+e^-\rightarrow Li^7+\eta$, where η denotes the neutrino.[2]

Later Roberts, Heydenburg, and Locher[3] discovered a gamma-ray accompanying the decay of Be^7 and from absorption of this radiation in lead obtained a value of its energy quantum of 0.425 ± 0.025 Mev. A similar result (0.425 ± 0.020 Mev) obtained by using Be^7 from the reaction $B^{10}(p,\alpha)Be^7$ and the cloud-chamber method for determining the secondary electrons spectrum has been reported by Maier-Leibnitz.[4] The observed gamma-rays have been interpreted as an evidence of an excited state in Li^7 produced during the radioactive transmutation of Be^7: $Be^7+e^-\rightarrow Li^{7*}+\eta$ and $Li^{7*}\rightarrow Li^7+(h\nu)_\gamma$.

As a matter of fact there are several indications of the formation of Li^7 in an excited state at 0.4 to 0.5 Mev. The mean energy separation of the two states of Li^7 as measured from the proton groups occurring during the deuteron bombardment of Li^6 was computed to be $0.455+0.015$ Mev.[5] From the apparent absorption coefficient in lead and aluminum of gamma-rays emitted during the bombardment of separated Li^7 target with protons Fowler and Lauritsen[6] found that the excitation energy was equal to 0.495 ± 0.025 Mev. Hudson, Herb, and Plain[7] obtained a value of 0.459 Mev for the energy of these gamma-rays, due to excitation of Li^7 without capture of the incident proton. From the difference between the energy release of the reaction $Be^9(d,\alpha)Li^7$ deduced from the alpha-particle range and that calculated from the most recent mass determination, the higher energy level in Li^7 was computed to be 0.494 ± 0.016 Mev.[8] The excitation energy deduced from the recent range determination of the two groups of alpha-particles from the reaction $B^{10}(n,\alpha)Li^7$ was 0.470 Mev.[9] And finally the Li^7 excited level calculated from the difference between the energy release value of the latter reaction deduced from the alpha-particle range and that deduced from the exact mass values is estimated to be 0.48 Mev.[10]

Within the limits of experimental error the above results are in good agreement with each other, the mean value being equal to 0.475 ± 0.020 Mev. However, there is an evident discrepancy between this result and the above discussed energy of gamma-rays from Be^7. The question

[1] L. H. Rumbaugh, R. B. Roberts, and L. R. Hafstad, Phys. Rev. **54**, 657 (1938).
[2] R. B. Roberts and N. P. Heydenburg, Phys. Rev. **53**, 929 (1938).
[3] R. B. Roberts, N. P. Heydenburg, and G. L. Locher, Phys. Rev. **53**, 1016 (1938).
[4] H. Maier-Leibnitz, Naturwiss. **26**, 614 (1938).
[5] J. H. Williams, W. G. Shepherd, and R. O. Haxby, Phys. Rev. **52**, 390 (1937); L. H. Rumbaugh, R. B. Roberts, and L. R. Hafstad, reference 1.
[6] W. A. Fowler and C. C. Lauritsen, Phys. Rev. **56**, 841 (1939).
[7] C. M. Hudson, R. C. Herb, and G. J. Plain, Phys. Rev. **57**, 587 (1940).
[8] E. R. Graves, Phys. Rev. **57**, 885 (1940).
[9] M. S. Livingston and J. G. Hoffman, Phys. Rev. **53**, 227 (1938).
[10] J. C. Bower, E. Bretcher, and C. W. Gilbert, Proc. Camb. Phil. Soc. **34**, 290 (1938).

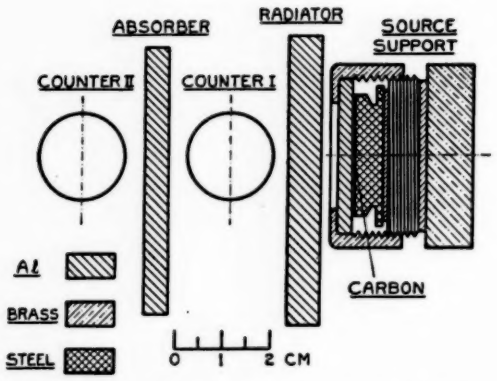

FIG. 1. Counters and source disposition in the absorption experiments.

arises as to whether in both cases one has to do with the same excitation level or with two different energy states if not two different nuclear phenomena.

EXPERIMENTAL METHOD

Since the energy of gamma-rays can be determined with much greater accuracy from the measurement of the range of the recoil electrons projected by incident radiation than from direct measurement of its absorption coefficient, the method used by Rumbaugh, Roberts, and Hafstad, we determined the energy of the Be^7 gamma-rays by measuring the maximum range of Compton electrons in aluminum placed between two Geiger-Müller counters in a coincidence circuit.[11]

We have investigated the gamma-rays from a thick target of LiOH which was previously bombarded with 15 μa-hours of 2.7-Mev deuterons accelerated by the Minnesota pressure Van de Graaff generator.[12]

We used two glass G-M counters filled with a mixture of argon ($p=10$ cm of Hg) and ethyl alcohol ($p=1$ cm of Hg). They were 1.8 cm in diameter and 10 cm long. A thin platinum layer evaporated on the inside of the glass tubes served as the cathode. The effective thin portions of the glass envelopes were 0.12 to 0.16 mm thick. The thickness of the aluminum plate used as a source of secondary electrons was 7 mm. The arrangement of target, secondary radiator, absorbers, and counters was similar to that shown for the case of a N^{13} source in Fig. 1.

The Neher-Harper method of quenching the discharges was used. The pulses from the amplifier were recorded through a scale-of-eight circuit. The threshold for both counters was the same (910±15 volts) and the length of the flat portions of their characteristics about 125 volts. The small regular increase in the single counting rate with counter overvoltage within the flat portion limits never exceeded 0.2 percent per volt. Our coincidence circuit had a resolving time of $3.6\pm0.5\times10^{-6}$ sec. The experimental results collected in Table I show that it was practically independent of the single counting rates in the counters. The gamma-rays from a well-shielded radium source were used in order to get the number of chance coincidences (C_t-C_c) as a function of the single counting rates (s_{I} and s_{II}). Sufficient precautions were taken with regard to the geometry of the system to exclude the possibility of an error due to the presence of some genuine coincidences. The errors in the table represent the root-mean-square values.

The gamma-rays from the annihilation of N^{13} positrons were first studied to obtain a calibration of our absorbing system in the region of 0.5 Mev. Radioactive nitrogen was prepared by deuteron bombardment of a carbon target prepared by deposition of pure acetylene carbon black onto a sheet of tantalum, a metal giving no products of disintegration with observable gamma-rays. The measurements over an hour gave a value of 10.1±0.2 minutes for the radio-nitrogen half-life, in excellent agreement with some recent evalua-

TABLE I. Counting rates.

Single counts per min. Counter I s_{I}	Single counts per min. Counter II s_{II}	Total coincidence rate per minute C_t	Cosmic-ray coincidences per minute C_c	Resolving time $\tau=\frac{60(C_t-C_c)}{2s_{\mathrm{I}}s_{\mathrm{II}}}$ sec.
2760	2810	1.07±0.06	0.09	$3.8\pm0.3\times10^{-6}$
2690	2740	0.99±0.08	0.08	$3.7\pm0.4\times10^{-6}$
1920	2045	0.53±0.04	0.06	$3.6\pm0.4\times10^{-6}$
1309	1428	0.26±0.03	0.07	$3.1\pm0.5\times10^{-6}$
1215	1244	0.24±0.03	0.07	$3.6\pm0.4\times10^{-6}$
1120	1272	0.25±0.04	0.06	$4.1\pm0.8\times10^{-6}$

Mean value $3.6\pm0.5\times10^{-6}$ sec.

[11] For details see: W. Bothe and J. Becker, Zeits. f. Physik **76**, 428 (1932); F. Rasetti, Zeits. f. Physik **97**, 64 (1935); S. C. Curran, P. I. Dee and V. Petržilka, Proc. Roy. Soc. (London) **A169**, 269 (1939).

[12] The experimental arrangement is described in the paper by J. H. Williams, L. H. Rumbaugh, and J. T. Tate, Rev. Sci. Inst. **13**, 202 (1942).

tions.[13] Without attempting to explain why, it is to be noted however that in order to get a regular decay curve it is necessary to heat the carbon target after bombardment for at least three minutes.

Figure 2 shows the absorption curves of the secondary electrons from both kinds of gamma-rays. All data obtained have been corrected for chance coincidences calculated as a function of single counts for each counter and the resolving time of our coincidence circuit. The maximum ranges are, respectively: $(a+0.37\pm0.03)$ millimeters of aluminum for electrons from Be^7 gamma-rays and $(a+0.46\pm0.04)$ millimeters for those from the annihilation radiation. a denotes the absorption power of three counter walls in aluminum equivalent.

CALCULATIONS

For gamma-rays of energy between 0.1 and 30 mc^2, the absorption in aluminum is principally due to the Compton scattering. From the relativistic relation between momentum and energy of an electron projected by a light quantum as a result of a collision, the amount of energy transferred to the electron is given by the formula.

$$E=E_0-E_0\cdot\mu/[\mu+E_0(1-\cos\theta)], \qquad (1)$$

where E_0 is the initial energy of the incident gamma-ray quantum, θ is the angle between the initial and final directions of its momentum and μ denotes as usual the rest energy of an electron.[14] Since the frequency shift of the scattered radiation is maximum for $\theta=180°$, the maximum energy transferred is

$$E_{max}=2E_0^2/2E_0+\mu.$$

In the case of the annihilation radiation $E_0=\mu$, and

$$E_{max}=(\tfrac{2}{3})\mu=0.340 \text{ Mev}.$$

The range-energy relation in aluminum for beta-rays between 0.25 and 0.40 Mev is represented in Fig. 3. The curve shows the values obtained by numerical integration from a graph of the reciprocal of $(-dE/dR)$ plotted against E, the average energy-loss per unit of path being calculated from Bloch's equation.[15]

By use of these data the total range of 0.86 $\pm$0.04 mm of aluminum is obtained for the 0.340 Mev beta-rays. Hence the absorption power a of the three counter walls which each secondary electron is passing through in our coincidence set-up is equivalent to: $0.86-0.46\pm0.04=0.40$ ±0.04 millimeters of aluminum. Since the same counter walls acted as an additional absorber in the case of secondary electrons from the Be^7 gamma-rays, it may be readily calculated that

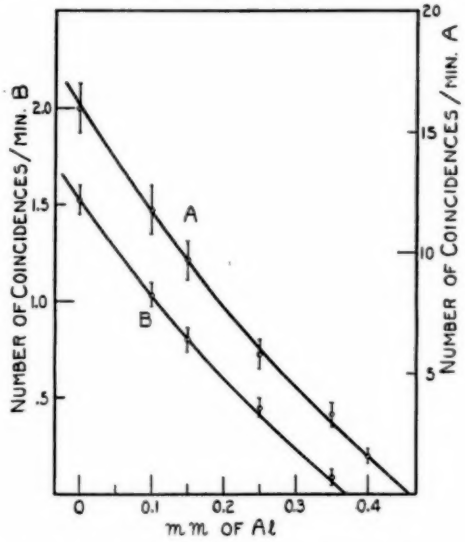

FIG. 2. Absorption curves (in aluminum) of secondary electrons from (A) the N^{13} annihilation radiation and (B) the gamma-rays accompanying the decay of Be^7.

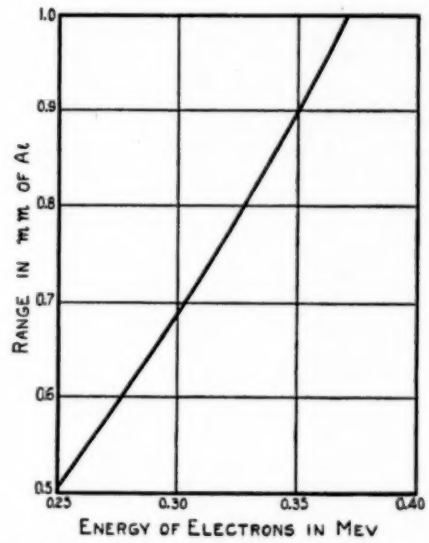

FIG. 3. Range-energy relation in aluminum for low energy electrons.

[13] See: A. G. Ward, Proc. Camb. Phil. Soc. **35**, 523 (1939); G. T. Seaborg, Chem. Rev. **27**, 199 (1940).

[14] W. Heitler, *Quantum Theory of Radiation* (Oxford, 1936), p. 217.

[15] F. Bloch. Zeits. f. Physik **81**, 363 (1933); E. E. Widdowson, Proc. Phys. Soc. (London) **50**, 185 (1938).

the total range of these electrons was equal to $0.40+0.37\pm0.03=0.77\pm0.03$ mm of Al. Their maximum energy computed from the energy-range graph should be 0.320 ± 0.005 Mev. By substituting this value into formula (1) it follows immediately that the initial energy of the gamma-rays accompanying the radioactive decay of Be^7 is 0.485 ± 0.005 Mev.

CONCLUSIONS

It should be mentioned that the presence of 0.28 Mev gamma-rays of N^{13}, reported by several authors,[16] could not affect our calculations based upon the maximum range of secondary electrons from radio-nitrogen gamma-radiation. On the other hand it is apparent from the experimental absorption curve for these electrons that there is a very little if any amount of incident gamma-rays with energy above 0.510 Mev.

Owing to the large value of the slope of the energy-range curve for soft beta-rays the accuracy of our range determination permits us to evaluate the corresponding energies and therefore the energies of the incident gamma-rays within 1 percent. The reasonably close agreement between our experimental result and the mean value of the low excited level of Li^7 deduced from other reactions provides considerable support for the original suggestion to associate the Be^7 gamma-rays with the energy separation of the two states of Li^7 built up by electron capture from the parent body.

ACKNOWLEDGMENTS

The senior author wishes to thank the Rockefeller Foundation for financial support during the course of these investigations. We are very much indebted to Mr. R. G. Nuckolls for the construction and maintenance of the coincidence circuit used in these experiments.

[16] J. R. Richardson, Phys. Rev. **55**, 609 (1939); E. M. Lyman, Phys. Rev. **55**, 1123 (1939).

JULY 1 AND 15, 1942 PHYSICAL REVIEW VOLUME 62

Density of Sodium Chloride

The Atomic Weight of Fluorine by Combination of Crystal Density and X-Ray Data

HERRICK L. JOHNSTON AND DWIGHT A. HUTCHISON
Department of Chemistry, The Ohio State University, Columbus, Ohio

(Received January 5, 1942)

The densities of carefully purified crystals of sodium chloride have been determined by the method of "crystal flotation" in pure ethylene dibromide. The results yield

$$d_{27.634°C}=2.16165\pm0.00002 \text{ g/ml},$$

which reduces to

$$d_{20°}=2.16366\pm0.00003 \text{ g/ml}.$$

It is found that six successive precipitations of NaCl in the manner employed by Richards and Wells in their determination of the atomic weights of sodium and of chlorine are required to effect purification to constant density (± about 4×10^{-6} g/ml), and also that exposure to air produces surface contamination sufficient to cause erratic changes in apparent density that may amount to as much as 5×10^{-4} g/ml within a few minutes. Combination of our value for d_{NaCl} with that of C. A. Hutchison and H. L. Johnston for d_{LiF} and with Straumanis, Ievins, and Karlsons' value for the lattice constant of LiF relative to the Siegbahn value for NaCl yields 0.443640 ± 0.000025 for the ratio of the molecular weights of LiF and NaCl, respectively. With the adoption of 22.997 (International Atomic Weight Committee) for the atomic weight of sodium, this ratio yields 18.994 ± 0.001 for the atomic weight of F. With the adoption of 22.994 (Birge) for sodium, the F atomic weight comes out 18.992. Either of these figures is in reasonable agreement with the value 22.995 ± 0.002, based on densities and lattice constants of fluorite and calcite, and with the gas density determinations for compounds of F, but are somewhat lower than the mass spectrograph value of 18.999 ± 0.001 for F^{19}. It appears that the determination of relative molecular weights by combination of x-ray and density data are as reliable, in favorable cases, as by other standard atomic weight methods. In calcite, fluorite, and rock salt crystals, used to obtain the data underlying these computations, there is no evidence of any appreciable influence of "crystal mosaic" patterns which Zwicky thought might influence crystal densities by as much as 1 percent.

THE most accurate determinations of the density of sodium chloride, reported in the literature, appear to be those of Defoe and Compton[1] and of Tu,[2] made for the purpose of

[1] O. K. Defoe and A. H. Compton, Phys. Rev. **25**, 618 (1925).
[2] Y. Tu, Phys. Rev. **40**, 662 (1932).

determining standards of x-ray wave-length. Defoe and Compton obtained the value

$$d_{20°} = 2.1632 \pm 0.0004 \text{ g/cm}^3,$$

while Tu obtained the value 2.16418 ± 0.00014 at 18°C. The latter reduces to

$$d_{20°} = 2.16365 \pm 0.00014 \text{ g/cm}^3,$$

when correction is made for the coefficient of thermal expansion of NaCl.[3] Both Defoe and Compton and Tu used natural crystals of rocksalt. Neither made a chemical analysis of the mineral. Defoe and Compton observed differences between different rocksalt crystals that exceeded the error of their density measurements. These differences might be accounted for by traces of chemical impurity or, as we find, by density errors that result from exposure to air.

A recent paper from this laboratory[4] dealt with the accurate determination of the density of chemically pure lithium fluoride, by the method of crystal flotation. We have completed a similar investigation with very carefully purified crystals of sodium chloride. Reduced to 20°C, we obtain the value

$$d_{20°} = 2.16366 \pm 0.00003 \text{ g/ml}$$
$$= 2.16360 \pm 0.00003 \text{ g/cm}^3$$

in good agreement with the value reported by Tu,[2] but with reduced limits of error.

EXPERIMENTAL DESCRIPTION

I. Preparation of Chemically Pure NaCl

Our method of preparing chemically pure NaCl was similar to that employed by Richards and Wells,[5] in their determination of the atomic weights of sodium and of chlorine.

Pure H_2SO_4 was prepared by distillation of Graselli C.P. reagent H_2SO_4 with a distilling flask and condenser made from pure fused quartz. Two successive distillations were carried out and the middle third of the distillate saved from each distillation.

Pure hydrochloric acid was prepared in a similar manner by double distillation of Graselli C.P. reagent hydrochloric acid, to which a few small crystals of C.P. $KMnO_4$ had been added.

Pure NaCl (preliminary) was precipitated from a saturated aqueous solution of Baker and Adamson's reagent quality NaCl mixed with pure hydrochloric acid (as prepared above) by the addition of HCl gas. The HCl gas for this precipitation was prepared by dropping pure H_2SO_4 (as prepared above) into an aqueous mixture of pure hydrochloric acid (cf. above) and Graselli reagent quality NaCl.

Pure HCl gas, used in subsequent steps in the purification, was prepared by dropping pure H_2SO_4 (cf. above) into an aqueous mixture of pure hydrochloric acid (cf. above) and pure NaCl (preliminary). The evolving gas was passed through two bead towers containing glass beads covered with pure H_2SO_4 (cf. above) and a final drying tube containing Coleman and Bell C.P. P_2O_5. The latter substance had been sublimed into the drying tube.

All aqueous solutions, in the above preparation of reagents, were made up with double distilled water (distilled from a tin still).

The purification of NaCl was continued by dissolving the preliminary preparation of pure NaCl (cf. above) in double-distilled water to which pure hydrochloric acid (cf. above) was added and precipitating with pure HCl gas (cf. above). The precipitated NaCl was centrifuged to remove adhering solution. This treatment was repeated with the precipitate until, in all, six successive precipitations had been made. Sensitive determinations of density revealed that the NaCl produced by this procedure showed small changes in density through five recrystallizations but that NaCl from the sixth, seventh, and eighth crystallizations was of constant density (cf. Table III, *seq.*).

Following the six successive precipitations by HCl gas and the subsequent centrifugations, the purified NaCl was fused in a platinum crucible to expel HCl.

Finally, the solidified melt was dissolved in warm triple-distilled water in a silver dish and given two recrystallizations from pure water.

---

[3] $\alpha_l = 40.5 \times 10^{-6}$, Straumanis, Ievins, and Karlsons, Zeits. f. anorg. allgem. Chemie **238**, 175 (1938). Cf. also Eucken and Dannohl.

[4] Clyde A. Hutchison and Herrick L. Johnston, J. Am. Chem. Soc. **62**, 3165 (1940).

[5] T. W. Richards and R. C. Wells, "A revision of the atomic weights of sodium and chlorine," Carnegie Institution of Washington, Publication No. 28 (1905).

TABLE I. Density of ethylene dibromide as a function of the temperature. 28.00°C = 3.843° Beckmann.

Temperature (Beckmann scale)	Densities (g/ml) d_T	$d_{3.477°B}$
0.000	2.16879	2.16158
1.000	2.16673	2.16160
2.000	2.16474	2.16168
2.500	2.16370	2.16167
3.000	2.16265	2.16166
3.500	2.16158	2.16163
4.000	2.16053	2.16162
5.000	2.15843	2.16159

II. The Density Determination

(a) *Calibration of the Flotation Medium*

The density was determined by floating fragments of pure single crystals in a calibrated flotation medium of pure ethylene dibromide. Details of the procedure have been described elsewhere.[6]

The ethylene dibromide used for this purpose was prepared from Merck's reagent quality $C_2H_4Br_2$ (boiling point range 129°–132°C), first dried over C.P. $CaCl_2$, by distillation in vacuum. The middle third of the distillate was retained. As shown best by the constancy of the temperature of crystal flotation the isothermal density of the purified ethylene bromide did not change by more than experimental limits of error ($\pm 4\times10^{-6}$ g/ml) during the several days that measurements were in progress.

The density of the ethylene bromide, as a function of the temperature, was determined by weighing an approximate 9-ml Pyrex sinker immersed in the ethylene bromide. To compensate for possible small effects of surface tension on the 0.004″ suspension wire an auxiliary sinker, of lead, was attached to the lower end of the wire suspension and weighings were taken on: (1) the wire suspension with attached auxiliary sinker immersed in the liquid and (2) the complete suspension assembly, with both the 9-ml sinker and the auxiliary sinker immersed in the liquid.[7]

The exact volume of the 9-ml sinker was 9.10542±0.00002 ml at 27.145°C. This is the average of ten independent determinations, each consisting of four weighings: (1) suspension +auxiliary sinker in air; (2) suspension+auxiliary and 9-ml sinkers in air; (3) suspension +auxiliary sinker in triple-distilled water at 27.145°; (4) suspension+auxiliary and 9-ml sinkers in triple-distilled water at 27.145°. The density of pure water at 27.145°C was taken to be 0.996502 g/ml.[8] The average deviation from the mean, among the ten determinations of volume, was ±0.00007 ml and the extreme deviation +0.00014 ml. All weighings were corrected to vacuum.

Densities of ethylene dibromide, determined at eight temperatures covering a range of five degrees, are given in the second column of Table I. For convenience, densities were determined at temperatures which corresponded to even divisions of the Beckmann thermometer used with the crystal flotations. The scale of this thermometer was quite uniform, as shown by calibration by the U. S. Bureau of Standards. To convert to degrees Centigrade, the Beckmann was compared with a standard mercury in glass thermometer, with a temperature range 27° to 32°C and graduated at intervals of 0.02°, which was calibrated by the U. S. Bureau of Standards shortly after use. The comparison gave

28.00°C = 3.843° Beckmann.

(b) *Preparation of Flotation Crystals*

Fragments of single crystals for the flotations were prepared from the purified NaCl (cf. I above) by the method developed by Kyropolous,[9] in the same manner as described previously.[4] It was found necessary to use an annealing period of four hours at a temperature 50° below the melting point of NaCl, and to allow at least four hours for the crystals to cool. It was also found that the densities of the crystals changed erratically when they were exposed to the atmosphere for several minutes. To avoid this erratic behavior it was found necessary to store them over P_2O_5, under vacuum.[10] When

[6] H. L. Johnston and C. A. Hutchison, J. Chem. Phys. **8**, 869 (1940).

[7] This is the procedure followed by Osborne, McKelvey, and Bearce, Bull. U. S. Bur. Stand. Reprint No. 197 (1912).

[8] *International Critical Tables* (McGraw-Hill Book Company, 1928), Vol. 3, p. 25.

[9] S. Kyropolous, Zeits. f. anorg. Chemie **154**, 308 (1926).

[10] These observations apply to the crystals at room temperature. Exposure to air during the high temperature annealing had no apparent effect on the density. In the subsequent cooling, which was carried out in the annealing furnace, P_2O_5 was introduced into the furnace, around the platinum crucible that contained the crystals, at about

immersed in the purified $C_2H_4Br_2$, so that they were not exposed directly to the atmosphere, the crystals maintained constant density.

Tables II and III illustrate these observations. Table II is a record of crystal flotations made with crystals that were grown from Baker and Adamson's reagent quality NaCl, without further purification. Table III is a record of crystal flotations with crystals that were grown from purified NaCl (cf. Section I) with varying numbers of HCl precipitations.

It is at once apparent that even C.P. NaCl experiences some manner of surface contamination when exposed to the atmosphere. It is noteworthy that the magnitude of density variations among exposed C.P. crystals is comparable to the density differences among natural crystals reported by Defoe and Compton.[1]

III. The Absolute Density

The average flotation temperature of the last eight crystals recorded in Table III is 3.477° Beckmann with an average deviation from the mean of $\pm 0.002°$—equivalent to $\pm 3.6\times10^{-6}$ g/ml in the density of NaCl (cf. infra).

A large scale plot of the experimental densities of ethylene dibromide (column 2 of Table I) against the temperatures gives a near linear relationship. The best straight line through the data has a slope of $-2.074\pm0.01\times10^{-3}$ g/ml/degree. Making use of this value for the temperature coefficient of density we have corrected each of the entries in column 2 of Table I to the common temperature 3.477° Beckmann. These corrected values are entered in column 3 Table I. The small systematic trend of the values recorded in this column is evidence of a slight curvature in the density temperature plot. By plotting the entries in column 3 against temperature and drawing in a smooth curve we obtain 2.16165 g/ml as the best value for the density of our purified ethylene dibromide at T Beckmann = 3.477°. We regard this as reliable to within about ± 0.00002 g/ml. Comparison of

TABLE II. A record of crystal flotations with crystals that were grown from Baker and Adamson's reagent quality NaCl (unpurified).

Explanation: Crystals designated as 1*a*, 1*b*, and 1*c* were three fragments from a crystal that was annealed for only two hours and that was stored with exposure to the atmosphere. Crystals designated as 2*a*, 2*b*, 2*c*, and 2*d* were annealed for only two hours but were stored over P_2O_5 under vacuum. Crystals designated as 3*a*, 3*b*, and 3*c* were annealed at a temperature 50° below the melting point for four hours and were stored over P_2O_5 under vacuum.

Crystal designation	Flotation temperatures (° Beckmann) Newly prepared	After 2 days	After 4 days	After 5 days	cf. Footnote[a]
1*a*	3.682	3.670			
1*b*	3.249	3.320			
1*c*	3.506	3.517			
2*a*	3.427		3.431		
2*b*	3.399		3.396		
2*c*	3.437		3.446		
2*d*	3.510		3.483		
3*a*	3.422			3.424	3.544
3*b*	3.497			3.495	3.458
3*c*	3.477			3.478	3.479

[a] After the five-day flotations made with crystals 3*a*, 3*b*, and 3*c*, crystals 3*a* and 3*b* were exposed to the atmosphere for twenty minutes and flotation temperatures redetermined. 3*c* was not exposed to the atmosphere. The entries in this column are the values obtained in the redetermination.

150°C. At 70°C the crystals were removed from the furnace and placed in the desiccator, which was immediately evacuated. Similar precautions were taken with the original melts prior to annealing. Crystals which had been once altered by exposure to air, at room temperature, were not restored to their original densities by a second annealing.

TABLE III. Crystal flotations made with crystals that were grown from purified Baker and Adamson reagent quality NaCl, in accordance with the purification scheme outlined in Section I.

Explanation: The crystals that are designated as 4*a*, 4*b*, 4*c*, and 4*d* were grown from purified NaCl that was given 4 precipitations with HCl gas, followed by fusion in platinum and 2 recrystallizations from triple-distilled water. Those designated as 6*a*, 6*b*, 6*c*, and 6*d* were given 6 precipitations with HCl gas, followed by fusion in platinum and 2 recrystallizations from triple-distilled water. Those designated as 8*a*, 8*b*, 8*c*, and 8*d* were given 8 precipitations with HCl gas, followed by fusion in platinum and 2 recrystallizations from triple-distilled water. All crystals were given a four-hour annealing at a temperature 50° below their melting point and were stored over P_2O_5 under vacuum.

Crystal designation	Flotation temperatures (° Beckmann)
4*a*	3.469
4*b*	3.456
4*c*	3.471
4*d*	3.461
6*a*	3.477
6*b*	3.472
6*c*	3.476
6*d*	3.476
8*a*	3.476
8*b*	3.477
8*c*	3.482
8*d*	3.477

Four crystal fragments were selected from the cooled melt of each preparation, and were annealed and floated. The table is therefore a record of *all* crystals that were floated from these three melts. With NaCl we did not experience the situation reported for LiF (reference 6): namely, that about one-half of the crystal fragments floated at diverse high temperatures, apparently due to internal cracks.

the Beckmann with the standard thermometer calibrated by the U. S. Bureau of Standards, at 28.00°C, yields 27.634°C for 3.477° Beckmann.

We can thus write for the absolute density of NaCl

$$d_{27.634°C} = 2.16165 \pm 0.00002 \text{ g/ml.}$$

Corrected to 20°C by use of the thermal coefficient of expansion for NaCl, this yields

$$d_{20°C} = 2.16366 \pm 0.00003 \text{ g/ml.}$$
$$= 2.16360 \pm 0.00003 \text{ g/cm}^3.$$

IV. Atomic Weight of Fluorine, Lattice Constant of Lithium Fluoride, Structure Constants of Calcite

In an earlier paper by C. A. Hutchison and one of us[11] we made use of the densities of LiF and of calcite, in conjunction with x-ray data to compute a value for the atomic weight of fluorine. The result obtained was 18.994 ± 0.002, based on 100.085 for the molecular weight of calcite. Corrected to the latest values[12] for M_{CaCO_3} this becomes

$$18.995 \pm 0.002,$$

a figure which is a little below the mass spectrograph value of 18.999 ± 0.001[13] but in excellent agreement with gas density determinations. This suggests the possible existence of a trace of some lighter isotope.

We can make a similar calculation from the densities of LiF and NaCl in conjunction with the ratio of their lattice constants and the molecular weight of NaCl. With true a_{LiF} taken to be 2.00904 ± 0.00002A[14] at 25°C; true a_{NaCl} at 25° set equal to 2.815058A;[15] and with 2.63899 ± 0.0001 and 2.16228 ± 0.00002 taken for the densities of LiF[4] and of NaCl, respectively, the *ratio* of the molecular weights of LiF and of NaCl comes out

$$0.443640 \pm 0.000025.$$

With the atomic weight of lithium taken as 6.9390 ± 0.0002[16] and those of Na and Cl as correct at 22.997[12b] and 35.457,[12b] respectively, the atomic weight of F comes out

$$18.994 \pm 0.001.$$

With Birge's[12b] adoption for the atomic weight of sodium, namely 22.994 ± 0.003, the F value comes out

$$18.992 \pm 0.002.$$

It is apparent that the agreement of the atomic weight values for fluorine from calcite and rock-salt data, respectively, in conjunction with the x-ray and density data for fluorite, is as close as is permitted by the small uncertainties that exist in the atomic weights of Ca and of Na, respectively. It is also apparent that the comparison of molecular weights by combination of accurate x-ray and density data is as reliable as by other standard methods of atomic weight determination. In particular, it is apparent that there is no serious influence of "crystal mosaic" patterns such as postulated by Zwicky,[17] who thought that densities computed from crystal lattice constants might be in error by as much as 1 percent in some cases.

Avogadro's number is not used in this computation of relative molecular weights from x-ray and density data.

---

[11] C. A. Hutchison and H. L. Johnston, J. Am. Chem. Soc. **63**, 1580 (1941).

[12] (a) 100.09. "Eleventh annual report on atomic weights of the International Union of Chemistry," J. Am. Chem. Soc. **63**, 845 (1941). (b) 100.091 ± 0.005, R. T. Birge, Rev. Mod. Phys. **13**, 233 (1941).

[13] A. K. Brewer, Phys. Rev. **49**, 867 (1936).

[14] Straumanis, Ievins, and Karlsons, Zeits. f. physik. Chemie **B42**, 143 (1939). This value is based on the Siegbahn scale (*effective* $a_{calcite}$ in the first order = 3.02904A at 18°C) through close agreement of the wave-length assumed for copper $K_{\alpha 1}$ (1.537395A) with that determined by J. A. Bearden and C. A. Shaw [Phys. Rev. **48**, 18 (1935)] through measurements on calcite (1.537400A) in which they assumed Siegbahn's value for the lattice constant.

[15] Based on the effective first order a calcite = 3.02904A at 18° with Siegbahn's experimental determination of the ratio of the *effective* grating spaces as 0.929007 and corrected for refraction (± 0.000260A) and for thermal expansion (reference 3) to 25°.

[16] T. W. Richards and H. H. Willard, J. Am. Chem. Soc. **32**, 4 (1910); Zeits. f. anorg. allgem. Chem. **66**, 237 (1910); Carnegie Inst. Publication No. 25, 1 (1910).

[17] F. Zwicky, Proc. Nat. Acad. Sci. **16**, 211 (1930).

On the Inelastic Scattering of Neutrons by Crystal Lattices

R. J. SEEGER AND E. TELLER*
The George Washington University, Washington, D. C.
(Received March 4, 1942)

Previous theoretical results on the inelastic scattering of neutrons in ideal crystals are reviewed. Restrictive conditions imposed by crystal interference on inelastic scattering are discussed. It is found that if the velocity of the incident neutrons is smaller than the sound velocity in the crystal, neutrons from a monochromatic, well-defined beam are scattered by inelastic processes into sharply limited areas. On the other hand, inelastic scattering of faster neutrons should give rise to diffuse spots similar to those observed in inelastic scattering of x-rays.

OWING to the comparatively great mass of neutrons the theory of inelastic scattering of neutrons by crystal lattices differs from the corresponding theories for electrons and for x-rays. Theoretical treatment[1] of the scattering of neutrons in crystals has led to two simple results. First, elastic collisions are predominant if the neutron energy is less than ME_0^2/E_v (M = mass number of an appropriate atom in the crystal, $E_v \equiv$ vibrational energy of such an atom in the crystal; the latter quantity becomes equal to kT at high temperatures and to the zero-point energy E_0 at low temperatures). Second, the total scattering probability of neutrons having sufficiently low energies becomes zero if the temperature of the crystal is equal to 0°K. While the absence of elastic scattering processes at sufficiently low neutron energies follows from the impossibility of fulfillment of the Bragg interference conditions, the disappearance of the inelastic scattering processes is owing to the relatively great value of the mass of the neutron.

The purpose of the present note is a discussion of the restrictions on inelastic scattering processes imposed by the crystal interference conditions. We shall see that these restrictions not only lead at low neutron energies to the disappearance of the scattering probabilities, but continue to operate at somewhat higher neutron energies. Actually they influence the inelastic scattering processes whenever the velocity of the neutron is not great as compared to the sound velocity in the crystal.

The following considerations will be restricted to crystals in which the neutrons are scattered in the same way by each lattice cell. This condition is fulfilled if no atomic species occurring in the crystal is a mixture of isotopes and if all nuclear spins are equal to zero.

We shall consider only such inelastic processes in which one quantum of a lattice vibration is emitted or absorbed. These processes are more probable than processes involving emission or absorption of several quanta if $a_m|\Delta k|$ is small compared to one.[2] Here a is the mean vibrational amplitude of an atom in the crystal. Different atomic species possess different a values and a_m is the greatest of these values. The quantity $|\Delta k|$ is the amount by which the neutron's wave number k has changed during the collision. The inequality $a_m|\Delta k| \ll 1$ is the general condition for processes involving a greater number of vibrational quanta to be progressively less probable. The condition is the same for neutrons, electrons, and x-rays. If one considers scattering through all possible angles the average value of $|\Delta k|$ will be equal to the initial wave number k. The above condition may then be replaced by $a_m k \ll 1$. If one now averages over the orientations of the crystal one may compare the average number of elastic collisions, which occur with high probability in the neighborhood of certain orientations, with the number of inelastic collisions, which occur with small probability, but in many cases for all orientations. It is then found that the average number of elastic collisions is great compared to the average number of inelastic collisions if $a_m k \ll 1$. This condition is valid as long as the crystals are small enough so that the dynamical

* Temporarily at Columbia University, New York.
[1] G. C. Wick, Physik. Zeits. **38**, 403 (1937); I. Pomerantschuk, Physik. Zeits. d. Sowjetunion **13**, 65 (1938).
[2] See Pomerantschuk, reference 1.

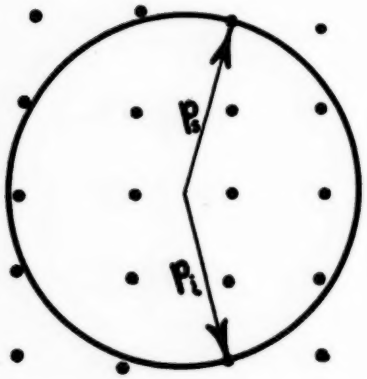

FIG. 1. Momentum of incident and scattered quantum.

theory of crystal interference need not be applied. For neutrons the condition $a_m k \ll 1$ may be transformed into $E_n E_v \ll M E_0^2$, where E_n is the energy of the incident neutron and M is the mass number of that atomic species which vibrates with the greatest amplitude. Thus we see that in the energy region where processes involving one lattice quantum are more probable than processes involving several quanta the elastic processes are, in turn, even more probable than the one-quantum processes.

We shall now review the theory of inelastic scattering processes involving one quantum of a lattice vibration for electrons and for x-rays. This theory is in its essential parts similar to the theory of neutron-scattering, but the relatively small velocity of the neutrons makes the latter theory somewhat more complicated. The influence of lattice vibrations on x-ray scattering has been discussed recently by Zachariasen[3] whose treatment we shall summarize below.

The Bragg interference conditions for an elastic scattering process can be stated simply with the help of the reciprocal lattice. This is a lattice in momentum space; the vectors connecting any two of its points are the momentum changes which an incident particle (photon, electron, or neutron) can suffer during an elastic scattering process. The vector p_i in Fig. 1 shows the momentum of an incident x-ray quantum. We construct the reciprocal lattice in such a way that one lattice point coincides with the end point of the vector p_i. Those lattice points which lie in the plane of the drawing are shown in Fig. 1.

After an elastic scattering the momentum of the scattered photon may be represented by a vector which connects the origin of p_i with a point on the surface of the sphere of radius $|p_i|$ drawn around the origin of p_i as center. The circle in Fig. 1 shows the intersection of this sphere with the plane of the drawing. If this sphere passes through a lattice point of the reciprocal lattice which is different from the end point of p_i, then the interference conditions are fulfilled and elastic scattering takes place. In Fig. 1 the vector p_s shows the momentum of a scattered x-ray quantum.

If the sphere mentioned above does not pass through any lattice point different from the end point of p_i, no elastic scattering occurs. Inelastic scattering, however, is still possible. In this case the interference conditions require that the momentum represented by the vector p_L in Fig. 2 shall be given to a lattice vibration. This may happen either by the emission of a vibrational quantum carrying the momentum p_L or by the absorption of a quantum with momentum $-p_L$. The vector p_L is constructed by connecting the end point of p_s with the closest point of the reciprocal lattice. (The momentum of a lattice vibration is defined as its wave number vector k_L multiplied by Planck's constant h.)

The intensity of the inelastic scattering[3] is proportional to the square of the amplitude of

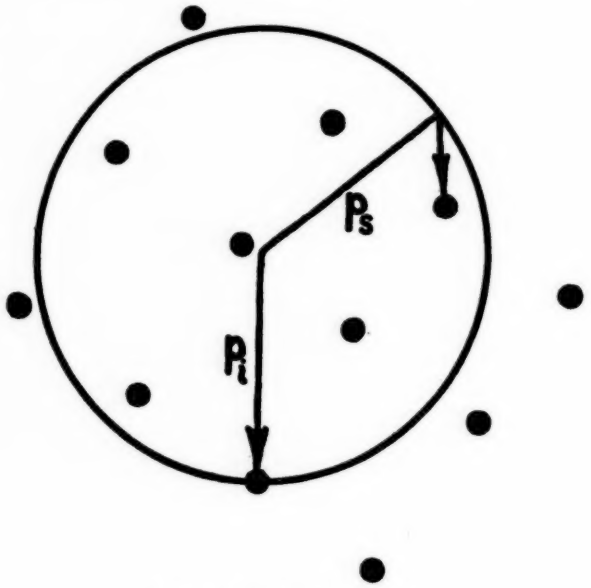

FIG. 2. Inelastic scattering.

[3] W. H. Zachariasen, Phys. Rev. **57**, 597 (1940).

the lattice vibration which has been emitted or absorbed during the process. In thermal equilibrium the amplitude of the vibrations increases with decreasing frequency. Thus the most probable inelastic scattering processes will be those in which a vibration of small frequency, and therefore of small wave number, participates.[4] Returning to the notation of Fig. 2 one may say that the intensity of inelastic scattering is greatest if p_L is as small as possible, or in other words if the Bragg condition is as nearly fulfilled as possible. This explains[3] the diffuse spots observed by Preston[5] around Laue spots and also in other positions in which the Bragg conditions are nearly fulfilled.

In using Fig. 2 it was tacitly assumed that the magnitudes of the momenta $|p_i|$ and $|p_s|$ are equal; or in other words the energy change of the x-ray during the inelastic scattering process has been neglected. This is permissible for x-ray quanta and also for electrons because in all cases of practical interest the energy of these particles is great compared to any vibrational quantum of the lattice. For neutrons, however, the change in energy must be taken into account.

We shall restrict this discussion to the inelastic processes of highest intensity, i.e., to those processes in which vibrations of small frequency participate. Then the change in the neutron energy ΔE_n remains relatively small and is given by

$$\Delta E_n = v_n \Delta p_s,$$

where v_n is the velocity of the incident neutron and Δp_s, defined by the relation $|p_s| \pm \Delta p_s = |p_i|$, is the distance between the end point of p_s and the sphere of radius $|p_i|$ around the origin of p_i. On the other hand ΔE_n must be equal to the quantum of lattice vibration

$$\Delta E_n = h\nu = hk_L v_L = p_L v_L,$$

where v_L is the sound velocity in the lattice. Since we consider vibrations of small frequencies and long wave-lengths sound dispersion need not be taken into account. But even so v_L will depend on the state of polarization of the lattice vibration and also on the orientation of the vector p_L.

[4] We consider only the acoustical branch.
[5] G. D. Preston, Proc. Roy. Soc. **A172**, 116 (1939).

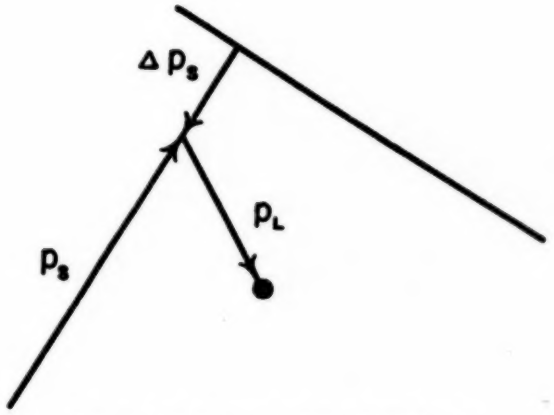

FIG. 3. Inelastic scattering, enlarged scale.

From the two above equations we find

$$\Delta p_s / p_L = v_L / v_n. \qquad \text{(A)}$$

To represent the relevant momentum vectors for inelastic neutron-scattering we show in Fig. 3 the region around the end point of p_s on an enlarged scale. Because of the change in scale the circle appearing in Fig. 1 and Fig. 2 may now be replaced by a straight line. Only one point of the reciprocal lattice is shown in Fig. 3. This point is supposed to be very close to the circle which appears in the figure as a straight line. The vector p_s coincides in direction with one of the radii of the "circle" and is, therefore, drawn at right angles to the straight line. In the particular case shown in Fig. 3, p_s ends inside the circle. Thus $|p_s| < |p_i|$ which means that E_n is diminished and emission of a sound wave has taken place. Processes in which a vibrational quantum is absorbed are represented by vector diagrams in which the end point of p_s lies outside the circle.

In order to obtain a crude picture of the possible inelastic processes we shall assume the sound velocity v_L to be a constant. Then for a definite velocity v_n of the incident neutrons the lengths of the vectors Δp_s and p_L have, according to (A), a constant ratio. Approximating the sphere around the origin at p_i by a plane, one finds that the end points of the vector p_s lie on a surface of the second order. If $|\Delta p_s| / p_L = v_L / v_n < 1$ this surface is a rotational hyperboloid. Its two sheets lie on opposite sides of the plane which we have substituted for the sphere, and the two sheets correspond to processes involving absorption and emission of vibrational quanta. (See

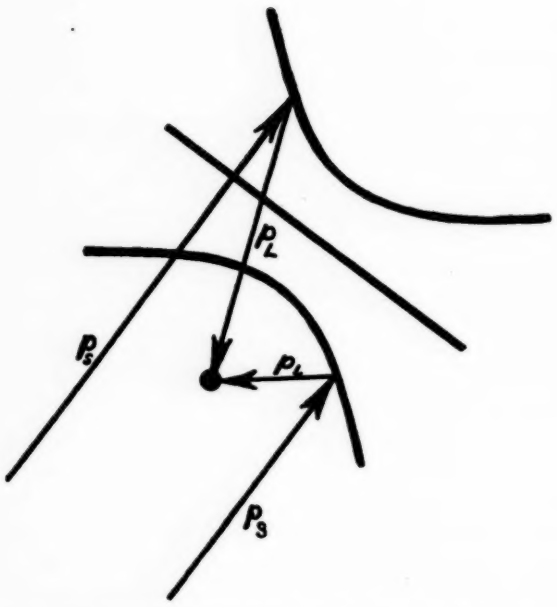

FIG. 4. Absorption and emission of vibrational quanta.

Fig. 4.) For similar reasons as mentioned above in connection with x-ray scattering those processes will be most probable in which the Bragg conditions for elastic scattering are most nearly satisfied. Thus we shall expect greatest intensity for inelastic scattering processes in the neighborhood of the sharp maxima corresponding to elastic scattering. With increasing v_n values the two sheets of the hyperbola mentioned above approach the plane (or sphere) defined by the relation $|p_s| = |p_i|$. In this limiting case the theory of inelastic neutron scattering becomes identical with the corresponding theory for x-rays or electrons. If, on the other hand, $\Delta p_s/p_L = v_L/v_n > 1$ the end points of the possible p_s vectors lie on a rotational ellipsoid surrounding the point of the reciprocal lattice. This whole surface will lie on one side of the sphere around the origin of p_i. The ellipsoid will lie completely inside the sphere if the same is true of the reciprocal lattice point, and completely outside the sphere if the reciprocal lattice point lies outside. In the former case only such inelastic processes occur in which a quantum is emitted, in the latter case only absorption is to be expected. In addition the finite extension of the ellipsoid limits the possible angular deviations of the inelastically scattered neutrons from the directions in which elastic scattering may occur. If, therefore, the incident momentum p_i is given, the inelastically scattered neutrons will be scattered into sharply delimited areas. The intensity per unit solid angle will actually become infinite at the rim of these areas. This is owing to the fact that near the rim an extended part of the surface of the ellipsoid corresponds to p_s vectors whose direction varies but very little. The integrated intensity over the whole spot remains, of course, finite. Figure 5 shows the end points of possible p_s vectors for the case $(v_L/v_n) > 1$.

If $v_L/v_n > 1$ and if at the same time p_i is small enough, it may happen that no points of the reciprocal lattice lie inside the sphere of radius $|p_i|$. Then according to our above argument only such inelastic processes are permitted in which a vibrational quantum is absorbed. If in addition the temperature of the lattice is very low so that no lattice vibrations are available, no inelastic scattering processes may occur. For sufficiently small p_i values the Bragg interference conditions cannot be satisfied so that elastic scattering cannot occur either. One may, therefore, expect that under these conditions neutrons will not be scattered at all. This particular result is essentially the same as that which has been obtained by Wick.[1]

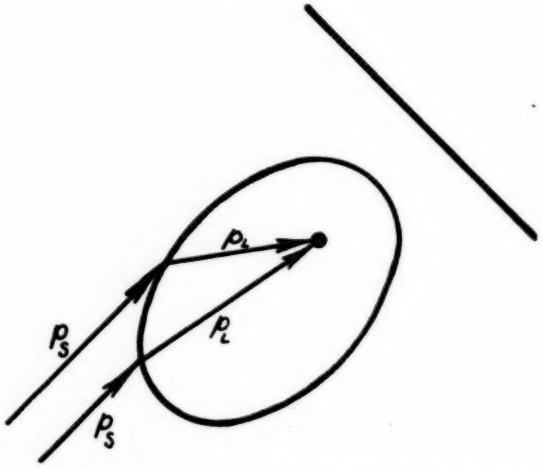

FIG. 5. End points of possible p_s vectors for $(v_L/v_n) > 1$.

Mobilities in Some Free Electron Gases

WILLARD H. BENNETT, *Electronic Research Corporation, Newark, Ohio*

AND

L. H. THOMAS, *Mendenhall Laboratory, Ohio State University, Columbus, Ohio*

(Received February 27, 1942)

Mobility coefficients for free electrons and mobilities of positive ions are reported for hydrogen, deuterium, and some mixtures of hydrogen and nitrogen, and of hydrogen and helium, for field strengths between 1 and 2 volts per cm per mm of mercury gas pressure. The relation between free electron drift velocity and field strength is found to be parabolic in this range for all these gases. Discussion of these observations shows that they can be explained qualitatively if electrons excite rotations of the hydrogen molecules by collision, and the cross sections for this process are estimated. A mathematical appendix states the theoretical results required in the discussion and derives those details not previously obtained.

A. THE EXPERIMENTAL DATA

DURING the past year, measurements of the mobilities of electrons and positive ions in various free electron gases have been made with refinements of the technique reported previously.[1] This technique is applicable where the drift velocity, $\bar{u}$, of electrons (or ions) is related to the field intensity per unit pressure, E/p, by a relation of the form

$$\bar{u}=K(E/p)^n,$$

where n is a constant and K is a generalized mobility coefficient. In these gases the relation has been shown to be $\bar{u}=K(E/p)^{\frac{1}{2}}$ for electrons within the range of field intensities used.

Further measurements have shown that the previous use of wire 0.0075 cm in diameter introduced a small uncertainty in the data for hydrogen which could be reduced by using wire 0.0025 cm in diameter. The finer wire had a tendency to vibrate and break, but it was found that tying the wire around a short segment of cord, near the supports, dampened out the vibrations completely. The finer wire was used in all the measurements being reported here.

Measurements were made in hydrogen, deuterium, mixtures of hydrogen and nitrogen, and mixtures of helium and hydrogen. The deuterium gas behaved similarly to hydrogen in conditioning and appearance of the discharge. Nitrogen containing less than 1 percent hydrogen when the wire is negative produces intensely hot spots on the wire where the discharge is taking place and melts the tungsten wire in two. Helium containing 10 percent hydrogen or less has a much lower electron mobility than hydrogen, and the wire breaks, probably owing to an incipient arc.

Small pieces of rubber or traces of carbon tetrachloride vapor in the tube introduce a gaseous impurity which falsifies the results unpredictably and which is not eliminated by long continued discharge from a point-to-cylinder in a side arm of the tube. Such a discharge was used for cleaning up the gas and was quickly effective if sulphur—and chlorine—containing impurities were avoided.

Table I compares the mobility coefficients for hydrogen and deuterium. Although these values for K are probably not accurate to better than

TABLE I. Mobility in hydrogen and deuterium.

	K[(cm/sec.)/(e.s.u./atmos.)$^{\frac{1}{2}}$]	C[(cm/sec.)/(e.s.u./atmos.)]
H_2	7.8×10^5	3.06×10^3
D_2	7.5×10^5	2.26×10^3

TABLE II. Values of the mobility coefficient K for electrons and the positive ions mobility C for mixtures of gases.

	K[(cm/sec.)/(e.s.u./atmos.)$^{\frac{1}{2}}$]	C[(cm/sec.)/(e.s.u./atmos.)]
100% H_2	7.8×10^5	3.06×10^3
30% H_2+70% N_2	8.7×10^5	1.13×10^3
20% H_2+80% N_2	8.7×10^5	0.99×10^3
10% H_2+90% N_2	7.9×10^5	0.92×10^3
1% H_2+99% N_2	7.5×10^5	0.90×10^3
100% N_2	——	0.78×10^3
30% H_2+70% He	8.7×10^5	3.00×10^3
10% H_2+90% He	($\bar{u}\neq K(E/p)^{\frac{1}{2}}$)	2.77×10^3

[1] W. H. Bennett, Phys. Rev. **58**, 992 (1940).

5 percent, the repeated checks with the same tube make it likely that the relative values are correct to better than 2 percent.

Table II shows the changes in K and C (the positive ion mobility) produced by decreasing the amount of hydrogen in nitrogen and for mixtures of He and H_2. As the concentration of hydrogen in nitrogen is decreased, the value of K increases, then decreases. A similar effect seems to be taking place when helium is introduced in hydrogen.

In these measurements of K, the value of E/p varied between about 1 and 2 volts per cm per mm of mercury pressure at 0°C, so that the consistency of the values of K for each gas or mixture for the various currents[2] shows that the electron drift velocity follows $\bar{u}=K(E/p)^{\frac{1}{2}}$ in that range.

B. DISCUSSION OF THE OBSERVATIONS

1. The Positive Ion Mobilities

The positive ion mobilities may be discussed with the aid of Langevin's formula

$$C=\frac{3}{16Y}\cdot\left\{\frac{1+m/M}{(D-1)d}\right\}^{\frac{1}{2}},$$

where m is the mass of a molecule, M is the mass of an ion, D is the polarizability of the gas, d is the density, and Y is a function of pressure, collision area, and polarizability. Of these, m should equal M for hydrogen and for deuterium, and Y and D should be the same for both. The only difference should appear in the density, d, so the mobilities should be related by

$$C_H=\sqrt{2}\,C_D.$$

The ratio of the mobilities measured is 1.36 instead of the value 1.41 expected.

The positive ion mobility in nitrogen is

$$0.78\times10^3 \text{ (cm/sec.)/(e.s.u./atmos.)}$$

or

$$2.61 \text{ (cm/sec.)/\{(volt/cm)/atmos.\}},$$

which compares favorably with

$$2.67 \text{ (cm/sec.)/\{(volt/cm)/atmos.\}},$$

the value usually cited.[3]

The values of the positive ion mobilities for mixtures of hydrogen and nitrogen are compared in Table III with those calculated from a formula given by Loeb.[4]

$$C=\frac{1}{x_1/C_1+x_2/C_2},$$

where x_1 and x_2 are the respective fractional concentrations of the components whose mobilities are C_1 and C_2. In the second column we calculated with C_2 from 1 percent H_2 in N_2 and in the third column we used C_2 from pure N_2.

Tyndall[5] does not report a mobility for H_2^+ in He but the result for the 10 percent hydrogen in helium mixture can be used to calculate mobility for hydrogen ions in helium. The result is 2.75×10^3 (cm/sec.)/(e.s.u./atmos.).

TABLE III. Calculated and observed values of positive ion mobilities. $C/10^3$[(cm/sec.)/(e.s.u./atmos.)].

	Observed	Calculated H_2^+ in N_2	Calculated N_2^+ in N_2
30% H_2+70% N_2	1.13	1.14	1.00
20% H_2+80% N_2	0.99	1.04	0.93
10% H_2+90% N_2	0.92	0.97	0.84
1% H_2+99% N_2	0.90	—	0.79

2. Electron Drift Velocities

The drift of electrons through gas under an applied field is well understood theoretically from the smallest up to large fields of the order of 1000 volts per cm per mm of mercury pressure at 0°C.[6] Up to such fields the velocity distribution of the electrons remains nearly isotropic, and Lorentz' method of expansion in spherical har-

[2] For test of data see W. H. Bennett, reference 1.

The following relations are used in this paper between units or notations. Mobility:

1 (cm/sec.)/{(volt/cm)/atmos.}
$=300$ (cm/sec.)/(e.s.u. of field/atmos.).

Mobility coefficient ($n=\frac{1}{2}$):

1.59 (cm/sec.)/{(volt/cm)/mm Hg}$^{\frac{1}{2}}$
$=1$ (cm/sec.)/(e.s.u. of field/atmos.)$^{\frac{1}{2}}$.

Cross section:

$$p\alpha=NQ.$$

Drift velocity:

$$(e/m)^{\frac{1}{2}}=4.20\times10^7 \text{ (cm/sec.)/(volt)}^{\frac{1}{2}}.$$

[3] J. H. Mitchell and K. E. W. Ridler, Proc. Roy. Soc. **146**, 911 (1934).

[4] L. B. Loeb, *Fundamental Processes of Electrical Discharge in Gases* (Wiley, 1939), p. 42.

[5] A. M. Tyndall, *The Mobility of Positive Ions in Gases* (Cambridge University Press, 1938).

[6] L. B. Loeb, reference 4, Chapters 4 and 5; S. Chapman and T. E. Cowling, *The Mathematical Theory of Non-Uniform Gases* (Cambridge University Press, 1939), pp. 345 ff. M. J. Druyvesteyn and F. M. Penning, Rev. Mod. Phys. **12**, 90–99 (1940). Many references, especially to the earlier work, will be found in the above.

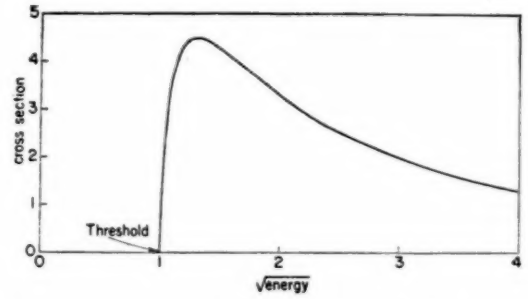

FIG. 1. Cross section for inelastic collision with a dipole (Massey).

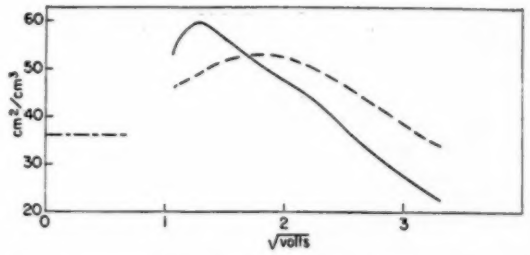

FIG. 2. ——— Value indicated for α assumed constant; ——— Observed values for α (cross section for momentum transfer) (Ramsauer and Kollath); — — — The usual collision cross section (Ramsauer and Kollath).

monics about the direction of the field and drift can be used. The most likely collision process between electrons and gas molecules is elastic scattering, and transfer to the gas molecules of the momentum gained by the electron in the direction of the field between collisions is almost entirely due to this. Owing to the small mass of an electron relative to an ion, however, transfer to the gas molecules by elastic scattering of the energy gained between collisions is slow; as a result the electrons acquire large energy not in general distributed according to Maxwell's law, and the first two equations of the Lorentz expansion must be solved simultaneously to give the velocity dependence of the isotropic part and of the term in "cos θ" in the distribution; further, in the first (energy transfer) equation the effects of inelastic collisions become as important as, or more important than, those of elastic collisions, except for lower fields in monatomic gases when all collisions are elastic.

In the absence of knowledge of the collision cross sections for elastic and inelastic collisions it is not possible to compute the drift velocities when inelastic collisions occur; it may, however, be possible to infer some information about the collision cross sections from the observed drift velocities. The drift velocity observed as a function of field strength is plainly inadequate to give both the cross section for momentum transfer in elastic impact as a function of speed and the cross sections for various losses of energy in inelastic impact. We have, however, knowledge of the former from direct observation of angle scattering[7] for electrons of energy more than 0.6 electron volt; moreover the sideways diffusion observed by Townsend[8] as a function of field strength gives us an independent set of observational data, while the data may be observed as functions of fractional concentration in gas mixtures as well as of the field.

3. Electron Mobility Coefficients

In the range of field strengths of these observations, Townsend's results show that in pure H_2 the average energy of the electrons varies from 0.35 to 0.54 electron volt. This is less than the threshold for excitation of the first vibrational state of H_2 at 0.54 ev. If the variation of drift velocity as the square root of the field strength is produced, as it could be, by collision cross section for momentum transfer α, nearly independent of speed (up to energies of 0.5 ev) and average fractional loss of energy per such collision (by amounts small compared to 0.1 ev) f, also independent of speed, we have[9] (Section C (2.4) below)

$$\bar{\epsilon} = 0.604 \frac{E}{p\alpha} f^{-1}, \tag{3.1}$$

$$\bar{u} = 3.17 \times 10^7 \left(\frac{E}{p\alpha} f \right)^{\frac{1}{2}}, \tag{3.2}$$

where E is field in volts per cm and p is gas pressure in mm Hg at 0°C, α is expressed as an "absorption coefficient" in ($cm^2/\{cm^3 \cdot mm\ Hg\}$), and $\bar{\epsilon}$ and $\bar{u}$ are the mean electron energy in electron volts and drift velocity in cm/sec., respectively. Using $\bar{\epsilon} = 0.35$ ev (from Townsend's

[7] C. Ramsauer and R. Kollath, *Handbuch der Physik*, Vol. 22, Part 2 (1933), p. 243; C. E. Normand, Phys. Rev. **35**, 1217 (1930).

[8] J. S. E. Townsend, J. Frank. Inst. **200**, 563 (1934).

[9] See M. J. Druyvesteyn and F. M. Penning, reference 6, for references.

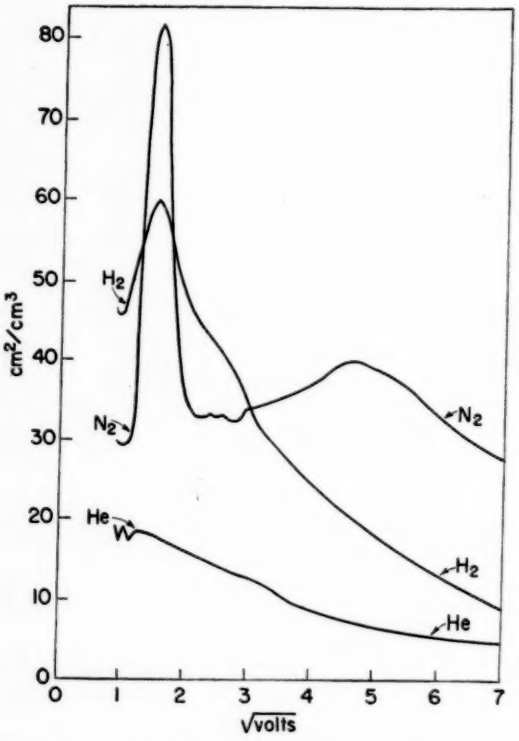

FIG. 3. Total collision cross section after Normand.

observations) and $\bar{u}=12.4\times10^5$ cm/sec. (from the observations reported here) for

$$E/p=1 \text{ (volt/cm)/mm Hg},$$

we obtain

$$\alpha=32 \text{ (cm}^2/\text{cm}^3\cdot\text{mm Hg)}, \tag{3.3}$$

$$f=0.0026. \tag{3.4}$$

This value of f is five times that $(2m/M=0.00055)$[10] which would arise from the elastic collisions, and must be assigned to excitation of the rotational energy states (0.015 ev for the first state of H_2). Such an inelastic collision would have to occur about once in five elastic collisions. This is entirely possible, the only difficulty being to explain why the loss of energy per cm, $f\alpha\bar{\epsilon}p$, should increase with the speed. If all the H_2 molecules were in their zero rotational state, and if only the first state could be excited, we should expect the loss of energy per cm to fall off inversely as the energy, as the speed (well above the threshold) increased[11] (Fig. 1). Many H_2 molecules, however, will be, at 300°K, in excited rotational states, and we might well expect interchange of angular momentum by two or more quanta with a symmetrical molecule. Indeed, if there were collision cross sections for losses of energy ϵ_r to various excitations.

$$\begin{aligned}\alpha_r(\epsilon)&=2f\alpha(\epsilon_{r+1}-\epsilon_r)/\epsilon \quad \epsilon>\epsilon_r\\ &=0 \qquad\qquad\qquad\quad \epsilon<\epsilon_r,\end{aligned} \tag{3.5}$$

(close together compared to 0.1 ev, but covering the whole range from 0 to 0.5 ev) we would obtain (Section C, (3.2 below)

$$\bar{\epsilon}=0.612\frac{E}{p\alpha}f^{-\frac{1}{2}}, \tag{3.11}$$

$$\bar{u}=3.50\times10^7\left(\frac{E}{p\alpha}f^{\frac{1}{2}}\right)^{\frac{1}{2}}, \tag{3.21}$$

differing little from (3.1) and (3.2), and agreeing with the observations if

$$\alpha=37 \text{ (cm}^2/\text{cm}^3\cdot\text{mm Hg)}, \tag{3.31}$$

$$f=0.0022. \tag{3.41}$$

This value of α cannot be compared directly with observed values since the latter[12] do not extend below 0.5 ev; however, it is not out of line with them (Fig. 2).

For D_2 we should expect the same value of α as for H_2, and to a first approximation the same chance of excitation of a rotational level. If only the first rotational level could be excited there would be only half the loss of energy in D_2 as in

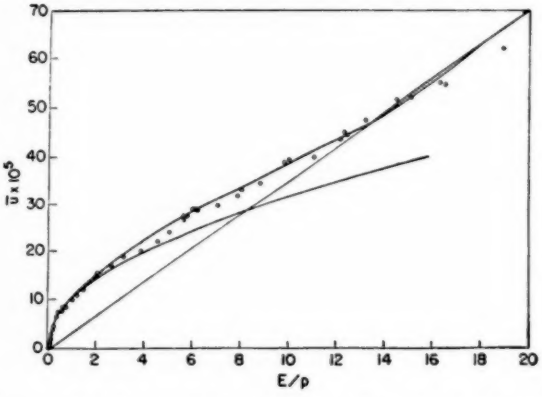

FIG. 4. Bradbury and Nielsen's drift velocities in H_2. Parabola, straight line, and theoretical interpolation.

[10] L. B. Loeb, reference 4, p. 212.
[11] H. S. W. Massey, Proc. Camb. Phil. Soc. **28**, 99 (1932).
[12] C. Ramsauer and R. Kollath, Ann. d. Physik **12**, 538 (1932).

H_2, and $\bar{u}$ should be smaller by the factor $2^{-\frac{1}{2}}=0.841$; if, on the other hand, (3.5) were correct $\alpha_r(\epsilon)$ should be halved, but so should $\epsilon_{r+1}-\epsilon_r$, and so α and $\bar{u}$ would be unchanged. (Moreover the threshold for excitation of the first vibrational state in D_2 is only 0.38 ev.) It is thus not unreasonable that $\bar{u}$ for D_2 is 0.96 that for H_2.

In the range of field strengths used, Townsend's results show that in pure N_2, $\bar{\epsilon}$ varies from 0.80 to 1.13 ev and in pure He from 2.0 to 3.9 ev. In the former this range contains the minimum at which the total cross section falls to 28 ($cm^2/cm^3 \cdot mm$ Hg); in the latter (as indeed in the same range of energy for H_2 and N_2), the total cross section is falling off [13] (Fig. 3). In all these cases and ranges the rate of loss of energy in H_2 is considerably greater for electrons of the same energies than in either N_2 or He (*viz.* 7 and 14 times, respectively). Thus up to 80 percent of H_2 or of He the loss of energy is almost entirely to H_2 molecules, and we may expect, as observed, nearly the same form of dependence of $\bar{u}$ on E/p with a coefficient varying with the concentration. If both α and f varied in the same way with speed for both gases, the form of dependence of mobility coefficient on concentration could be predicted, e.g., for α and f constant at values α_1 and f_1 and α_2 and f_2 for gases with concentrations x_1 and x_2,

$$\bar{u}=3.17\times10^7\left(\frac{E}{p}\right)^{\frac{1}{2}}\frac{(x_1f_1\alpha_1+x_2f_2\alpha_2)^{\frac{1}{2}}}{(x_1\alpha_1+x_2\alpha_2)^{\frac{1}{2}}}. \quad (3.5)$$

Although α and f probably do not vary in this way we should still expect a slight gradual rise of $\bar{u}$ to a maximum as the concentration of H_2 diminishes, followed at last by a rather sudden fall to the drift velocity for pure N_2 or He as the average energy of the electrons approaches that for pure N_2 or He only as the last of the hydrogen is withdrawn.

It may be noted that if the collision cross section for momentum transfer $\alpha(\epsilon)$ is proportional inversely to the speed, as is nearly true at above 1.5 ev in H_2 or He or above 16 ev in N_2, the drift velocity (Section C, (1.6) below)

$$\bar{u}=3.0\times10^7\frac{E}{p}/\{\epsilon^{\frac{1}{2}}\alpha(\epsilon)\}, \quad (3.6)$$

[13] C. E. Normand, reference 7.

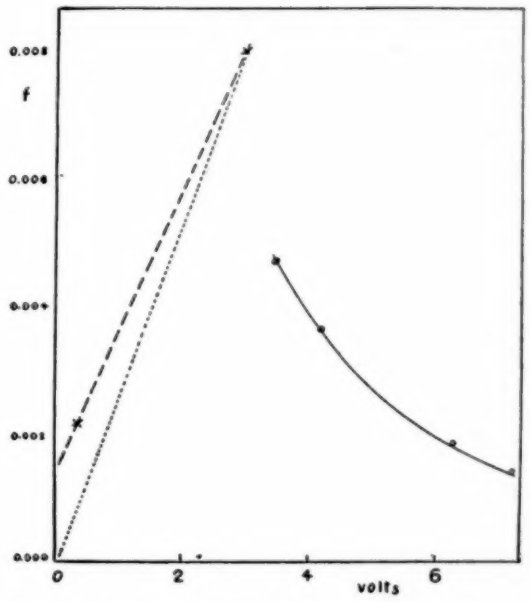

FIG. 5. Fraction of energy lost per collision. ——— Ramien; — — — Used in this paper; ---------- Used by Nielsen and Bradbury.

no matter how energy is lost. (If f were constant, we should then have a Maxwell distribution with

$$\bar{\epsilon}=\frac{1}{2f}\frac{(E/p)^{\frac{1}{2}}}{\{\epsilon^{\frac{1}{2}}\alpha(\epsilon)\}^2};$$[14]

if f varied as ϵ, we should have a Druyvesteyn distribution with

$$\bar{\epsilon}=0.604\frac{(E/p)}{\alpha(\epsilon)f(\epsilon)^{\frac{1}{2}}}.$$

In fact any values of $\alpha(\epsilon)$ agreeing with Normand's values (above 0.5 ev) and of $f(\epsilon)$ giving with these values of $\alpha(\epsilon)$ the observed values of $\bar{u}(E/p)$ between $E/p=1$ and 2 (volt/cm)/mm Hg, will give also values of $\bar{u}$ indistinguishable from those observed over the whole range (up to $E/p=20$).[15] (Fig. 4.) The curve computed (from Section C, 2.52 below) agrees with the observations simply because it smoothly joins the parabola given by 3.2 or 3.21 for small E/p (for small ϵ depending on $\alpha/f^{\frac{1}{2}}$ only) to the straight line through the origin for large E/p given by 3.6 (for large ϵ depending on $\epsilon^{\frac{1}{2}}\alpha(\epsilon)$ only). That the curve approaches the

[14] Reference 9, p. 90.

[15] N. E. Bradbury and R. A. Nielsen, Phys. Rev. **49**, 391 (1936).

straight line from below is to be expected theoretically.

(Because they use Townsend's values of $\bar{\epsilon}$ together with Normand's values of α and $f=2m/M$ to obtain their curve (B) (Fig. 5, reference 15), Bradbury and Nielsen reach the conclusion that the large values of f are necessary to explain the drift velocity values. The discrepancy between their curve (B) and the observed values of $\bar{u}$ arises from the inconsistency of Normand's α and $f=2m/M$ with Townsend's values of $\bar{\epsilon}$, not from any inconsistency between these values of α and f and the observed values of $\bar{u}$, and the conclusion that the values of f are large can only be obtained if Townsend's values of $\bar{\epsilon}$ are used.)

Townsend's value $\bar{\epsilon}=2.9$ ev for $E/p=20$ ((volt/cm/mm Hg), thus implies that f increases to 0.008 for an electron energy of about 3 ev,[15] so that while the collision cross section for momentum transfer is decreasing, that for loss of energy is still increasing as the energy increases. While this value of f fits in with Ramien's direct observations[16] for energy 4 ev, the fairly steady increase from 0.0022 at 0.35 ev to 0.008 at 3 ev does not agree with his assumption that the only important process is the excitation of the first vibrational state, nor does the trend fit in with his observation that at 7 ev f has fallen to 0.0015. The trend seems indeed difficult to explain unless, as sufficient energy becomes available, molecular vibrational states of higher and higher energies may be excited (Fig. 5).

It should be emphasized that these conclusions about f might be greatly modified if it should turn out that Townsend's energies are unreliable.

C. MATHEMATICAL APPENDIX

1. Druyvesteyn's Equation

We shall adopt the notation used by Morse[17] with an electron distribution function

$$f(v,\theta)=f_0(v)+f_1(v)\cos\theta+\cdots. \tag{1.1}$$

Supposing that momentum transfer takes place almost entirely by elastic collisions, we can express f_1 in terms of the derivatives of f_0.[18] When effects of diffusion on $f(v,\theta)$ are to be ignored,

$$f_1(v)=\frac{1}{NvQ(v)}\frac{eE}{m}\frac{\partial f_0(v)}{\partial v}. \tag{1.2}$$

(Here $f(v,\theta)v^2dvd\omega$ is the number of electrons per unit volume of charge $-e$ and mass m moving with speed in range dv about v in direction within solid angle $d\omega$ about a direction making angle θ with an applied electric field E. N is the number of gas molecules per unit volume with "collision cross section for momentum transfer" $Q(v)$ for electrons of speed v; so that $NQ(v)$ is the same as $p\alpha(v)$ above.)

We neglect ionization and suppose that the cross section for an inelastic collision of an electron of speed v in which energy δ_r is lost (or a superelastic collision in which $-\delta_r$ is gained) is $q_r(v)$, so that the probability of such a collision per unit time is $Nvq_r(v)$ and the net gain to the distribution function at v per unit time due to this is

$$(N/v)\{v'^2q_r(v')f_0(v')-v^2q_r(v)f_0(v)\}, \tag{1.3}$$

where $v'^2=v^2+(2/m)\delta_r$ (since the number of electrons of speed in dv' about v' per unit volume per unit solid angle is $f_0(v')v'^2dv'$, and since $v'dv'=vdv$).

The function $f_0(v)$, in order that it shall not change appreciably over a free path, must satisfy Druyvestyn's equation in the form

$$-\frac{e^2E^2}{m^2}\frac{4}{3v}\frac{\partial}{\partial v^2}\left\{\frac{v^2}{NQ(v)}\frac{\partial}{\partial v^2}f_0(v)\right\}=\sum_r\frac{N}{v}\{v'^2q_r(v')f_0(v')-v^2q_r(v)f_0(v)\}, \tag{1.4}$$

with

$$\frac{v^2}{NQ(v)}\frac{\partial}{\partial v^2}f_0(v)\to 0 \quad \text{as} \quad v\to 0.$$

The mean drift velocity of the electrons

$$\bar{u}=\frac{1}{3}\int_0^\infty f_1(v)v^3dv\Big/\int_0^\infty f_0(v)v^2dv=\frac{eE}{m}\int_0^\infty\frac{1}{3}\frac{\partial}{\partial v}\left(\frac{v^2}{NQ(v)}\right)f_0(v)dv\Big/\int_0^\infty f_0(v)v^2dv \tag{1.5}$$

in this case.

If $vQ(v)$ is constant, then the mean drift velocity is

$$\bar{u}=eE/mNvQ(v), \tag{1.6}$$

no matter how energy is lost.

2. Solutions for Small Energy Loss per Collision

We shall suppose that the electric field is so large that the electronic energy is large compared with the thermal molecular energy. The contribution to the right-hand side of (1.4) from elastic collisions with molecules of mass M is then

$$2\frac{m}{M}\frac{1}{v}\frac{\partial}{\partial v^2}(v^4NQ(v)f_0(v)). \tag{2.1}$$

If the energy, δ_r, lost in a type of inelastic collision is only a small fraction of the total energy, the contribution from this inelastic scattering can be written

$$\frac{2}{m}\frac{\delta_r}{v}\frac{\partial}{\partial v^2}\{v^2Nq_r(v)f_0(v)\}. \tag{2.2}$$

[16] Hans Ramien, Zeits. f. Physik **70**, 353 (1931).
[17] P. M. Morse, W. P. Allis, and E. S. Lamar, Phys. Rev. **48**, 412 (1935).
[18] Reference 17, p. 414.

Thus Druyvesteyn's equation becomes

$$-\frac{e^2E^2}{m^2}\frac{4}{3v}\frac{\partial}{\partial v^2}\left\{\frac{v^2}{NQ(v)}\frac{\partial}{\partial v^2}f_0(v)\right\}=\frac{1}{v}\frac{\partial}{\partial v^2}[v^4Nq(v)f_0(v)], \quad (2.3)$$

where

$$q(v)=2\frac{m}{M}Q(v)+\sum_r\frac{\delta_r}{\frac{1}{2}mv^2}q_r(v). \quad (2.31)$$

$q(v)/Q(v)$ is often[19] called the "fraction of energy lost per collision" and denoted by f.

If $Q(v)$ and $q(v)$ are known (2.3) can be integrated by quadrature.[20] In particular, if $Q(v)=Q$ and $q(v)=fQ$ are constant, we have the original case of Druyvesteyn:

$$f_0(v)=A\exp\left(-\frac{3}{8}\frac{m^2N^2fQ^2}{e^2E^2}v^4\right), \quad (2.41)$$

so that

$$\bar{u}=\frac{\pi^{\frac{1}{2}}}{3\Gamma(\frac{3}{4})}\left(\frac{3f}{2}\right)^{\frac{1}{4}}\left(\frac{2eE}{mNQ}\right)^{\frac{1}{2}}=0.7546f^{\frac{1}{4}}\left(\frac{eE}{mNQ}\right)^{\frac{1}{2}}, \quad (2.42)$$

while the mean energy of the electrons

$$\bar{\epsilon}=\frac{\Gamma(\frac{5}{4})}{\Gamma(\frac{3}{4})}\left(\frac{2e^2E^2}{3fN^2Q^2}\right)^{\frac{1}{2}}=0.6039f^{-\frac{1}{2}}\frac{eE}{NQ}. \quad (2.43)$$

More generally, if $Q(v)=Q_0/(1+(v/v_0)^4)^{\frac{1}{4}}$, and $q(v)=fQ(v)$, where Q_0, v_0, and f are constant, so that the cross sections are constant for small v and vary inversely as v for large v, but remain in the same ratio;

$$f_0(v)=A\exp\left[-\gamma v_0^4\{(1+(v/v_0)^4)^{\frac{1}{2}}-1\}\right], \quad (2.51)$$

and we obtain

$$\bar{u}=\frac{\pi^{1/2}}{3\Gamma(\frac{3}{4})}\left(\frac{3f}{2}\right)^{1/4}\left(\frac{2eE}{mNQ_0}\right)^{1/2}\frac{K_{1/4}(\gamma)^2+3K_{3/4}(\gamma)K_{5/4}(\gamma)}{8(\pi/4\gamma)^{1/2}K_{5/4}(2\gamma)}, \quad (2.52)$$

and

$$\bar{\epsilon}=\frac{\Gamma(\frac{5}{4})}{\Gamma(\frac{3}{4})}\left(\frac{2e^2E^2}{3fN^2Q_0^2}\right)^{1/2}\frac{K_{7/4}(2\gamma)}{K_{5/4}(2\gamma)}, \quad (2.53)$$

where $\gamma=\frac{3}{8}(m^2N^2fQ_0^2/e^2E^2)v_0^4$, and $K_n(\gamma)$ is the Bessel function of order n and of pure imaginary argument, $\sim(\pi/2\gamma)^{\frac{1}{2}}e^{-\gamma}$ as $\gamma\to\infty$.

3. Solutions if the Loss of Energy in a Collison May be Large

If energy can be lost by an electron of speed v' by amounts δ_r with cross sections $q_r(v')$ distributed nearly continuously from 0 to $\frac{1}{2}mv'^2$, and if we write

$$q_r(v')=q(v',v)\frac{\delta_{r+1}-\delta_r}{\frac{1}{2}mv'^2} \quad v'^2>\frac{2}{m}\delta_r$$

$$=0 \quad v'^2<\frac{2}{m}\delta_r$$

so that

$$\sum_r(\ )\frac{2}{m}(\delta_{r+1}-\delta_r)$$

becomes $\int(\ )2vdv$, we obtain for the right-hand side of (1.4)

$$\frac{1}{v}\left[\int_v^\infty Nq(v',v)f_0(v')2v'dv'-\int_0^v Nq(v,v')2v'dv'f_0(v)\right]. \quad (3.1)$$

If we neglect loss of energy in other ways, (1.4) can be reduced to a linear differential equation of the second order when $q(v,v')$ is of the form $\alpha(v')\beta(v)$. In particular, if $Q(v)=Q$ and $q(v',v)=2fQ$ (so that f is still the "fraction of energy lost per collision") are constant, the distribution is Maxwellian;

$$f_0(v)=A\exp\left(-(\tfrac{3}{2}f)^{\frac{1}{2}}\frac{mNQ}{eE}v^2\right), \quad (3.21)$$

and

$$\bar{u}=\frac{2^{\frac{1}{2}}}{3\pi^{\frac{1}{2}}}(\tfrac{3}{2}f)^{\frac{1}{4}}\left(\frac{2eE}{mNQ}\right)^{\frac{1}{2}}=0.8325f^{\frac{1}{4}}\left(\frac{eE}{mNQ}\right)^{\frac{1}{2}}, \quad (3.22)$$

$$\bar{\epsilon}=\frac{3}{4}\left(\frac{2e^2E^2}{3fN^2Q^2}\right)^{\frac{1}{2}}=0.6123f^{-\frac{1}{2}}\frac{eE}{NQ}. \quad (3.23)$$

4. Townsend's Data

Townsend's experiments lead to values for other averages over the electron distribution than $\bar{u}$ and $\bar{\epsilon}$.[21] In fact his

$$U^2=\int_0^\infty\frac{v}{NQ(v)}f_0(v)v^2dv\Big/\int_0^\infty\frac{1}{3}\frac{\partial}{\partial v}\left(\frac{v^2}{NQ(v)}\right)f_0(v)dv, \quad (4.1)$$

and

$$W=\frac{eE}{m}\int_0^\infty\frac{\partial}{\partial v}\left(\frac{v}{(NQ(v))^2}\right)f_0(v)dv\Big/\int_0^\infty\frac{\partial}{\partial v}\left(\frac{v^2}{NQ(v)}\right)f_0(v)dv, \quad (4.2)$$

and $W=\bar{u}$ in general only if $Q(v)\propto 1/v$; $\frac{1}{2}mU^2=\bar{\epsilon}$ only if $Q(v)\propto 1/v$ or if the distribution is Maxwellian. However, in all the cases we have considered, the ratios $W/\bar{u}$ and $\frac{1}{2}mU^2/\bar{\epsilon}$ differ inappreciably from unity.

[19] Reference 9, p. 93.
[20] Reference 17, p. 416.
[21] W. P. Allis and H. W. Allen, Phys. Rev. **52**, 703 (1937).

The Mercury Arc Cathode

CHARLES G. SMITH
Raytheon Manufacturing Company, Newton, Massachusetts
(Received March 13, 1942)

Conduction electrons in the liquid at the arc spot are considered to be heated to about 4000°K by electronic bombardment from the vapor while the atomic temperature of the liquid is near 150°C. Thermionic emission apparently yields the arc current plus that returning from the vapor. An arc spot was driven around a circular mercury track by a radial magnetic field. The spot traveled opposite to the ponderomotive force for fields below approximately 5000 gauss with velocity proportional to field strength and showed a negative temperature coefficient. The Righi-Leduc effect considered as a thermomotive force operative in the hot layer of conduction electrons was assumed to drive the spot. The velocity was evaluated in terms of the vertical thermal gradient and compared with the observed, yielding a gradient of about 5×10^8 degrees cm. Arcs were extinguished by current pulses of about 10^{-7} sec. in the same direction as the arc current. This gave means for calculating the total energy of the hot electronic layer, and finally the vertical thermal gradient in good agreement with the value above. The Thomson heat stops losses along this gradient, and is apparently the factor causing the characteristic arc current density.

TO explain the escape of electrons from the apparently non-thermionic arc spot on the liquid cathode, yielding currents of 4000 amperes per square centimeters more or less, the theory has been advanced that most of the electrons bearing the current are pulled from the cathode by the electrostatic force of the field of ions just above the cathode.[1] This well-known extraction theory has been analyzed,[2] and has been apparently the most acceptable for a number of years. However, new phenomena and new considerasions to be brought forward lead to a different concept.

We advance the theory that electronic bombardment of the cathode results in an efficient transfer of energy to conduction electrons in the liquid mercury, raising them to a temperature sufficient to cause a kind of thermionic emission great enough to yield the observed arc current plus that coming down from the vapor; and that the atomic configuration is at a very much lower temperature. The Thomson heat is apparently operative to arrest most of the heat flow tending to go down into the liquid by way of the electronic part of the thermal conductor.

We discuss first the relationship between liquid and vapor at the arc spot. In the quantitative discussion that follows we assume a current density of 4000 amperes per sq. cm, which according to our observations given below and in agreement with observations of one other[3] seems to be a characteristic of the ordinary mercury arc.

Probe measurements of electronic temperature and number of electrons in the plasma though generally considered to be very trustworthy in mercury vapor will not be relied upon for the region adjacent the arc spot because of the smallness of the region in relation to the necessary size of the probes and other practically insurmountable difficulties leading to doubts[4] concerning such measurements. We shall have to be content with finding reasonable relationships between plasma and liquid in harmony with the present theory; and shall point out that the plasma factors, cathode drop, electronic temperature, and electronic density, will take on different values for different arcs. Confirming evidence for the general theory will go beyond the fitting of the phenomena in the vapor to the phenomena in the liquid and will come from new considerations of the liquid mercury. We have the following notation:

D = observed arc current density in amp./sq. cm,
L = electronic current in amp. cm^{-2} leaving the cathode,
I = electronic current in amp. cm^{-2} entering the cathode from the gas,
N = number of electrons per cc in the plasma just on the anode side of the cathode fall space,

[1] I. Langmuir, Science **58**, 290 (1923); Gen. Elec. Rev. **26**, 735 (1923).
[2] K. T. Compton, Phys. Rev. **37**, 1077 (1931).
[3] A. Gunther-Schulze, Zeits. f. Physik **11**, 74 (1922).
[4] R. C. Mason, Phys. Rev. **51**, 28 (1937).

T = electronic temperature of the vapor,
C = cathode drop in volts,
$q = 1.6\times10^{-19}$ coulomb, being the electronic charge,
ϕ = work function of Hg,
k = Boltzmann gas constant per molecule,
θ = temperature of the conduction electrons in the liquid cathode.

Three equations will be written down involving T, N, I, and L subject to the assumptions of the present theory.

$$L = D + I, \tag{1}$$

$$I = Nq(kT/2\pi m)^{\frac{1}{2}}\mathcal{E}^{-11600C/T}. \tag{2}$$

The energy balance equation:

$$2(I/q)kT + \phi I\times10^{7} = \phi L\times10^{7} + 2(L/q)k\theta. \tag{3}$$

In (3) we have considered the energy brought in due to the kinetic energy of the electrons and the operation of the work function. The energy going out is treated in a similar way. Energy due to ions has been neglected in comparison to that of the electrons. Furthermore, thermal conduction along the electronic medium in the mercury is neglected because we assume the Thomson effect to nullify such conduction. This will be discussed later.

The last term of (3) is relatively small and can be evaluated for our purposes now. θ can be taken from the thermionic equation

$$L = 120\theta^{2}\mathcal{E}^{-11600\phi/\theta},$$

provided we assume a reasonable value for L. If our estimate of L turns out poor we can use our final results to get a better value and proceed anew. However, as we shall see later, a value of 4000°K will be a good estimate for θ. The work function ϕ is taken to be 4.26 volts. This was obtained from the contact potential between Hg and platinum[5] as observed by Moore and by using the work function of platinum as observed by DuBridge.[6]

Then (3) becomes

$$2IkT/q + \phi I\times10^{7} = (\phi + 0.69)L\times10^{7}, \tag{4}$$

or

$$2IkT/q\times10^{-7} = 4.95D + 0.69I, \tag{5}$$

and

$$D/I = 3.48T\times10^{-5} - 0.139. \tag{6}$$

[5] D. H. Moore, Phys. Rev. **50**, 344 (1936).
[6] L. A. DuBridge, Phys. Rev. **32**, 961 (1928).

T is reasonably expected to be in the neighborhood of 4×10^{4}. Hence I is approximately equal to D. The electronic emission at the arc spot is therefore approximately $2D$ or about 8000 amperes per sq. cm. Note that the cathode drop is not explicit in Eq. (6). Evidently a change in cathode drop must cause changes in T and N which maintain the validity of (6).

By combining (6) and (2) we have

$$N = \frac{46.2\times10^{20}}{(T-4000)T^{\frac{1}{2}}}\mathcal{E}^{11600C/T}. \tag{7}$$

If there were another relation between N and T known from experiment we could find the value of either. It is known that the cathode is subjected to a mechanical pressure, which by the observations of Kobel[7] upon a given arc was approximately 6.5 cm of mercury. The pressure $p = NkT$ could be called upon provided we accept the idea of Tonks that the mechanical pressure[8] is that of the electrons. The concept seems very reasonable although the kinetic picture of how the momentum is transferred to the cathode must depend upon conditions. However, we shall make only small use of the relation here since the observations are not as extensive as would be desirable, and do not include a value of C. It is of interest, however, to evaluate N from (7) for various values of T and C.

Results are recorded in Table I for cathode drops of 6, 8, 10, and 12 volts and for values of T that seem to cover the expected range. C would not be expected to go below about five volts in any case because of the minimum energy needed to excite the mercury atom. It is known, however, that the cathode drop for a thermionic cathode may be below 7 volts.[9] Measurements

TABLE I. Number of electrons (N) per cc in the plasma. T = Electronic temperature in plasma. C = Cathode drop in volts.

	$C=6$	$C=8$	$C=10$	$C=12$
$T\times10^{-3}$	$N\times10^{-15}$	$N\times10^{-15}$	$N\times10^{-15}$	$N\times10^{-15}$
30	10.5	22.7	49.3	105.0
40	3.66	6.54	11.7	20.6
50	1.80	2.87	4.58	7.25
60	1.07	1.59	2.32	3.44
70	.710	1.01	1.38	1.93

[7] E. Kobel, Phys. Rev. **36**, 1636 (1930).
[8] L. Tonks, Phys. Rev. **46**, 278 (1934).
[9] R. C. Mason, Phys. Rev. **38**, 427 (1931).

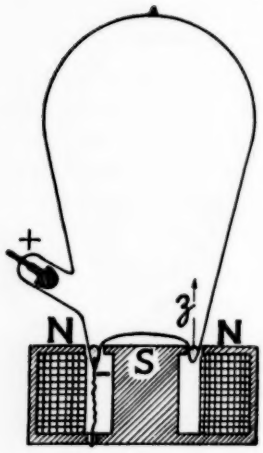

FIG. 1. Arc tube with annular mercury cathode. $N-S$ = concentric poles of electromagnet driving the arc spot around circle 30 cm in circumference. z = coordinate of text.

upon a particular mercury arc have yielded 10 volts[10] for C.

If we assume C was 10 volts when Kobel observed a pressure of about 80,000 dynes per sq. cm and equate this pressure to NkT we find that $T=37{,}000°\text{K}$ approx. and $N=15\times10^{15}$ electrons per cc. These values seem reasonable. The phenomena in the plasma apparently fit on to those expected in the liquid. The table shows that a smaller N goes with a larger T. We know from experiments with the plasma that a small atomic density usually requires a larger T. The arc for various vapor pressures is visualized, therefore, as accommodating itself to the conditions by variations of C, N, and T. An increase in T is assumed to be caused by an increase in C. The arc according to the present, or *emission theory* is adaptable to a wide range of vapor pressure.

Before going further with the emission theory more observations are needed. A magnetic field transverse to the arc current drives the spot in a direction transverse to the field but in a sense opposite to the ponderomotive force. We set up a tube having an annular ring of mercury for the cathode. A radial magnetic field was employed as shown in Fig. 1.

With a south pole at the center, the arc spot raced around clockwise as viewed from above. The mercury circulated slowly in the opposite direction. The arc stream curled backward as the spot rushed forward. Velocity was measured by focusing light from the spot upon a photo-cell arrangement and using the amplified current to deflect the beam of a cathode-ray oscillograph. Deflection along the other coordinate was made by the 60-cycle power circuit, or by other known frequency. Definite patterns were observable upon the screen of the oscillograph from which the number of excursions per second made by the arc spot around its track was deduced. Speeds above about 3000 cm per second gave an arc track with very smooth edges and a very definite resulting pattern on the oscillographic screen. Lower speeds showed a ragged arc path and a variable oscillographic indication.

The arc track sought the region where the horizontal component of the magnetic field was strongest (the path where it could go fastest). The spot could be made to race around near the inner glass wall or the outer or could be made to follow a circle half way between the two walls by varying the disposition of the magnetic field to give the strongest horizontal component in the desired region.

A plot of velocity of spot as a function of magnetic field strength is shown in Fig. 2. The result for a constant temperature of the mercury is a straight line through the origin. The velocity has a large but undetermined negative temperature coefficient at any field strength. The steeper straight line was observed with cooler mercury. The magnet was turned on and the speed ob-

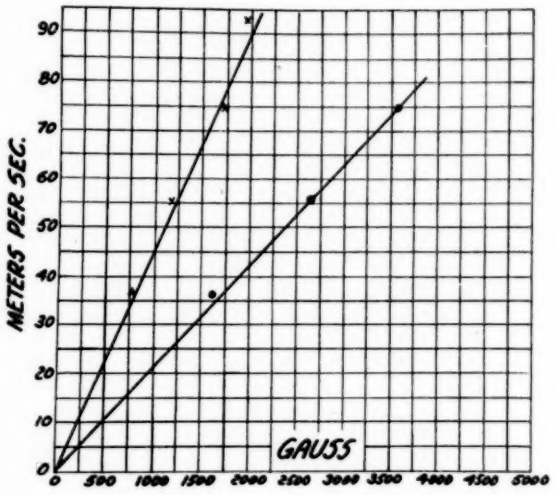

FIG. 2. Velocity of arc spot *versus* horizontal component of magnetic field. Arc current six amp. Steeper line observed with cooler mercury.

[10] E. S. Lamar and K. T. Compton, Phys. Rev. **37**, 1069 (1931).

served in less than a second. Then the magnet was shut off and after several minutes another reading at a higher field strength was made. In this way the mercury temperature was at about the same low value for each observation. The lower curve was taken by allowing the arc to race around till it reached a constant lower limit of speed, the mercury presumably reaching a constant temperature. We regret that an accurate determination of temperature of the mercury at the arc path was not possible in the time available.

The velocities in the region considered are too high for mechanical effects to cause turbulence of the liquid surface. The large condenser for the vapor insured an inconsiderable pressure everywhere except at the arc spot. We obviously have an arc spot racing over a smooth mercury surface, and going in the direction opposite to that determined by the effect of the field on the arc stream; the speed is accurately proportional to the magnetic field, and has a negative temperature coefficient; the determining temperature is that of the liquid or the hot conduction electrons and probably has little or no connection with that of the vapor, except at very high field strength and low vapor pressure. Phenomena in these regions are dealt with later.

A transverse galvano-magnetic effect suggests itself as a prime cause of the observed phenomena. The Hall effect seems to be too small to be of direct importance. The Nernst and the Ettingshausen effects also seem to be of a low order of magnitude. A negative Righi-Leduc effect, however, seems to be the one involved directly, provided the thermal gradient of the conduction electrons along a vertical line in the liquid is large enough. The magnetic field transverse to the large thermal gradient is visualized as giving rise to a thermomotive[11] force in the liquid at the moving arc spot acting to transfer heat in the observed direction of motion.

We can write the thermotive force per cm as

$$\Delta\theta/B = SIH(d\theta/dz),$$

where B = breadth of arc spot along line of motion; S = Righi-Leduc coefficient; H = magnetic field strength; and $d\theta/dz$ = vertical thermal gradient. $\Delta\theta$ represents the total driving thermomotive force in an element of the spot.

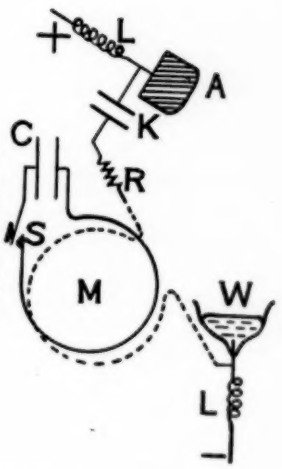

FIG. 3. Arc quenching circuit. S = switch. C = 0.02 μf condenser. M = closely coupled primary and secondary each being one turn of ½″ ribbon about 11 cm in diameter. R = non-inductive resistance of six ohms. K = 0.06 μf. W = Hg cathode. A = carbon anode. LL = r-f chokes.

Let K = the thermal conductivity of the highly excited region in the liquid; E = the energy per unit volume of the excited electrons; and V = velocity of the excited spot. Then $VE = KSIH(d\theta/dz)$ = rate of transfer of heat in the direction of motion. Hence

$$V/H = (KS/E)(d\theta/dz).$$

The velocity seems to be independent of B and hence of the size of the spot. Therefore, velocity is apparently independent of changes of arc current. Trebling the arc current suddenly was observed to cause an increase in velocity of about 15 percent. Since the magnetic field due to the arc current has been neglected in its effect upon the thermomotive force, we consider the observations to give a result consistent so far with the formula.

The ratio KS/E may be evaluated approximately from theory.[12]

$$S = \frac{2el}{h}\left(\frac{\pi}{3n}\right)^{\frac{1}{3}}.$$

$$K = \frac{2\pi^3 lk^2\theta}{9h}\left(\frac{3n}{\pi}\right)^{\frac{2}{3}}.$$

$E = \theta C_v$ Approx.

C_v = Specific heat of the electrons.

$$C_v = \frac{4\pi^3 mk^2}{3h^2}\left(\frac{3n}{\pi}\right)^{\frac{1}{3}}\theta.$$

[11] P. L. Bridgman, *The Thermodynamics of Electrical Phenomena in Metals* (The Macmillan Company, 1934), p. 137.

[12] A. Somerfeld and N. H. Frank, Rev. Mod. Phys. **3**, 1 (1931).

Finally

$$(V/H)=\tfrac{1}{3}(e/m)(l^2/\theta)(d\theta/dz)$$
$$=5.9\times10^6(l^2/\theta)(d\theta/dz),$$

where l = mean free path of electron; m = mass of the electron; and e = charge of electron in e.m.u.

The formula as derived is approximate. The quantity l is of the order of magnitude of 2×10^{-6} cm. We take θ to be 4000°K, the value near the emitting or top surface of the spot. Then

$$d\theta/dz=1.7\ V/H\times10^8.$$

The observed V/H is between 2 and 4. Hence $d\theta/dz$ is approximately 5×10^8 degrees/cm by this method of evaluation. Fortunately there is an independent method, wherein the total energy of the excited layer of electrons is evaluated from energy necessary to extinguish the arc.

Pulses of current lasting about 10^{-7} sec. were superposed upon the arc current already flowing, by discharging a capacity C of 0.02 microfarad connected in series with one turn of a closely coupled transformer M and a damping resistance R about equal to the critical damping resistance (see Fig. 3). W is the liquid cathode and A is the anode. LL are radiofrequency chokes. K is a condenser about four times as large as C, which served to transmit the pulse but to prevent passage of steady current. The arc was invariably extinguished, when the superposed current was comparable to that already flowing. The voltage of C necessary to extinguish the arc was consistently less if the sign of the charge were such that the first rush of current were added to the arc current. A higher voltage of C was necessary if it were charged to cause a subtraction from the arc current. This observation evidently shows that a superposed added current can extingish the arc. Currents up to twenty amperes were thus interrupted. The mechanism of this action depends upon our ability suddenly to raise the cathode drop of the arc. Evidently the bombarding electronic current I of Eq. (2) ceases for a moment because of a sudden increase of the factor C. The degree of ionization and electronic temperature in the vapor respond relatively slowly as would be expected from other observations.[13] The outflowing current L carries away energy from the spot and it is cooled below that necessary for sustaining the arc. The energy taken away is approximately 4.78 $Lt\times10^7$ ergs per sq. cm where $t=10^{-7}$ sec. Hence only about 30,000 ergs are removed. The arc would not have gone out if this were very much less than the total energy involved. We therefore consider the excited region to be limited in energy.

Let us assume about 4×10^{22} electrons per cc and let Z be approximately the thickness of the activated layer. Then the total energy is roughly $Z\times\theta C_v=550\ Z\theta^2$. θ is an average, taken here to be 2000°K. Then $2.2\times10^9\ Z=30{,}000$ and $Z=1.4\times10^{-5}$ cm. A reasonable estimate of Z of the order of magnitude seems to be about 10^{-5} cm.

The thermal gradient downward among the conduction electrons is therefore approximately 4000×10^5 or 4×10^8 degrees per cm. The experiments with the moving spot and those involving blowing out of arcs are each in harmony with the emission theory and each yields essentially the same value for the thickness of the excited region of conduction electrons.

Such an enormous thermal gradient in the liquid would cool the spot and extinguish the arc if the ordinary thermal conduction had free play. Arcs were also extinguished within 10^{-7} sec. by pulses of current in the direction opposite to the arc current. The arc spot in the absence of arc current cools down to an inoperative value within the 10^{-7} sec. Evidently the arc current normally prevents the cooling. The convection of heat upward with the electronic current must approximately equal the thermal conduction downward. Therefore, we assume the Thomson heat to counteract the thermal conduction. We look first at the order of magnitudes necessary and write $10^7\sigma D(d\theta/dz)=-K(d\theta/dz)$ approx., or, $\sigma=-(K/D)\times10^{-7}$ volt, where σ = Thomson coefficient; D = current density = 4000 amp./sq. cm; K = thermal conductivity = 8×10^5 ergs/cm sec. deg. Hence $\sigma=-2\times10^{-5}$ volt. We can evaluate σ approximately from the theory[12] of metals.

$$\sigma=300U_E=\frac{-8\pi^2mk^2\theta}{3eh^2}\left(\frac{\pi}{3n}\right)^{\frac{1}{3}}\times300\text{ volts.}$$

Here U_E is the Thomson coefficient in e.s.u. as calculated for a case of no variation of electronic free path with temperature. The formula

[13] C. G. Smith, Phys. Rev. **59**, 997 (1941).

is therefore not expected to yield a correct result. Nevertheless, it is of some interest to note that for $n=4\times10^{22}$ and $\theta=2000°$ we find $\sigma=-1.1\times10^{-5}$ volt, a magnitude close to that required by the arc theory. Evaluation of σ from observation is possible from the relation

$$\sigma_m-\sigma_r=\theta(dQ/d\theta)=\text{difference in Thomson heats of two metals, } m \text{ and } r.$$

Here Q equals the thermoelectric power. From the *International Critical Tables 6*, page 214, we find data for mercury and lead, which give

$$\sigma=-3.3\times10^{-8}\theta.$$

Extrapolation to $\theta=2000°$ gives a value of the order of magnitude needed for the arc theory.

At this point we cannot feel sure that our procedure is correct in detail, although it evidently indicates that we are dealing with factors of real significance. We have not explained why the current density is 4000 amperes per sq. cm. If it were more than this the Thomson coefficient could be less. In view of the present theory we feel that the current density is a characteristic of the liquid mercury and is determined among other things by the behavior of the Thomson heat. Evidently currents below some limit are too small to nullify the possible thermal losses. The 4000 amperes is probably this minimum current. There is a back e.m.f. associated with the Thomson heat and proportional to the thermal gradient, which must tend to limit the current density since it supplies a spreading tendency for the arc spot. We shall not make mental constructions now to fit the situation in more detail, since experimental results to accompany them are not at hand. We therefore return to other observations.

The rapidly moving arc spot in a definite track when viewed through a filter that transmits only the red, appears like a red hot streak whose width is readily measured by optical means. Measurements were made for currents ranging from 2 to 12 amperes, and the resulting current density evaluated by assuming the moving spot to be circular. Values only slightly below 4000 amperes per square centimeter were found.

The most interesting observation, however, is that the intensity of the red streak seems to be exactly the same regardless of the angle between the mercury surface and the line of vision. This suggests the operation of Lambert's cosine law of brightness, and shows clearly that the red light is coming from the liquid mercury. If it were coming from the gas immediately above the liquid, then the brightness when viewed along a line nearly parallel with the surface would be greater than that observed when looking normal to the surface; just as an end on view of a discharge tube yields greater brightness than that encountered across the tube. The inference is that the electrons in the liquid in the activated arc region are emitting the light, and any such emission from the adjacent vapor is of secondary importance. Time was not available for determining the color temperature of the streak, although the spectrum was observed to be continuous.

The arc spot appears to be incandescent. However, the vaporization from the spot has been estimated[2] to be that expected from a liquid surface at approximately 200°C. Our observations with the transverse magnetic field confirm this. With a strong field, an electron leaving the liquid to enter the vapor will in general start along a cycloidal path which will lead back to the cathode unless the trajectory is disturbed by a collision with atom or electron in the vapor. A field of 5000 gauss stopped the contrary motion of the spot attributed to the Righi-Leduc effect and reversed it, giving rise to a very slow opposite motion. If the vapor pressure were allowed to rise, this new motion ceased and the direction changed back to that characteristic of a lesser magnetic field. Apparently the electronic free path for a spot barely stopped is nearly that of the expected cycloidal path. It appears that we can evaluate approximately the electronic free path. The length of the cycloid expected is about 0.008 cm for an electron whose kinetic energy at the crest of the cycloid is about nine electron volts. The free path of an electron in normal mercury vapor[14] at 1-mm pressure is approximately 0.015 cm. We infer that the vapor density just above the arc spot under the conditions above corresponds very roughly to that of vapor at 2-mm pressure under standard condi-

[14] K. T. Compton and I. Langmuir, Rev. Mod. Phys. **2**, 123 (1930).

tions. The liquid surface is therefore estimated to be about 150°C by this independent method.

The conduction electrons in the liquid at the arc spot are at a temperature of 4000°K according to this emission theory. The observations indicate they emit light as an incandescent body. The atomic constituent of the excited region is at approximately 150°C. If these things be true, then the cooling of the liquid by evaporation and by ordinary thermal conduction along the atomic constituent plus losses due to convection are together able to keep pace with the energy transfer from the excited electronic medium over to the atomic matrix. This rate of transfer is expected to be low but no attempt at a theoretical estimation of it will be made at this time.

For the sake of clarity, however, we recall in this connection the well-known fact that sputtering of a cathode is readily produced by bombardment with masses of atomic magnitude, namely, ions; whereas the plate of a radio tube bombarded by electrons suffers little or no sputtering. Evidently the transfer of energy to the atomic lattice is direct in the ionic case but indirect in the electronic. Where the mass of colliding particle and target particle are nearly equal the efficiency of direct energy transfer would be considered greatest. The electronic bombardment must heat electrons in the metal first and these in turn transfer energy to the atoms.

The emission theory, therefore, seems to introduce ideas in harmony with those previously acceptable. It fits in with known factors in the vapor above the arc spot. It seems to be the only theory compatible with the characteristic behavior of the arc spot in a transverse magnetic field and the extinction phenomena cited, and leading to an explanation of the characteristic current density. The lack of equilibrium between the hot electronic medium and the relatively cool atomic matrix involves an account that can possibly be elaborated upon later.

JULY 1 AND 15, 1942 PHYSICAL REVIEW VOLUME 62

The Loss of Energy of Hydrogen Ions in Traversing Various Gases

CRAIG M. CRENSHAW
Department of Physics, New York University, New York

(Received April 14, 1942)

The loss of energy of hydrogen and deuterium ions having initial energies in the range from 60 to 340 kev has been measured as a function of their path in various gases at various pressures. The measurements are expressible in terms of the energy loss in kev per cm of path per mm of pressure as well as in terms of stopping power relative to air. The gases examined are air, water vapor, hydrogen, deuterium, and helium.

APPARATUS

FIGURE 1 shows the general plan of the apparatus. The hydrogen or deuterium ions after being accelerated by means of a Cockcroft-Walton voltage quadrupler pass into the field of the resolving magnet. Here a mass beam is selected and properly deflected so as to pass on through the gas absorption chamber. After traversing the gas the beam is again brought into a high vacuum and passed through the field of a measuring magnet. This magnet is so adjusted as always to bend the beam a definite amount as determined by the ion beam fluorescence on the observation screen. Thus the magnetic field of the measuring magnet measures the energy of the ions after passing through the gas.

Figure 2 gives a detailed sketch of the absorption chamber. The gas is confined by means of a fine capillary system of diaphragms at each end of the chamber. The gas which does escape through these capillaries is removed by a liquid air trap and a system of high speed pumps.

Several features in the design and operation of the apparatus have been given special attention. Energy measurements are all made in

terms of a carefully constructed and calibrated resistance voltmeter. The energy of the exit beam as given by the magnetic field of the measuring magnet depends for its conversion into kev upon calibrations made with no gas in the absorption chamber. Under such conditions the exit beam has the same energy as the known incident beam.

The beam is brought in and out of the gas absorption chamber through the capillary systems. There it encounters pressure gradients. The upper capillary system is movable and these end effects are evaluated by taking data for a second position. Pressure in the various parts of the system has been carefully watched with suitable gauges. The pressure in the absorption chamber is accurately measured with an oil manometer.

Arrangements are such that the position of the high energy edge of the spot on the viewing screen is relatively insensitive to adjustments of the analyzing magnet and minor adjustments of the beam. A slight shift changes only the portion of the beam used in the finer apertures of the absorption chamber. Thus a correspondence between the most energetic particles in the incident and exit beam is a real one and repeatable.

The field strength of the measuring magnet is measured by a ballistic galvanometer and a flip coil. The galvanometer throw is read three times. If these readings do not agree with 0.04 cm on a fifty-centimeter scale, the throws are repeated until consistent results are obtained. The galvanometer series resistor is adjusted to give a fifty-centimeter throw for the fastest ions measured.

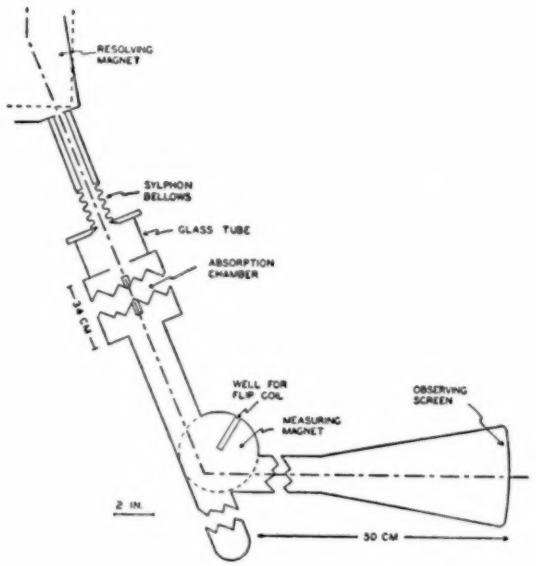

FIG. 1. General plan of the apparatus.

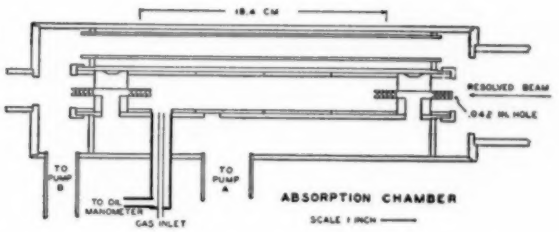

FIG. 2. The absorption chamber showing the pumping and pressure connections.

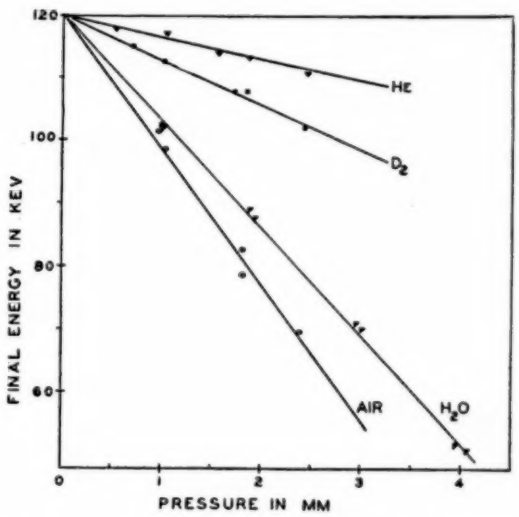

FIG. 3. Energy of the exit beam as a function of pressure in the absorption chamber.

DISCUSSION OF DATA

Tests have been run first to determine the linearity of the loss of energy with respect to the pressure of the absorbing gas. Figure 3 is a sample plot of such data. These measurements, repeated at forty-kilovolt intervals throughout the whole range, show in general that the relation between loss of energy and pressure is linear. A slight departure from linearity is to be expected for large pressures if the loss of energy depends upon the incident energy. For water vapor at a pressure of 5 mm, this deviation from linearity

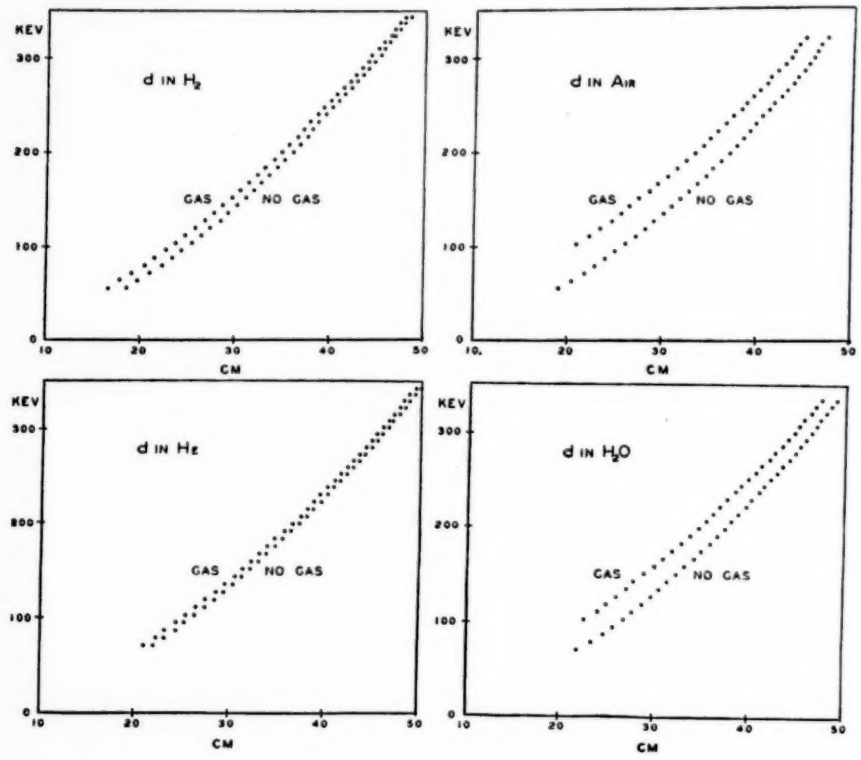

FIG. 4. Incident energy of deuterons as a function of galvanometer deflection for four gases.

is observed in the range where the energy loss is dependent on the incident energy.

To evaluate the energy dependence of the energy losses and to get the most accurate measurements of the magnitude of the loss of energy, data like those shown in Fig. 4 have been taken. It was found that gross changes in the focusing properties of the accelerator tube did affect the energy calibration of the measuring magnet. To overcome this difficulty calibration data were taken concurrently with the energy loss data.

First the field of the measuring magnet is adjusted so that the beam strikes the screen at the fiducial mark with no gas in the absorption chamber. This field strength is then measured by the flip coil and galvanometer. Next gas is admitted to the absorption chamber until the pressure is 2 mm and the field of the measuring magnet is readjusted and measured. This process is repeated in steps of about eight kilovolts throughout the whole available range from 60 to 340 kilovolts. Any disturbance that might affect the galvanometer reading or the beam position will then influence both the observation curve and the calibration curve in the same manner. If some adjustment has to be made, such as the shifting of the galvanometer zero or refocusing the beam, then by repeating the last point after the adjustment the points can be shifted to agree at this value. Since the

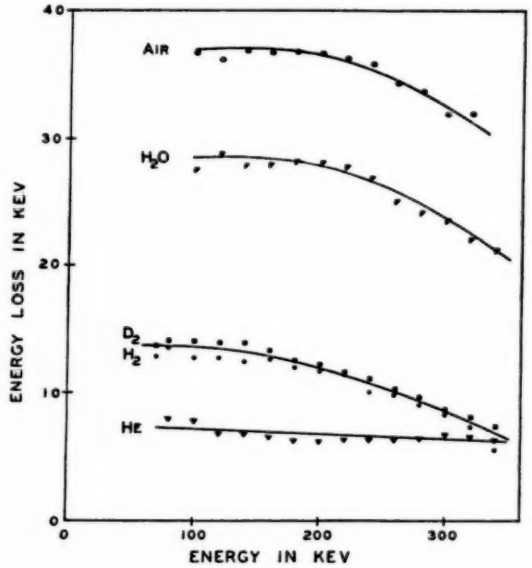

FIG. 5. Loss of energy of deuterons in kev for 18.4-cm path at 2-mm pressure in various gases as a function of incident energy.

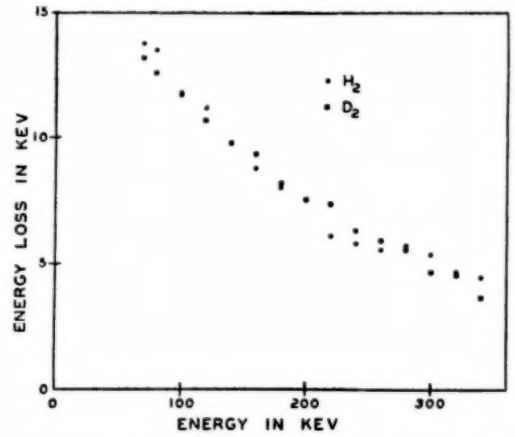

FIG. 6. Loss of energy of protons in kev for 18.4-cm path at 2-mm pressure in H_2 and D_2 as a function of incident energy.

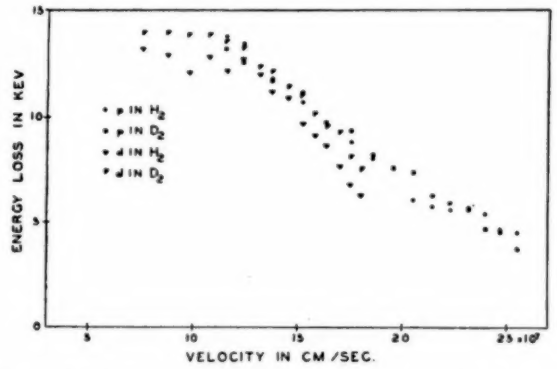

FIG. 7. Loss of energy of protons and deuterons in kev for 18.4-cm path at 2-mm pressure as a function of velocity.

resulting curve always joins smoothly, this shifting is justifiable.

These values are plotted as indicated in Fig. 4. The ordinate is the energy of the particles as they enter the absorbing chamber as measured by the voltmeter. The field strength of the measuring magnet is expressed in terms of the galvanometer deflection of the flip circuit. This deflection is plotted as abscissa. When there is no gas in the chamber, the emergent and incident energies are the same. Thus the curve obtained with no gas, shown on the right in each plot, is a calibration curve showing the energy of the particle corresponding to any galvanometer deflection. In the curve obtained with gas in the absorption chamber, the galvanometer deflection is that corresponding to the energy of the emergent beam. Points on the two

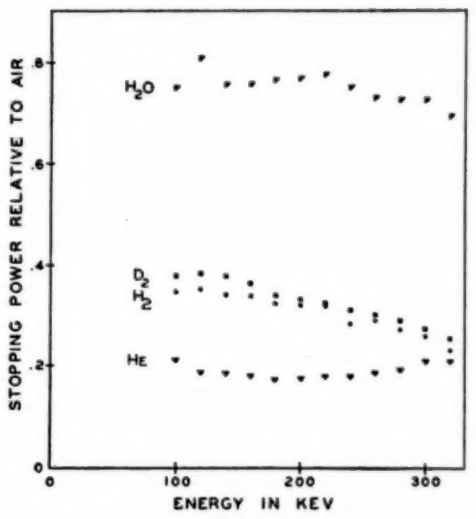

FIG. 8. Stopping power relative to air for various gases as a function of incident energy.

curves having the same abscissa have thus the same energy for the emergent particles. This energy is shown by the ordinate of the point on the curve with no gas. The incident energy is the ordinate of the point on the curve with gas, and the loss of energy is the difference of the ordinates of the two points.

Figures 5 and 6 show plots of the loss of energy in various gases as a function of incident energy. Values for the ordinate were obtained from large scale plots of the observed data. A least squares analysis was also made for some of the data and yielded almost identical results. The difference in the loss of energy in the hydrogen isotope gases is of the same order of magnitude as the accuracy of the observations. This is contrary to preliminary measurements reported in an abstract.[1]

The loss of energy of protons and deuterons of the same velocity is shown in Fig. 7. The values agree sufficiently well to indicate that no difference exists between the isotopic projectiles.

Figure 8 shows stopping powers relative to air.

ACKNOWLEDGMENTS

The author wishes to express his indebtedness to Dr. Victor J. Young and Mr. Henry P. Manning, Jr., for aid and encouragement throughout the course of the work.

[1] C. M. Crenshaw, V. J. Young, H. P. Manning, Phys. Rev. **61**, 388A (1942).

The Propagation of Electromagnetic Waves in Parabolic Pipes

R. D. SPENCE AND C. P. WELLS
Michigan State College, East Lansing, Michigan

(Received May 2, 1942)

The properties of parabolic pipes for the transmission of electromagnetic waves are here analyzed. Formulae are given for the field configurations, critical frequencies, and attenuation constants. The results resemble those obtained by Chu for the elliptical pipe.

IT is the purpose of this paper to present the theory of the transmission of electromagnetic waves in pipes of parabolic cross section. According to Eisenhart[1] the scalar wave equation is separable in only four distinct systems of cylindrical coordinates. On the basis of Eisenhart's criterion the only types of pipes for which the scalar wave equation may be separated are those whose cross sections are either rectangular, circular, elliptical, or parabolic. The first three have been well investigated theoretically, but the fourth has received little if any attention.[2]

The parabolic coordinate system (Fig. 1) used to describe the parabolic pipe is defined by the transformation:

$$x=\tfrac{1}{2}(\eta^2-\xi^2),$$
$$y=\eta\xi,$$
$$z=z.$$

The z axis is taken to be the axis of the pipe and the surface of the pipe itself is formed by the intersection of the two parabolic cylinders $\xi=\eta=$constant.

Plane waves, non-homogeneous in ξ and η, are assumed propagated down the pipe in a positive z direction. This and the assumption of a simple periodic time variation is equivalent to postulating an electromagnetic field of the form:

$$\left.\begin{matrix}\mathbf{E}\\ \mathbf{H}\end{matrix}\right\}=\mathbf{F}(\eta,\,\xi)e^{-hz+\iota\omega t}, \qquad (1)$$

in which ω is equal to 2π times the frequency of the source, and h is the propagation constant in the positive z direction. The propagation constant is itself complex and equal to $\alpha+\beta\iota$ where α is the attenuation constant and β is the phase constant.

The scalar components of the electromagnetic field are obtained from the wave equation and from Maxwell's equations. In parabolic coordinates these are:

$$\left\{\frac{\partial^2}{\partial\eta^2}+\frac{\partial^2}{\partial\xi^2}+\gamma^2(\eta^2+\xi^2)\right\}\left\{\begin{matrix}E_z\\ H_z\end{matrix}\right\}=0, \qquad (2)$$

$$\gamma^2(\eta^2+\xi^2)^{\frac{1}{2}}H_\xi=-h(\partial H_z/\partial\xi)+(\iota\omega\epsilon+\sigma)(\partial E_z/\partial\eta), \qquad (3a)$$

$$\gamma^2(\eta^2+\xi^2)^{\frac{1}{2}}H_\eta=-h(\partial H_z/\partial\eta)-(\iota\omega\epsilon+\sigma)(\partial E_z/\partial\eta), \qquad (3b)$$

$$\gamma^2(\eta^2+\xi^2)^{\frac{1}{2}}E_\xi=-h(\partial E_z/\partial\xi)-\iota\nu\omega(\partial H_z/\partial\eta), \qquad (3c)$$

$$\gamma^2(\eta^2+\xi^2)^{\frac{1}{2}}E_\eta=-h(\partial E_z/\partial\eta)+\iota\nu\omega(\partial H_z/\partial\xi), \qquad (3d)$$

where $\gamma^2=k^2+h^2$ and $k^2=\omega^2\epsilon\nu-\iota\omega\nu\sigma$. We shall call γ the wave guide constant. It will depend only on the physical size of the pipe and the mode of wave excited.

The practical system of units is used, where:

$\epsilon=$dielectric constant $10^{-11}/36\pi$ farads per cm (in air)
$\nu=$permeability $4\pi\times10^{-9}$ henries per cm (in air)
$\sigma=$conductivity in mhos per cm
$H=$magnetic field in amperes per sq. cm
$E=$electric field in volts per cm.

Separating variables in the wave equation leads to the two ordinary differential equations:

$$d^2U/d\xi^2+(\gamma^2\xi^2+m)U=0, \qquad (4a)$$

$$d^2V/d\eta^2+(\gamma^2\eta^2-m)V=0, \qquad (4b)$$

where m is the separation constant, restricted

[1] L. P. Eisenhart, Ann. Math. **35**, 284–305 (1934).
[2] See Lord Rayleigh, Phil. Mag. **43**, 125–132 (1897); G. C. Southworth, Bell Sys. Tech. J. **15**, 284–309 (1936); Carson, Meade, and Schelkunoff, Bell Sys. Tech. J. **15**, 310–333 (1936); W. L. Barrow, Proc. I. R. E. **24**, 1298–1328 (1936); and L. J. Chu, J. App. Phys. **9**, 583–591 (1938).

here to positive integral values. Both of these are forms of the confluent hypergeometric equation[3] or as they are sometimes called, parabolic cylinder equations. Solutions in the form of definite integrals were given by Weber[4] for the problem of the parabolic membrane. Later all solutions were classified by Epstein[5] in connection with the problem of diffraction of light by a parabolic cylinder.

Both even and odd solutions of order m exist for Eqs. (4a) and (4b). We shall designate the even solutions as ${}_eU_m$, ${}_eV_m$ and the odd solutions as ${}_oU_m$, ${}_oV_m$. The solution of the wave equation can then be written:

$$\left.\begin{matrix}E_z\\H_z\end{matrix}\right\}=\sum_{m=0}^{\infty}[b_m\,{}_eU_m(\xi)\,{}_eV_m(\eta)+c_m\,{}_oU_m(\xi)\,{}_oV_m(\eta)]e^{-hz+i\omega t},\quad(5)$$

where b_m and c_m are complex constants and depend upon the strength of excitation.

PERFECTLY CONDUCTING PIPES

The boundary conditions depend upon the assumptions made regarding the conductivity σ. In this section we consider σ to be infinite in the walls of the pipe and zero in the dielectric inside the pipe. Under this condition the tangential components of the electric field vanish at the walls and the propagation constant h reduces to $i\beta$, since the attenuation constant must be zero. Boundary conditions of this type can be satisfied by considering two partial fields to exist in the pipe. The first, called an E wave is defined by $H_z=0$ everywhere inside the pipe, and the second, called an H wave is defined by $E_z=0$ everywhere inside the pipe. Thus for the two partial fields the boundary conditions are:

$$E\text{ wave}\begin{cases}E_z=0, & \xi=\eta=a\\E_\xi=0, & \eta=a\\E_\eta=0, & \xi=a\end{cases}\quad(6a)$$

$$H\text{ wave}\begin{cases}E_\eta=0, & \xi=a\\E_\xi=0, & \eta=a\end{cases}\quad(6b)$$

where $\xi=a$ or $\eta=a$ determines the boundary of the pipe. The boundary conditions are exceptional in that the walls of the pipe are formed by two cylindrical surfaces rather than just one as in the case of the circular or elliptical pipe.[2]

The above boundary conditions can be satisfied by using only one term of the series given by (5). For the E wave the components of the field are:

$$E_z=[b\,{}_eU_m(\xi)\,{}_eV_m(\eta)+c\,{}_oU_m(\xi)\,{}_oV_m(\eta)]e^{-hz+i\omega t},\quad(7a)$$

$$E_\xi=\frac{\beta}{\omega\epsilon}H_\eta=\frac{-i\beta}{\gamma^2(\eta^2+\xi^2)^{\frac{1}{2}}}[b\,{}_eU_m'(\xi)\,{}_eV_m(\eta)+c\,{}_oU_m'(\xi)\,{}_oV_m(\eta)]e^{-hz+i\omega t},\quad(7b)$$

$$E_\eta=\frac{-\beta}{\omega\epsilon}H_\xi=\frac{-i\beta}{\gamma^2(\eta^2+\xi^2)^{\frac{1}{2}}}[b\,{}_eU_m(\xi)\,{}_eV_m'(\eta)+c\,{}_oU_m(\xi)\,{}_oV_m'(\eta)]e^{-hz+i\omega t},\quad(7c)$$

where the primes indicate differentiation with respect to either ξ or η.

In order that the tangential components of the electric field vanish at the boundary, it is

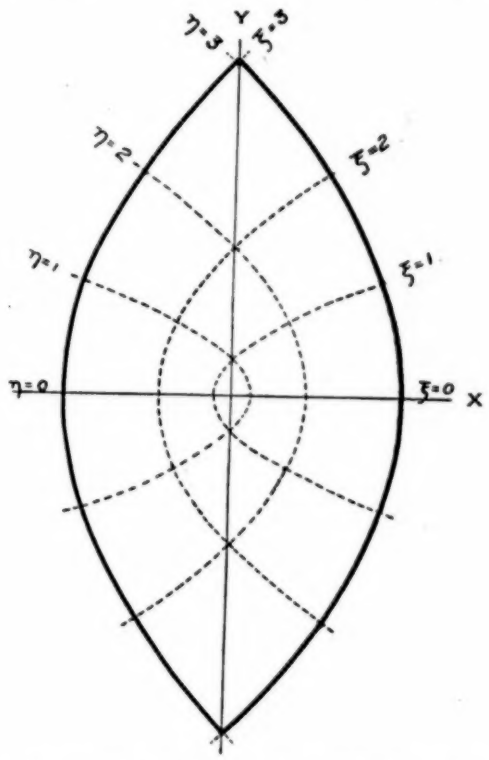

FIG. 1. Cross section of pipe showing parabolic coordinates.

[3] E. T. Whittaker and G. N. Watson, *Modern Analysis* (Cambridge University Press, 1915), second edition, p. 341.

[4] H. Weber, *Die partiellen Differentialgleichungen der math. Physik* (Braunschweig, 1912), fifth edition, Vol. 2, p. 258.

[5] P. S. Epstein, Diss. Munich.

necessary that U and V satisfy the equations:

$$ {}_eU_m(a)=0 \quad {}_eV_m(a)=0, \tag{8a}$$

$$ {}_oU_m(a)=0 \quad {}_oV_m(a)=0. \tag{8b}$$

The roots of these equations serve to determine the critical wave-length. Corresponding to a root a_{nm} where n indicates the number of root and m the order, the critical wave-length is: $\lambda_{nm}=2\pi/\gamma_{nm}$.

For $m=0$ the functions of U and V are identical. In this case it is not hard to verify that they can be written in terms of Bessel functions of $\frac{1}{4}$ and $-\frac{1}{4}$. The even solution is:

$$ {}_eU_o(\xi)=c_1\xi^{\frac{1}{2}}J_{-1/4}(\gamma\xi^2/2); \tag{9a}$$

and the odd solution is:

$$ {}_oU_o(\xi)=c_2\xi^{\frac{1}{2}}J_{1/4}(\gamma\xi^2/2), \tag{9b}$$

where c_1 and c_2 are constants.

In terms of γa^2 a few of the roots of ${}_eU_o(a)=0$ are:

$$\gamma_{10}a^2=4.013, \quad \gamma_{20}a^2=10.246.$$

For the odd solution ${}_oU_o(a)=0$:

$$\gamma_{10}a^2=5.562, \quad \gamma_{20}a^2=11.812.$$

The longest critical wave-length for these modes is given by the even solution:

$$\lambda_{10}=2\pi/\gamma_{10}=2\pi a^2/4.013=0.783y_0,$$

where y_0 is the latus rectum of the parabola $\xi=a$.

For values of $m\neq 0$, there appears to be no simple method of calculating the roots of Eqs. (8a), (8b).

The components of the field for the H wave are:

$$H_z=[b\ {}_eU_m(\xi)\ {}_eV_m(\eta) + c\ {}_oU_m(\xi)\ {}_oV_m(\eta)]e^{-hz+\iota\omega t}, \tag{10a}$$

$$E_\xi=\frac{\omega\nu}{B}H_\eta=\frac{-\iota\omega\nu}{\gamma^2(\eta^2+\xi^2)^{\frac{1}{2}}}[b\ {}_eU_m(\xi)\ {}_eV_m'(\eta) + c\ {}_oU_m(\xi)\ {}_oV_m'(\eta)]e^{-hz+\iota\omega t}, \tag{10b}$$

$$E_\eta=\frac{-\omega\nu}{\beta}H_\xi=\frac{\iota\omega\nu}{\gamma^2(\eta^2+\xi^2)^{\frac{1}{2}}}[b\ {}_eU_m'(\xi)\ {}_eV_m(\eta) + c\ {}_oU_m'(\xi)\ {}_oV_m(\eta)]e^{-hz+\iota\omega t}. \tag{10c}$$

The boundary conditions here are:

$$ {}_eU_m'(a)=0, \quad {}_eV_m'(a)=0,$$
$$ {}_oU_m'(a)=0, \quad {}_oV_m'(a)=0.$$

Again for $m=0$ we can reduce these to fairly simple expressions in terms of Bessel functions. For:

$$ {}_eU_o'(\xi)=\frac{d}{d\xi}[c_1\xi^{\frac{1}{2}}J_{-1/4}(\gamma\xi^2/2)]=c_3\xi^{\frac{1}{2}}J_{3/4}(\gamma\xi^2/2).$$

Also:

$$ {}_oU_o'(\xi)=\frac{d}{d\xi}[c_2\xi^{\frac{1}{2}}J_{1/4}(\gamma\xi^2/2)]=c_4\xi^{\frac{1}{2}}J_{-3/4}(\gamma\xi^2/2).$$

From the equation ${}_eU_0'(a)=0$ we find:

$$\gamma_{10}a^2=6.982, \quad \gamma_{20}a^2=13.305;$$

and from ${}_oU_0'(a)=0$:

$$\gamma_{10}a^2=2.124, \quad \gamma_{20}a^2=8.597.$$

The longest critical wave-length here is:

$$\lambda_{10}=2\pi/\gamma_{10}=2\pi a^2/2.124=1.479y_0.$$

As in the case of the E wave there appears to be no simple method for calculating roots of higher orders.

IMPERFECTLY CONDUCTING PIPES

In this case we consider the conductivity σ to be finite though large. This requires modification of the boundary conditions which now are the continuity of the tangential electric and tangential magnetic fields. The actual fields that exist will be a superposition of the two partial fields which we previously designated as E waves or H waves. However, if the conductivity is large, it will be assumed that one of these partial fields will predominate and we shall still speak of E waves and H waves. For each case we shall define a set of associated impedances which will help clarify the physical statement of the problem.[6] A superscript (1) on the impedance will designate an E wave, and a (2) the H wave. Then by definition:

$$Z_z^{(1)}=E_\xi/H_\eta=-E_\eta/H_\xi=\omega\nu h/k^2=hZ_0/k, \tag{13a}$$

where $Z_0=\omega\nu/k$ is the characteristic impedance. The impedances for the coordinates ξ and η are

[6] J. A. Stratton, *Electromagnetic Theory* (McGraw-Hill, 1941), pp. 354–55.

defined by:

$$E_z = -Z_\xi^{(1)} H_\eta, \quad E_z = Z_\eta^{(1)} H_\xi. \tag{13b}$$

Likewise for the H wave:

$$Z_z^{(2)} = E_\xi/H_\eta = E_\eta/H_\xi = hZ_0/k \tag{14a}$$

and

$$E_\eta = Z_\xi^{(2)} H_z, \quad E_\xi = -Z_\eta^{(2)} H_z. \tag{14b}$$

Because of the similarity of the two boundaries $\xi=a$ and $\eta=a$ we shall limit the remainder of the discussion to the boundary $\xi=a$. Moreover, we shall no longer distinguish between even and odd U and V as the details are the same for both.

For the field outside the boundary of the pipe $\xi=a$ we shall take

$$E_z' = \sum_{m=0}^{\infty} b_m' T_m'(\xi) V_m(\eta) e^{-hz+\iota\omega t}, \tag{15}$$

where $T_m'(\xi)$ represents an asymptotic solution of the confluent hypergeometric equation. The primes will hereafter designate the value of the functions outside the pipe. As an approximation for $T_m'(\xi)$ we shall use:

$$T_m'(\xi) \sim \frac{\exp(-\iota\gamma'\xi^2/2)}{2\gamma'\xi} \cdot e^{\iota(2m+1)\pi/4}, \tag{16}$$

which is valid for values of $\xi \gg m$. Then (15) can be written:

$$E_z' = b' W(\eta) \frac{\exp(-\iota\gamma'\xi^2/2)}{2\gamma'\xi} \cdot e^{-hz+\iota\omega t}, \tag{17}$$

where

$$b'W(\eta) = \sum_{m=0}^{\infty} b_m' V_m(\eta) e^{\iota(2m+1)\pi/4}$$

and b' is a new constant.

The boundary conditions require $H_\eta = H_\eta'$ at $\xi=a$ where:

$$H_\eta = \frac{-\iota\omega\epsilon}{\gamma^2(\eta^2+\xi^2)^{\frac{1}{2}}} \frac{\partial E_z}{\partial \xi}, \quad H_z' = \frac{-\sigma}{\gamma'^2(\eta^2+\xi^2)^{\frac{1}{2}}} \frac{\partial E_z'}{\partial \xi}.$$

We have assumed for the second equation that $\sigma \gg \iota\omega\epsilon$ and $\gamma' \sim k' \sim (-\iota\omega\nu'\sigma)^{\frac{1}{2}}$. Equating H_η and H_η' and setting $V(\eta)/W(\eta)$ equal to unity since it is independent of ξ, gives a relation for the constant b' in terms of b:

$$b' = \frac{-2b\omega\epsilon\gamma'^2 \exp(\iota\gamma' a^2/2)}{\sigma\gamma^2} \frac{dU(a)}{da}. \tag{18}$$

In this expression we have assumed $\iota\gamma' a^2 \gg 1$.

Calculation of the attenuation constant is the principle objective in the imperfectly conducting pipe. This can be done by means of the definition:

$$\alpha = \tfrac{1}{2} w_\xi / w_z, \tag{19}$$

where w_ξ is the power lost through the wall $\xi=a$, and w_z is the power transmitted down the pipe.

In order to evaluate w_z it is necessary to integrate the real part of the Poynting vector in the z direction over the cross section of the pipe. For the E wave this yields:

$$w_z = \frac{|b|^2\beta\omega\epsilon}{2\gamma^4} \int_0^a \int_0^a \left\{ \left| V \frac{dU}{d\xi} \right|^2 + \left| U \frac{dV}{d\eta} \right|^2 \right\} d\xi d\eta. \tag{20}$$

The value of w_z for the H wave can be obtained by replacing ϵ by ν.

The power lost through the wall of the pipe is:

$$w_\xi = \tfrac{1}{2} R \int_0^a \{E_\eta' H_z'^* - E_z' H_\eta'^*\} (\eta^2+\xi^2)^{\frac{1}{2}} d\eta \tag{21}$$

for a unit length of pipe. Here R indicates the real part of the expression and * indicates the complex conjugate.

It is necessary to emphasize that for an imperfectly conducting pipe the so-called E wave actually has a small H_z component present and the so-called H wave has a small E_z component present. In computing the power lost through the pipe these cannot be neglected. Both a magnetic and an electric impedance will exist for either wave. For values of $\sigma \gg \iota\omega\epsilon$ the approximate values of the impedances are:

$$Z_\xi^{(1)} = -\left(\frac{\omega\nu'}{\sigma}\right)^{\frac{1}{2}} \frac{(\eta^2+\xi^2)^{\frac{1}{2}}}{\xi} e^{(\pi/4)\iota} \tag{22a}$$

$$Z_\xi^{(2)} = \left(\frac{\omega\nu'}{\sigma}\right)^{\frac{1}{2}} \frac{\xi}{(\eta^2+\xi^2)^{\frac{1}{2}}} e^{(\pi/4)\iota}. \tag{22b}$$

By means of Eqs. (13) and (14) we find

$$E_z' = \left(\frac{\omega\nu'}{\sigma}\right)^{\frac{1}{2}} \frac{(\eta^2+\xi^2)^{\frac{1}{2}}}{\xi} H_\eta' e^{(\pi/4)\iota},$$

$$E_\eta' = \left(\frac{\omega\nu'}{\sigma}\right)^{\frac{1}{2}} \frac{\xi}{(\eta^2+\xi^2)^{\frac{1}{2}}} H_z' e^{(\pi/4)\iota}. \tag{23}$$

These give for the E wave:

$$w_\xi=\frac{\sqrt{2}}{4}\left(\frac{\omega\nu'}{\sigma}\right)^{\frac{1}{2}}\frac{|b|^2\omega^2\epsilon^2}{a\gamma^4}\left|\frac{dU}{da}\right|^2\int_0^a|V|^2d\eta. \tag{24}$$

The attenuation for the E wave is:

$$\alpha=\frac{1}{2}\left(\frac{\pi\nu'\epsilon}{\nu\sigma}\right)^{\frac{1}{2}}\frac{f^{\frac{1}{2}}}{\left(1-\frac{f_{nm}^2}{f^2}\right)^{\frac{1}{2}}}\frac{\frac{1}{a}\left|\frac{dU}{da}\right|^2\int_0^a|V|^2d\eta}{\int_0^a\int_0^a\left\{\left|V\frac{dU}{d\xi}\right|^2+\left|U\frac{dV}{d\eta}\right|^2\right\}d\xi d\eta}, \tag{25}$$

where $f=\omega/2\pi$ and f_{nm} is the frequency corresponding to the wave-length λ_{nm}.

Following the same method, we find the value of w_ξ for the H wave to be

$$w_\xi=\frac{\sqrt{2}}{4}\left(\frac{\omega\nu'}{\sigma}\right)^{\frac{1}{2}}|b|^2|U(a)|^2\int_0^a\left\{|V|^2-\frac{1}{a}\frac{h^2}{\gamma^4}\left|\frac{dV}{d\eta}\right|^2\right\}d\eta. \tag{26}$$

The attenuation for the H wave is:

$$\alpha=\frac{1}{2}\left(\frac{\pi\nu'\epsilon}{\nu\sigma}\right)^{\frac{1}{2}}\frac{|U(a)|^2}{a}\frac{f_{nm}^{\frac{1}{2}}}{\left(1-\frac{f_{nm}^2}{f^2}\right)^{\frac{1}{2}}}\frac{\left(\frac{f_{nm}}{f}\right)^{\frac{1}{2}}\gamma^2a^2\int_0^a|V|^2d\eta+\left(\frac{f_{nm}}{f}\right)^{-\frac{1}{2}}\left(1-\frac{f_{nm}^2}{f^2}\right)\int_0^a\left|\frac{dV}{d\eta}\right|^2d\eta}{\int_0^a\int_0^a\left\{\left|V\frac{dU}{d\xi}\right|^2+\left|U\frac{dV}{d\eta}\right|^2\right\}d\xi d\eta}. \tag{27}$$

The values of the attenuation for both waves are in agreement with those found by Chu for the pipe of elliptical cross section. Both expressions for the attenuation have one term that varies as $f^{\frac{1}{2}}$, thus increasing with frequency. The attenuation for the H waves has also the term proportional to $f^{-\frac{1}{2}}$ which decreases with increasing frequency. Thus it is of interest to note that the behavior of electromagnetic waves, insofar as the above theory applies, is the same for all cylindrical pipes whose cross sections are defined by coordinates which separate the scalar wave equation.

Experimental work is now in progress to determine ways in which the various partial fields may be excited and to check the values of the critical frequencies and attenuation constants for various modes.

On the Statistical Mechanics of Change of State

H. SNYDER
Northwestern University, Evanston, Illinois
(Received January 10, 1942)

The nature of the pressure against density curve at constant temperature is investigated by the methods of the grand canonical ensemble for a system of identical molecules between which only short range forces act. It is shown that, except for surface effects, the total energy, entropy, etc., are proportional to the number of molecules in the system. The pressure is proven to be a non-decreasing function of the density which may have regions of constancy as a function of the density. This shows rather clearly the impossibility for any analytic equation of the Van der Waals' type being able to give a satisfactory account of condensation without *ad hoc* assumptions.

IT should be possible to understand the isothermal change of a vapor into a liquid in terms of the forces acting between the molecules. Since this change takes place for nearly every system of molecules, one would expect that the detailed nature of the forces is not important. Only such general considerations should enter, as whether the forces are attractive or repulsive, and their behavior for large distances of separation of the molecules.

We shall show for a system of molecules of one species between which only short range forces act that: (a) the pressure is a monotonically increasing function of the density at constant temperature, although there may be regions in which the pressure is independent of the density; (b) the energy, entropy, free energy, etc., are approximately proportional to the number of molecules present. It is only in the asymptotic approximation for a large number of molecules and where the dimensions of the space containing the molecules are large compared to the range of the molecular forces that (a) and (b) hold. The neglected terms may be regarded as giving rise to surface effects. It should not be implied that short range forces are necessary for (a) and (b), although we have been able to show that (a) and (b) are true only for this case.

The grand canonical ensemble will be used for the statistical description of the system because of its elegance and convenience. We will furthermore consider the system to obey the laws of classical mechanics. This has been shown by Kahn and Uhlenbeck[1] not to be an essential restriction. The appearance of Planck's constant in our equation is for dimensional purposes. It has no quantum mechanical implications.

The partition function of a classical grand canonical ensemble with generic phases is

$$e^{-\psi/\vartheta}=\sum_{N=0}^{\infty}\int\cdots\int\frac{\exp\left[-\dfrac{H(p_1,\cdots p_{3}N;x_1,y_1,\cdots z_N)-\alpha N}{\vartheta}\right]}{h^{3N}N!}dp_1\cdots dp_{3N}dx_1\cdots dz_N. \tag{1}$$

In terms of the function, ψ, the pressure, average number of particles in the system, and the mean square fluctuations in the number of particles are:

$$p=-\partial\psi/\partial V, \tag{2}$$

$$(N)_{Av}=-\partial\psi/\partial\alpha, \tag{3}$$

$$\langle[N-(N)_{Av}]^2\rangle_{Av}=-\vartheta\partial^2\psi/\partial\alpha^2. \tag{4}$$

Equations (2) and (3) do not insure the existence of an equation of state. For a general ψ the pressure is not necessarily a function of the temperature and particle density only. To investigate the conditions under which an equation of state exists we write

$$\psi=-V\varphi,\qquad \beta=\ln V. \tag{5}$$

[1] B. Kahn and G. E. Uhlenbeck, Physica **5**, 399 (1938).

Then Eqs. (2) and (3) take the form

$$p=\varphi+(\partial\varphi/\partial\beta), \tag{6}$$

$$\rho=(N)_{Av}/V=\partial\varphi/\partial\alpha, \tag{7}$$

where ρ is the particle density.

The necessary and sufficient condition that the pressure may be written as a function of the density and temperature independent of the volume is that the Jacobian

$$\begin{vmatrix} \frac{\partial p}{\partial\alpha} & \frac{\partial\rho}{\partial\alpha} \\ \frac{\partial p}{\partial\beta} & \frac{\partial\rho}{\partial\beta} \end{vmatrix} = \begin{vmatrix} \frac{\partial\varphi}{\partial\alpha}+\frac{\partial^2\varphi}{\partial\alpha\partial\beta} & \frac{\partial^2\varphi}{\partial\alpha^2} \\ \frac{\partial\varphi}{\partial\beta}+\frac{\partial^2\varphi}{\partial\beta^2} & \frac{\partial^2\varphi}{\partial\alpha\partial\beta} \end{vmatrix} = 0. \tag{8}$$

If φ is independent of β it is evident that (8) will be satisfied. There are, of course, many other functions which would satisfy (8). It is, however, the only form for which total energy, entropy, etc., are proportional to the number of particles. Thus our task of showing (a) and (b) is reduced to the problem of showing that φ is asymptotically independent of β for large dimensions. The truth of (a) follows readily from Eqs. (4), (6), and (7) for φ independent of β. For this condition we find

$$p=\varphi(\alpha), \tag{9}$$

$$\rho=\frac{\partial\varphi(\alpha)}{\partial\alpha}>0, \tag{10}$$

$$\langle[N-(N)_{Av}]^2\rangle_{Av}/\vartheta V=\frac{\partial^2\varphi(\alpha)}{\partial\alpha^2}>0, \tag{11}$$

where these derivatives exist. The inequality in (10) is obvious because the particle density is positive, and similarly that in (11) because the mean square fluctuations in the number of particles is certainly positive. Equation (10) tells us the pressure is an increasing function of α. Equation (11) shows that the density is an increasing function of α. This relation may be inverted to read that α is an increasing function of the density. The fact that α is an increasing function of the density and that the pressure is an increasing function of α implies that the pressure is an increasing function of the density.

However, if $\varphi(\alpha)$ is a continuous function of α with a discontinuity in slope at some point, say $\alpha=\alpha_0$, then the slope of $\varphi(\alpha)$, which is the density, may be considered as taking on all values between the limiting values of the slope from the left and from the right. We now see that this value of $\alpha=\alpha_0$ leads to a region of values of the density in which pressure is independent of the density. Such a point in the curve corresponds to a region in which there are two or more phases present.

The next stage in our development will be to show for systems for which the molecular forces are short range that $\varphi(\alpha, V)$ is asymptotically independent of the dimensions of the system, and that it may have the character indicated in the preceding paragraph. The method by which we do this is based on a power series development for $\varphi(\alpha, V)$ in terms of certain characteristic integrals of the interactions between the molecules and $e^{\alpha/\vartheta}$. Returning to expression (1) for $e^{-\psi/\vartheta}$ we can immediately evaluate the integrals over momentum space, for a Hamiltonian of the form

$$H(p_1, p_2, \cdots, p_{3N}; x_1, y_1, \cdots, z_N) = \frac{1}{2m}\sum_{k=1}^{3N} p_k^2+U(x_1, y_1, \cdots, z_N), \tag{12}$$

in which $U(x_1, y_1, \cdots, z_N)$ is the potential energy of N molecules. We now have

$$e^{-\psi/\vartheta}=\sum_{N=0}^{\infty}\frac{1}{N!}\left\{\frac{(2\pi m\vartheta)^{\frac{3}{2}}}{h^3}e^{\alpha/\vartheta}\right\}^N \times\int\cdots\int dx_1\cdots dz_N \times\exp\left[\frac{-U(x_1, y_1, \cdots, z_N)}{\vartheta}\right]. \tag{13}$$

To obtain the power series indicated above we define the following sequence of functions by the recursion relationships

$$\begin{aligned} W(1)&=S(1)\equiv 1, \\ W(1,2)&=S(1,2)+S(1)S(2), \\ W(1,2,3)&=S(1,2,3)+S(1)S(2,3)+S(2)S(1,3)+S(3)S(1,2)+S(1)S(2)S(3), \\ W(1,2,3,4)&=S(1,2,3,4)+\cdots, \end{aligned} \tag{14}$$

where

$$W(1, 2, \cdots, N) = \exp\left[-U(x_1, \cdots, z_N)/\vartheta\right].$$

The general law of formation, (14), for the functions $S(k_1, k_2, \cdots)$ is as follows. Partition all of the particles numbered 1 to N into sets such that each particle appears in one and only one set. For each set write the symmetric function $S(k_1, k_2, \cdots)$ for the particles appearing in that set. For each partition form the product of the S's for that partition, and sum over all possible partitions of the numbers 1 to N. This sum we set equal to $W(1, 2, \cdots, N)$. It is clear that this operation defines $S(1, 2, \cdots, N)$ in terms of $W(1, 2, \cdots, N)$ and other S's containing fewer than N particles, and consequently, in terms of all of the W's for the particles 1 to N which contain N and fewer of these particles.

We shall call these functions, S, cluster functions because all of them, except those containing only one particle, vanish if we take any one of the particles in them sufficiently far away from the remaining particles so that its interaction energy with them disappears. For short range forces this means that each particle of a particular S must be close to at least one other particle of this S if they are to contribute to the integrals in (13). This fact is quite evident for the case of an S containing only two particles, since $W(1, 2)$ equals one if the two particles are separated far enough. We prove the above for a general S by mathematical induction. Suppose that for $N>2$ the first particle is far away from the remaining ones. Then $W(1, 2, \cdots, N) = W(2, 3, \cdots, N)$. Now separate the right-hand side of (14) into three parts: the single terms $S(1, 2, \cdots, N)$ containing all of the particles; the sum of all the terms with $S(1)$ as a factor, which is $W(2, 3, \cdots, N)$; the sum of the remaining terms in each of which the first particle appears with at least one other particle, and no more than $N-2$ other particles, and each of which is zero by hypothesis. Thus we obtain $W(1, 2, \cdots, N) = W(2, 3, \cdots, N) + S(1, 2, \cdots, N)$ or $S(1, 2, \cdots, N) = 0$.

We define

$$b_l(V) = \frac{1}{Vl!}\int \cdots \int S(1, 2, \cdots, l)\,dx_1 dy_1 \cdots dz_l. \tag{15}$$

In terms of the functions, $b_l(V)$, (13) may now be written

$$e^{-\psi/\vartheta} = \prod_{l=1}^{\infty} \sum_{n_l=0}^{\infty} \frac{1}{n_l!}\left\{\left[\frac{(2\pi m\vartheta)^{\frac{3}{2}} e^{\alpha/\vartheta}}{h^3}\right]^l V b_l(V)\right\}^{n_l}. \tag{16}$$

On carrying out the sums indicated in (16) there results

$$\psi = -\vartheta V \sum_{l=1}^{\infty}\left[\frac{(2\pi m\vartheta)^{\frac{3}{2}}}{h^3} e^{\alpha/\vartheta}\right]^l b_l(V). \tag{17}$$

A comparison of (17) and (5) shows us that

$$\varphi = \vartheta \sum_{l=1}^{\infty}\left[\frac{(2\pi m\vartheta)^{\frac{3}{2}}}{h^3} e^{\alpha/\vartheta}\right]^l b_l(V). \tag{18}$$

A necessary condition that $\varphi(\alpha, V)$ be asymptotically independent of the size of the system is the asymptotic independence of the $b_l(V)$ of V. The independence of the $b_l(V)$ of the volume for large dimensions is a consequence of the fact that the S's vanish unless the particles form a cluster. For any value of l we shall now show that one can find dimensions of the system sufficiently large so that the effect of a given change in the size of the system is as small as one could wish. Consider now the integral which defines $b_l(V)$. Take the coordinates of all of the particles except the first one to be fixed. The value of the integral over the coordinates of the first particle will then depend only upon the relative coordinates of the remaining $(l-1)$ particles except when these particles are near some boundary of the system because the integrand of (15) vanishes unless the first particle is in the neighborhood of the remaining particles. Similarly integrate over the coordinates of the first $(l-1)$ particles. For short range forces the value of this integral is independent of the position of the lth particle unless it is near to a boundary of the system because the value of the integrand of (15) will vanish if any one of the other particles is too far from the lth one and because the integrand depends only upon the relative coordinates of the particles. The distance which we must keep the lth particle from the boundary, in order that the integrals over the remaining particles be independent of the position of the lth particle, will increase as l increases. We now see that the integral over the lth particles will give a factor

proportional to the volume of the system provided the dimensions of the system are so large that the last particle is near the boundary of the system for only a small fraction of the range of integration for which it is far from the boundary. In fact, the difference between the actual factor and the volume is roughly proportional to the surface area of the boundary with a proportionality factor which depends upon l. Thus, $b_l(V)$ may be written approximately as the sum of a term which is a function of l only plus a term proportional to the boundary area divided by the volume. The neglect of the part which depends upon the boundary is not uniform as a function of l, therefore the $b_l(V)$ are asymptotically independent of the volume and boundary.

This asymptotic independence of the $b_l(V)$ of the volume may be supplemented by a rough integration which will suffice to determine the behavior of $b_l(V)$. Integrate over the coordinates of the first particle. We get a contribution to the value of the integral roughly proportional to the cube of the range of the molecular interaction for each of the remaining particles, and consequently, a factor $(l-1)v$, where v is an appropriately defined interaction volume. Similarly, integrating over the coordinates of the second, third, etc., particles we would obtain factors $(l-2)v$, $(l-3)v$, $(l-4)v$, etc. We see that we obtain[2]

$$b_l(V)=f(l,\ V)v^{l-1}, \tag{19}$$

where $|f(l,\ V)|$ is a function of l which varies more slowly than an exponential. If we write

$$z=v\frac{(2\pi m\vartheta)^{\frac{1}{2}}e^{\alpha/\vartheta}}{h^3}$$

and place this expression in Eq. (18) then

$$\varphi(z,\ V)=\frac{\vartheta}{v}\sum_{l=1}^{\infty}f(l,\ V)z^l. \tag{20}$$

The asymptotic independence of the $b_l(V)$ of V is not sufficient to guarantee the asymptotic independence of $\varphi(z,\ V)$ of V. For this, one needs uniform convergence of the power series (20) as a function of V. We define

$$B_l=\frac{1}{Vl!}\int\cdots\int|S(1,2,\cdots,l)|\,dx_1dy_1\cdots dz_l, \tag{21}$$

in which we integrate the variables x_1, y_1, $\cdots$, z_{l-1} over all space, and $x_ly_lz_l$ over V, The B_l are independent of V and also

$$|b_l(V)|\leq B_l. \tag{22}$$

A crude estimation for B_l would show that

$$B_l=F(l)v_0^{l-1}, \tag{23}$$

with v_0 constant and $F(l)$ a slow varying function. Let

$$f(l,\ V)=f^0(l)+f'(l,\ V), \tag{24}$$

where $\lim_{V\to\infty}f'(l,\ V)=0$ and $f^0(l)$ is independent of V. Now write

$$\varphi(z,\ V)=\frac{\vartheta}{v}\left[\sum_{l=1}^{N}f^0(l)z^l+\sum_{l=1}^{N}f'(l,\ V)z^l+\sum_{l=N+1}^{\infty}f(l,\ V)z^l\right]. \tag{25}$$

Equations (22) and (23) give us

$$\left|\sum_{l=N+1}^{\infty}f(l,\ V)z^l\right|\leq\sum_{l=N+1}^{\infty}F(l)\left\{\frac{v_0}{v}|z|\right\}^l. \tag{26}$$

For $z<v/v_0$ the series on the right side of (26) converges. Therefore, there exists an N such that

$$\left|\sum_{l=N+1}^{\infty}f(l,\ V)z^l\right|<\frac{\epsilon}{2}, \tag{27}$$

with ϵ any positive quantity. For this fixed N there exists a sufficiently large V such that

$$\left|\sum_{l=1}^{N}f'(l,\ V)z^l\right|<\frac{\epsilon}{2}. \tag{28}$$

This implies that

$$\lim_{V\to\infty}\varphi(z,\ V)=\varphi(z) \tag{29}$$

exists, which is all that is required. The uniform convergence[3] of the series (20) enables us to

[2] This form for the $b_l(V)$ is also given by Mayer and Mayer, *Statistical Mechanics* (John Wiley and Sons, 1940), p. 298.

[3] The uniform convergence of series (20) follows if a series of the form $\sum_{l=1}^{\infty}B_lz^l$ has a finite radius of convergence.

consider the $b_l(V)$ to be independent of the dimensions of the system as long as they are sufficiently large.

For a slowly varying $f(l)$, the nearest singularities of $\varphi(z)$ are on the unit circle. At sufficiently low temperatures, and if the forces have regions where they are attractive, then it is true that the b_l are positive.[4] The only question which remains before us is whether a convergent power series can represent a function which for real z is continuous at $z=1$ with a discontinuity in slope.

We will show this by constructing a function with these properties. Take the function defined by the integral

$$g(z)=\frac{z-1}{2}\int_0^{\theta_0} h(\theta)\left[\frac{1}{z-e^{i\theta}}+\frac{1}{z-e^{-i\theta}}\right]d\theta, \quad (30)$$

in which θ_0 is less than π, and where $h(\theta)$ is a continuous positive function possessing derivatives of at least the third order, where $h'(0)<0$, and where $h(\theta)$ has a contact of at least the third order at $\theta=\theta_0$. This function, $g(z)$, is continuous at $z=1$, and for real z there is a discontinuity in the first derivative at this point. For $|z|<1$, $g(z)$ can be expanded into a convergent power series, $g(z)=\sum c_n z^n$, all of whose coefficients, c_n, except finitely many are positive. This defect in $g(z)$ could be readily remedied by the addition of an appropriate polynomial to the integral. The coefficients of z^n are, except for the first term,

$$c_n=\int_0^{\theta_0} h(\theta)[\cos n\theta-\cos(n+1)\theta]d\theta. \quad (31)$$

Integrating by parts three times we obtain

$$c_n=-h'(0)\left[\frac{2n+1}{n^2(n+1)^2}\right]-\int_0^{\theta_0} h'''(\theta)\left[\frac{\sin n\theta}{n^3}-\frac{\sin(n+1)\theta}{(n+1)^3}\right]d\theta. \quad (32)$$

[4] Reference 2, pp. 305–308.

It is clear that since the first term of c_n is positive and of order $-h'(0)/n^3$, and the second term, the integral, is of order $1/n^4$ or smaller, only finitely many of the c_n can be negative. To such a function $g(z)$ an appropriate entire function can be added so that the sum has the properties shown in Eqs. (10) and (11).

The fact that we have been able to construct a function possessing the appropriate properties is no guarantee that the functions defined by the power series (20) will have these properties. We must distinguish several possible cases for functions defined by power series such as (20):

(a) The functions $\varphi(z, V)$ do not have analytic continuations for real $z>1$.

(b) They do have an analytic continuation for real $z>1$, but for these z the $\lim_{V\to\infty}\varphi(z, V)$ does not exist. This means that the $\varphi(z, V)$ are not uniformly bounded for real $z>1$.

(c) The analytic continuation of the $\varphi(z, V)$ exists for real $z>1$ and $\varphi(z, V)$ approaches a limit as V tends to infinity. In this case the continuation of the function $\varphi(z)$ defined by (29) will exist and is the same as the $\lim_{V\to\infty}\varphi(z, V)$ for real $z>1$.

If conditions (a) or (b) hold, then one can only say that the grand canonical ensemble may not be used for the description of condensed systems. If (c) holds then all of our previous conclusions are valid. We would then be at considerable variance with the conclusions of K. Fuchs.[5] In his work the volume dependence of the cluster integrals was used to explain the vapor pressure curve between a solid and a gas. Also, in our development surface effects appear in a very general manner from the term in $b_l(V)$ which is proportional to the boundary area divided by the volume. This is quite different from the case where one uses the canonical ensemble where they appear in terms of very special properties assumed for the $b_l(V)$.[6]

[5] K. Fuchs, Proc. Roy. Soc. **179**, 194–301 (1941).
[6] Reference 2, p. 313.

A Generalized Electrodynamics

Part I—Non-Quantum

BORIS PODOLSKY
Department of Physics, University of Cincinnati, Cincinnati, Ohio

(Received March 23, 1942)

If one wishes to derive generalized field equations from a Lagrangian, at the same time preserving the linear character of the equations, one must admit terms involving derivatives of the field quantities. It turns out that the only non-trivial generalization of this kind, leading to differential equations of order below eighth, is obtained by taking $L_f=(1/8\pi)\{\frac{1}{2}F_{\alpha\beta}^2+a^2(\partial F_{\alpha\beta}/\partial x_\beta)^2\}$. This leads to a theory that contains the Landé-Thomas theory and accounts for the choice of sign required when one wishes to consider the total field as consisting of the Maxwell-Lorentz and the Yukawa fields.

1. INTRODUCTION

IF one assumes that the equations of electrodynamics are derivable from some Lagrangian L, and wishes to preserve the linear character of the field equations (The Principle of Superposition) in order to make the quantization easy, then, unless one is prepared to introduce new kinds of field quantities, the only way of generalizing the Maxwell-Lorentz theory appears to be by permitting the Lagrangian of the field to contain terms involving derivatives of the field quantities $\mathbf{E}$ and $\mathbf{H}$.

One then obtains, as the field equations, partial differential equations of an order higher than the usual second. Far from being objectionable, this appears to be what is needed. For, the various proposed methods of "cutting off" effects of higher frequencies seems to indicate clearly that the higher derivatives, which become important for higher frequencies, are not properly taken care of by the usual second-order equations. Further, the extra freedom of choice of a solution to be used in any particular problem, provided by equations of higher order, permits of an imposition of finiteness conditions, analogous to Schroedinger's procedure, which serves also to remove infinities inherent in the usual treatment of point charges.

2. NON-RELATIVISTIC CASE

The usual Lagrangian of the field in this case, in electrostatic units, is:

$$\bar{L}_f\equiv\int L_f dV=\frac{1}{8\pi}\int \mathbf{E}^2 dV. \qquad (2.1)$$

To preserve the linearity of the field equations the additional terms have to be quadratic in $\mathbf{E}$ and its derivatives. If we limit ourselves to field equations of an order not higher than *sixth*, the highest derivative of $\mathbf{E}$ that may occur is second. Investigating all possible combinations of the operator ∇ and $\mathbf{E}$ satisfying these requirements, one finds that all such combinations either vanish identically, by virtue of the condition $\mathbf{E}=-\nabla\varphi$ (the result of preserving unchanged the term in the total Lagrangian representing the interaction of the field and particles), or differ by a divergence from $(\nabla\cdot\mathbf{E})^2$. Since addition of a divergence to L_f does not alter the field equations, we may take, as the only generalization giving anything new,

$$L_f=(1/8\pi)[\mathbf{E}^2\pm a^2(\nabla\cdot\mathbf{E})^2]. \qquad (2.2)$$

The constant a thus introduced has the dimension of length, but otherwise remains arbitrary, as does also the sign of the whole additional term.

The field equations are now:

$$(1\mp a^2\nabla^2)\nabla\cdot\mathbf{E}=4\pi\rho \quad \text{and} \quad \nabla\times\mathbf{E}=\mathbf{0}. \qquad (2.3)$$

Although both choices of the sign admit of solutions without infinities, I am inclined to the belief, based on the study of the types of waves occurring in the corresponding relativistic generalization, that eventually only the upper sign will turn out to give physically significant results. The following investigation is therefore based on the tentative assumption that the upper sign is to be used in Eqs. (2.2) and (2.3).

The generalized Poisson equation is now:

$$(1-a^2\nabla^2)\nabla^2\varphi=-4\pi\rho; \qquad (2.4)$$

and if we put

$$\rho = e\delta(\mathbf{r}), \tag{2.5}$$

which corresponds to a point charge e located at the origin, the only solution of Eq. (2.4), finite everywhere and vanishing at infinity, is:

$$\varphi = (e/r)(1-e^{-r/a}). \tag{2.6}$$

This result is of the same form as the electrostatic potential obtained by Landé and Thomas.[1] However, we are here not limited to values of a consistent with their special assumption of meson involvement in the electronic interaction. In fact, later considerations seem to suggest that

$$a = h/mc, \tag{2.7}$$

which, on the Landé-Thomas theory, would correspond to the meson mass being equal to m (instead of 2×137 m). This would mean that the meson here is a neutrino. However, no such interpretation is here necessary, nor apparently desirable. In Section 4 we shall consider more fully the relation of the present theory to that of Landé and Thomas.

3. RELATIVISTIC EQUATIONS

Using $x_4 = ict$ and $-ds^2 = dx_\alpha{}^2$, with the usual summation convention, we need not distinguish between covariant and contravariant tensors. Letting

$$F_{\alpha\beta} = -F_{\beta\alpha} = (\partial\varphi_\beta/\partial x_\alpha) - (\partial\varphi_\alpha/\partial x_\beta) \tag{3.1}$$

with

$$\varphi_\alpha = (\mathbf{A}, i\varphi), \tag{3.2}$$

where $\mathbf{A}$ is the vector potential and φ the scalar potential, we have: $F_{12} = H_3$, $F_{23} = H_1$, $\cdots F_{14} = -iE_1$, $\cdots$ etc.; and, as usual,

$$\mathbf{E} = -\nabla\varphi - (1/c)\dot{\mathbf{A}} \quad \text{and} \quad \mathbf{H} = \nabla\times\mathbf{A}. \tag{3.3}$$

One set of the field equations is then the usual

$$\partial F_{\alpha\beta}/\partial x_\gamma + \partial F_{\beta\gamma}/\partial x_\alpha + \partial F_{\gamma\alpha}/\partial x_\beta = 0, \tag{3.4}$$

or

$$\nabla\times\mathbf{E} + (1/c)\dot{\mathbf{H}} = \mathbf{0} \quad \text{and} \quad \nabla\cdot\mathbf{H} = 0. \tag{3.5}$$

Equations of motion of a particle are, in the usual way,

$$(d^2x_\alpha/ds^2) = (e/mc^2)F_{\alpha\beta}(dx_\beta/ds), \tag{3.6}$$

or

$$\frac{d}{dt}\left[\frac{m\mathbf{v}}{(1-v^2/c^2)^{\frac{1}{2}}}\right] = e\left(\mathbf{E} + \frac{\mathbf{v}}{c}\times\mathbf{H}\right). \tag{3.7}$$

[1] A. Landé and L. H. Thomas, Phys. Rev. **60**, 514 (1941).

The only independent relativistically invariant generalization of Eq. (2.2) is found to be[2]

$$L_f = \frac{1}{8\pi}\left\{\frac{1}{2}F_{\alpha\beta}{}^2 + a^2\left(\frac{\partial F_{\alpha\beta}}{\partial x_\beta}\right)^2\right\} \tag{3.8}$$

$$= \frac{1}{8\pi}\left\{\mathbf{E}^2 - \mathbf{H}^2 + a^2\left[(\nabla\cdot\mathbf{E})^2 - \left(\nabla\times\mathbf{H} - \frac{1}{c}\dot{\mathbf{E}}\right)^2\right]\right\}. \tag{3.9}$$

The resulting field equations are:

$$\left(1 - a^2\frac{\partial^2}{\partial x_\alpha{}^2}\right)\frac{\partial F_{\beta\gamma}}{\partial x_\gamma} = 4\pi j_\beta, \tag{3.10}$$

or

$$(1-a^2\Box)\nabla\cdot\mathbf{E} = 4\pi\rho$$

and

$$(1-a^2\Box)\left(\nabla\times\mathbf{H} - \frac{1}{c}\dot{\mathbf{E}}\right) = 4\pi\rho\mathbf{v}/c, \tag{3.11}$$

where the four-vector j_α is defined by

$$j_\alpha = (\rho\mathbf{v}/c, i\rho), \tag{3.12}$$

with

$$\rho(\mathbf{r}) = \textstyle\sum_s e_s\delta(\mathbf{r} - \mathbf{r}_s). \tag{3.13}$$

The summation here is over all the particles; the sth particle having the charge e_s and the position $\mathbf{r}_s = \mathbf{r}_s(t)$.

With the usual restriction on the potentials,

$$(\partial\varphi_\alpha/\partial x_\alpha) \equiv \nabla\cdot\mathbf{A} + (1/c)\dot{\varphi} = 0, \tag{3.14}$$

we obtain:

$$(1-a^2\Box)\Box\varphi_\alpha = -4\pi j_\alpha, \tag{3.15}$$

a set of fourth-order partial differential equations.

4. RELATION TO THE LANDÉ-THOMAS THEORY

Although the present generalization consists merely of an addition of a comparatively simple term to the Lagrangian of the field, see Eq. (3.8), it contains the Landé-Thomas theory as a special case, and shows in a way why their particular way of combining Maxwell-Lorentz and Yukawa fields should work.

For, let

$$(1-a^2\Box)\varphi_\alpha \equiv \varphi_\alpha{}''; \tag{4.1}$$

[2] A possible addition of a term $b\mathbf{E}\cdot\mathbf{H}$ is trivial, since, by virtue of Eq. (3.4), $\mathbf{E}\cdot\mathbf{H} = \partial J_\alpha/\partial x_\alpha$, a four-dimensional divergence of the four-vector $J_\alpha = (i/4)\epsilon_{\alpha\beta\gamma\delta}F_{\beta\gamma}\varphi_\delta$, and does not affect the resulting field equations.

then Eq. (3.15) becomes

$$\Box\varphi_\alpha''=-4\pi j_\alpha, \tag{4.2}$$

so that φ_α'' is the usual Maxwell-Lorentz potential. If we now put

$$\varphi_\alpha\equiv\varphi_\alpha''-\varphi_\alpha', \tag{4.3}$$

substitution into Eq. (4.1), with the use of Eq. (4.2), gives

$$(1-a^2\Box)\varphi_\alpha'=4\pi a^2 j_\alpha. \tag{4.4}$$

Equations (4.2) and (4.4), with a suitable choice of a, are just the Landé-Thomas equations for the Maxwell-Lorentz and the Yukawa parts of the field, respectively. The minus sign in Eq. (4.3), which Landé and Thomas found necessary to introduce *ad hoc*, is here required to give Eq. (4.4). In other words, *if* we wish to consider φ_α as the sum of the Maxwell-Lorentz and Yukawa fields, these *must* be combined by subtracting the latter from the former. The same kind of analysis applies also to the energies. The choice of the opposite sign in Eq. (2.2) would lead to solutions of entirely different form, and has nothing to do with the present question.

5. ENERGY-MOMENTUM TENSOR

The derivation of the energy-momentum tensor is closely related to the problem of finding the Hamiltonian corresponding to the Lagrangian (3.8), which is necessary for the quantization of the field. I therefore reserve it for Part II of this report, giving here merely the result:

$$\begin{aligned}4\pi icT_{\mu\nu}&=F_{\mu\alpha}F_{\nu\alpha}-\tfrac{1}{4}F_{\alpha\beta}F_{\alpha\beta}\delta_{\mu\nu}\\&+(a^2/2)[F_{\alpha\beta}\Box F_{\alpha\beta}+(\partial F_{\alpha\beta}/\partial x_\beta)(\partial F_{\alpha\gamma}/\partial x_\gamma)]\delta_{\mu\nu}\\&-a^2[F_{\mu\alpha}\Box F_{\nu\alpha}+F_{\nu\alpha}\Box F_{\mu\alpha}\\&\qquad+(\partial F_{\mu\alpha}/\partial x_\alpha)(\partial F_{\nu\beta}/\partial x_\beta)].\end{aligned} \tag{5.1}$$

This leads to the expression for the energy

$$\begin{aligned}E=\frac{c}{i}\int T_{44}dV&=\frac{1}{8\pi}\int(\mathbf{E}^2+\mathbf{H}^2)dV\\&-\frac{a^2}{8\pi}\int\left\{(\nabla\cdot\mathbf{E})^2+\left(\nabla\times\mathbf{H}-\frac{1}{c}\dot{\mathbf{E}}\right)^2\right.\\&\left.+2(\mathbf{H}\cdot\Box\mathbf{H}+\mathbf{E}\cdot\Box\mathbf{E})\right\}dV.\end{aligned} \tag{5.2}$$

In electrostatics this reduces to

$$E=\frac{1}{8\pi}\int\{\mathbf{E}^2-a^2[(\nabla\cdot\mathbf{E})^2+2\mathbf{E}\cdot\nabla^2\mathbf{E}]\}dV. \tag{5.3}$$

Making use of $\nabla\times\mathbf{E}=\mathbf{0}$, and assuming that $\mathbf{E}\nabla\cdot\mathbf{E}$ vanishes at infinity faster than $1/r^2$, one finds that Eq. (5.3) can easily be put in the form

$$E=\frac{1}{8\pi}\int\{\mathbf{E}^2+a^2(\nabla\cdot\mathbf{E})^2\}dV, \tag{5.4}$$

which is obviously positive. For the field of a point charge given by Eq. (2.2) this turns out to be $e^2/2a$.

6. WAVES

In the absence of *electrified matter* Eq. (3.15) becomes

$$(1-a^2\Box)\Box\varphi_\alpha(\mathbf{r},t)=0. \tag{6.1}$$

When we assume $\varphi_\alpha(\mathbf{r},t)$ to be real, the general solution of this equation is:

$$\begin{aligned}\varphi_\alpha(\mathbf{r},t)=&\left(\frac{1}{2\pi}\right)^{\frac{1}{2}}\int\{\varphi_\alpha(\mathbf{k})\exp i(\mathbf{k}\cdot\mathbf{r}-ckt)\\&+\varphi_\alpha^*(\mathbf{k})\exp -i(\mathbf{k}\cdot\mathbf{r}-ckt)\}dk\\&+\left(\frac{1}{2\pi}\right)^{\frac{1}{2}}\int\{\tilde{\varphi}_\alpha(\mathbf{k})\exp i(\mathbf{k}\cdot\mathbf{r}-c\tilde{k}t)\\&+\tilde{\varphi}_\alpha^*(\mathbf{k})\exp -i(\mathbf{k}\cdot\mathbf{r}-c\tilde{k}t)\}dk;\end{aligned} \tag{6.2}$$

where $\mathbf{k}$ is the wave vector, the direction of which is the direction of propagation of the component plane wave and the magnitude of which is $k=2\pi/\lambda$, λ being the wave-length; $dk=dk_x dk_y dk_z$; $\tilde{k}=(1+a^2k^2)^{\frac{1}{2}}/a$; $\varphi_\alpha(\mathbf{k})$ and $\tilde{\varphi}_\alpha(\mathbf{k})$ are two arbitrary independent functions of $\mathbf{k}$; and the asterisk denotes the complex conjugate of the quantity to which it is attached. If the reality assumption is omitted, the asterisk then denotes merely another independent function of $\mathbf{k}$.

The first integral in Eq. (6.2) is the general solution of the ordinary wave equation, which was previously used and found convenient.[3] I shall refer to waves thus represented as the *ordinary waves*. The second integral gives the *extraordinary waves*, and are distinguished by a *tilde* ($\tilde{}$).

If a wave is considered as being associated with a particle, then, corresponding to a term

[3] V. Fock and B. Podolsky, Physik. Zeits. der Sowjetunion **1**, 801 (1932).

$\varphi_a(\mathbf{k}) \exp(i\mathbf{k}\cdot\mathbf{r}-i\omega t)$, quantum mechanics assigns the energy $E=\hbar\omega$ and the momentum $\mathbf{p}=\hbar\mathbf{k}$. Thus, corresponding to the ordinary waves, since in that case $\omega=ck$, the relation between the energy and momentum is

$$E^2=c^2p^2, \tag{6.3}$$

which is the relativistic relation between the energy and momentum for a free particle of *zero* mass.

For the extraordinary waves, however, $\omega=c\tilde{k}$, which gives

$$\tilde{E}^2=(ch\tilde{k})^2=c^2\tilde{p}^2+c^2h^2/a^2. \tag{6.4}$$

This is the relativistic relation between the energy and momentum of a free particle of a finite mass

$$m=h/ac. \tag{6.5}$$

Since we have assumed space to be free of electrified particles, we must suppose that the general electromagnetic field contains neutral particles, which I tentatively assume to be *neutrinos*. Then, m is the neutrino mass, and

$$a=h/mc. \tag{6.6}$$

Finally, we note that the second integral in Eq. (6.2) satisfies the differential equation

$$(1-a^2\Box)\psi=0, \tag{6.7}$$

and is the de Broglie wave for a particle of mass given by Eq. (6.5). In the non-relativistic approximation Eq. (6.7) is the Schroedinger equation for a neutral particle.

I am grateful to Professor Samuel J. M. Allen for his friendly interest in this problem.

JULY 1 AND 15, 1942 PHYSICAL REVIEW VOLUME 62

The Vibration of Piezoelectric Plates

A. W. LAWSON
Randal Morgan Laboratory of Physics, University of Pennsylvania, Philadelphia, Pennsylvania
(Received April 24, 1942)

The characteristic frequencies of infinite piezoelectric plates vibrating between the grounded electrodes of a plane parallel condenser have been rigorously investigated. It is found that the frequencies depend on the piezoelectric constants as well as the elastic constants of the crystal. The effective elastic constants for a piezoelectric crystal do not in general satisfy the same symmetry relations as the true elastic constants. For odd harmonics, which are the only modes which can be excited by a uniform electric field, the strain does not vanish at the surface of the plate for a finite gap between the electrodes. Consequently, the frequencies of free vibration also depend on the separation of the electrodes, and the rigorous theory shows this dependence should not be linear as hitherto supposed. The effect of the gap decreases as the square of the harmonic number and hence the higher frequencies of vibration are not exactly harmonics of the fundamental.

THE object of this paper is to give a rigorous treatment of the free vibrations of an infinite piezoelectric plate vibrating between two grounded infinite electrodes. These frequencies are the resonant frequencies of the plate when driven by an alternating voltage on the electrodes. This theory is an excellent approximation for a finite plate whose thickness is small compared to its lateral dimensions. The general theory of non-piezoelectric plates has been given by Koga,[1] and special cases of piezoelectric plates have been discussed by Cady.[2] The general theory for piezoelectric plates is similar to that of Koga for ordinary plates but is complicated by the fact that it is necessary to solve Maxwell's equations simultaneously with the differential equations for the propagation of elastic waves. It will appear that Cady's particular solution is an excellent first approximation but is not self-consistent.

If, in an anisotropic substance, u is the displacement vector, θ the strain tensor, ϕ the

[1] I. Koga, Physics **3**, 70 (1932).

[2] W. G. Cady, Physics **7**, 237 (1936).

stress tensor, c the elastic tensor, E the electric field intensity, P the polarization, e the piezoelectric tensor, k the susceptibility tensor, and ρ the density, we have for our fundamental elastic wave equations

$$\sum_i \partial\varphi_{ij}/\partial x_i=\rho\ddot{u}_j, \quad j=1, 2, 3; \tag{1}$$

where

$$\varphi_{ij}=\sum_{\alpha\beta} c_{ij\alpha\beta}\theta_{\alpha\beta}-\sum_{\gamma} e_{ij\gamma}E_\gamma, \tag{2}$$

and
$$\theta_{\alpha\beta}=\partial u_\alpha/\partial x_\beta, \quad \text{if} \quad \alpha=\beta;$$
$$\theta_{\alpha\beta}=\partial u_\alpha/\partial x_\beta+\partial u_\beta/\partial x_\alpha, \quad \text{if} \quad \alpha\neq\beta. \tag{3}$$

The use of this somewhat cumbersome notation is to ensure that the magnitudes of the elastic and piezoelectric constants will be the same as those employed by Voigt. Finally, we have

$$P_i=\sum_{\alpha\beta} e_{\alpha\beta i}\theta_{\alpha\beta}+\sum_{\gamma} k_{\gamma i}E_\gamma. \tag{4}$$

It is immediately evident from Eq. (4) that the polarization in the medium is not in general collinear with the electric field intensity.

Now, if we restrict our attention to the case of a plate oriented perpendicular to x_1, then we have

$$\partial/\partial x_2=\partial/\partial x_3=0. \tag{5}$$

In virtue of Eqs. (2), (3), and (5), we may write Eq. (1) as

$$\sum_\alpha\left\{\frac{\partial^2}{\partial x_1^2}(c_{1j\alpha1}u_\alpha)-e_{1j\alpha}\frac{\partial E_\alpha}{\partial x_1}\right\}=\rho\ddot{u}_j. \tag{6}$$

Moreover, we have from electromagnetic theory

$$c\nabla\times\mathbf{E}=-\dot{\mathbf{B}}, \tag{7}$$

where $\dot{\mathbf{B}}$ is the magnetic field intensity, and

$$\nabla\cdot\mathbf{D}=0, \tag{8}$$

where $\mathbf{D}$ is the electric induction vector. From Eqs. (5) and (8), we obtain

$$\frac{\partial E_1}{\partial x_1}+4\pi\sum_\alpha\left\{k_{\alpha1}\frac{\partial E_\alpha}{\partial x_1}+e_{\alpha11}\frac{\partial u_\alpha}{\partial x_1}\right\}=0, \tag{9}$$

where the quantities E_α are the components of the electric field along axes chosen perpendicular and parallel to the surface of the plate. Thus E_1 is the electric field intensity along x_1. Neglecting $\dot{\mathbf{B}}$ in Eq. (7), we have

$$\partial E_\alpha/\partial x_\beta-\partial E_\beta/\partial x_\alpha=0, \ \beta=\alpha-1; \ \alpha=1, 2, 3, \tag{10}$$

whence

$$\partial E_2/\partial x_1=\partial E_3/\partial x_1=0. \tag{11}$$

So Eq. (9) reduces to

$$K_{11}\frac{\partial E_1}{\partial x_1}+4\pi\sum_\alpha e_{\alpha11}\frac{\partial u_\alpha}{\partial x_1}=0, \tag{12}$$

where

$$K_{11}\equiv1+4\pi k_{11}, \tag{13}$$

which when substituted in Eq. (6) yields

$$\sum_\alpha\frac{\partial^2}{\partial x_1^2}\{c^*_{1j\alpha1}u_\alpha\}=\rho\ddot{u}_j, \tag{14}$$

where

$$c^*_{1j\alpha1}\equiv c_{1j\alpha1}+\frac{4\pi e_{1j1}e_{\alpha11}}{K_{11}}. \tag{15}$$

Taking the origin at the center of the plate, we shall now assume that

$$u_j^r=A_j^r\sin\frac{n\pi x_1}{s_r}\exp i\omega_r t, \quad n \text{ odd}; \tag{16}$$

and

$$u_j^r=A_j^r\cos\frac{n\pi x_1}{s_r}\exp i\omega_r t, \quad n \text{ even}. \tag{17}$$

We then have the secular system

$$\sum_\alpha c^*_{1j\alpha1}A_\alpha^r-\kappa_r^2A_j^r=0, \quad j=1, 2, 3; \tag{18}$$

where

$$\kappa_r^2=4\rho s_r^2f_r^2/n^2, \quad f_r=\omega_r/2\pi. \tag{19}$$

We define

$$\xi_r=\sum_j A_j^r u_j^r. \tag{20}$$

Then our differential equations become

$$\frac{\partial^2\xi_r}{\partial x_1^2}=\frac{\rho}{\kappa_r^2}\ddot{\xi}_r, \quad r=1, 2, 3; \tag{21}$$

where κ_1^2, κ_2^2, κ_3^2 are the roots of the cubic equation

$$\begin{vmatrix} c^*_{1111}-\kappa^2 & c^*_{1121} & c^*_{1131} \\ c^*_{1211} & c^*_{1221}-\kappa^2 & c^*_{1231} \\ c^*_{1311} & c^*_{1321} & c^*_{1331}-\kappa^2 \end{vmatrix}=0. \tag{22}$$

Corresponding to Eqs. (16) and (17), we assume that

$$\xi_r=\xi_r^0\sin\frac{n\pi x_1}{s_r}\exp i\omega_r t, \quad n \text{ odd}; \tag{23}$$

and

$$\xi_r=\xi_r^0\cos\frac{n\pi x_1}{s_r}\exp i\omega_r t, \quad n \text{ even}. \tag{24}$$

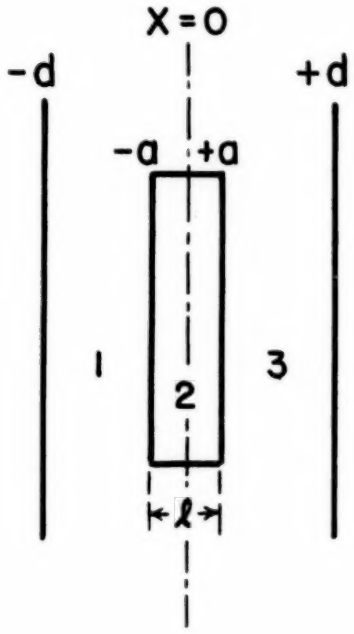

FIG. 1. Arrangement of crystal air gaps and electrodes.

Here we regard s_r as an unknown to be determined by the boundary conditions, which are at $x_1=\pm a$.

$$X_x=X_z=X_y=0, \tag{25}$$

$$\mathbf{n}\times(\mathbf{E}-\mathbf{E}^0)=0, \tag{26}$$

$$\mathbf{n}\cdot(\mathbf{D}-\mathbf{D}^0)=0, \tag{27}$$

when the origin is chosen at the center of the plate and $2a\equiv l$, the thickness of the plate.

The exact formulation of these conditions depends on the physical situation. In practice, the crystalline plate is inserted between two electrodes which are parallel to the surface of the plate. An alternating difference of potential between the two plates is used to excite resonant vibrations in the plate. We shall, however, assume that the plates are at zero potential and inquire into the characteristic frequencies of free vibration in this case. These are also the frequencies at which a driving voltage on the electrodes will produce resonance, but the expressions for the displacement are then considerably more complicated.[3] Since only the resonant frequencies are of practical interest, we shall not attempt to formulate the expressions for the displacements in the case of forced vibrations. Confining our attention to the case when the electrodes are grounded, we conclude by symmetry that the external electric field E^0 is entirely along the x_1 direction, that is, perpendicular to the surface of the plate, or

$$E^0{}_1=E^0, \quad E^0{}_2=E^0{}_3=0. \tag{28}$$

Consequently our boundary conditions at $x_1=\pm a$ reduce to

$$K_{11}E_1+4\pi\textstyle\sum_\alpha e_{\alpha 11}(\partial u_\alpha/\partial x_1)=E^0, \tag{29}$$

$$\textstyle\sum_\alpha c_{1j\alpha 1}(\partial u_\alpha/\partial x_1)-e_{1j1}E_1=0, \quad j=1,2,3; \tag{30}$$

and, solving these equations simultaneously, we obtain

$$\sum_\alpha c^*{}_{1j\alpha 1}\frac{\partial u_\alpha}{\partial x_1}=\frac{e_{1j1}}{K_{11}}E^0, \quad j=1,2,3. \tag{31}$$

It remains to determine E^0 in terms of the quantities u_j. This requires the solution of Poisson's equation, which is most conveniently carried out in a manner suggested by Cady.

We treat the cases n odd and n even separately. We assume that in both cases, however, the configuration is that shown in Fig. 1, where $2d$ is the total gap between the electrodes in which the specimen is symmetrically inserted. Denoting by 1, 2, and 3 the regions occupied by the first air gap, the specimen, and the second air gap, respectively, we have, since

$$\nabla^2 V_q=-4\pi\rho_q(x_1), \quad q=1,2,3, \tag{32}$$

the relation

$$V_q=-4\pi\left\{\int\left[\int\rho_q(x_1)dx_1\right]dx_1+C_qx_1+C_q'\right\}, \tag{33}$$

where V_q is the electrostatic potential and $\rho_q(x_1)$ is the charge density in the qth region. These latter quantities have the values:

$$\rho_1(x_1)=\rho_3(x_1)=0, \tag{34}$$

$$\rho_2(x_1)=-(d/dx_1)P_2'(x_1), \tag{35}$$

where $P_2'(x_1)$ is that part of the polarization arising from the strain. Confusion may arise at this juncture because some authors consider the strain to produce free charge, while others consider the strain to produce polarization. It

[3] See, for example, P. M. Morse, *Vibration and Sound* (McGraw-Hill, 1936).

is clear that we have assumed the strain to produce polarization equivalent to that arising from a free charge distribution $\rho_2(x_1)$. While both points of view lead to the same result, confusion may arise due to the difference in definition of **P** and **D**. In order to proceed further and evaluate the constants C_q and C_q', it is necessary to know the space dependence of $P_2'(x_1)$. Here, and until further notice, we omit the index r, since it is understood that these equations obtain for each value of r.

For n odd, we have according to Eqs. (4) and (16)

$$P_2'(x_1)\equiv P_0\cos\frac{n\pi x_1}{s}=\frac{n}{s}\sum_\alpha e_{\alpha 11}A_\alpha\cos\frac{n\pi x_1}{s}. \quad (36)$$

Consequently, we obtain for the electrostatic potentials

$$V_1=-4\pi[C_1x_1+C_1'], \quad (37)$$

$$V_2=-\frac{4\pi}{K_{11}}\left[-\frac{P_0s}{n\pi}\sin\frac{n\pi x_1}{s}+C_2x_1+C_2'\right], \quad (38)$$

$$V_3=-4\pi[C_3x_1+C_3']. \quad (39)$$

We seek to evaluate the undetermined constants. By symmetry,

$$C_1=C_3. \quad (40)$$

Moreover, at $x=-d$:

$$V_1=-4\pi[-C_1d+C_1']=0, \quad (41)$$

so

$$C_1'=Cd, \quad (42)$$

and, at $x=d$:

$$V_3=-4\pi[C_3d+C_3']=0, \quad (43)$$

so

$$C_3'=-C_3d. \quad (44)$$

Consequently, we obtain

$$V_1=-4\pi C_1(x+d), \quad (45)$$

and

$$V_3=-4\pi C_1(x-d). \quad (46)$$

At $x=-a$, $V_1=V_2$, so

$$-4\pi[-a+d]C_1=-\frac{4\pi}{K_{11}}\left[-\frac{P_0s}{n\pi}\sin\frac{-n\pi a}{s}-C_2a+C_2'\right] \quad (47)$$

and $D_1=D_2$, so

$$-4\pi C_1+4\pi\left[-P_0\cos\frac{-n\pi a}{s}+C_2\right]=-4\pi P_0\cos\frac{-n\pi a}{s}, \quad (48)$$

whence immediately

$$C_1=C_2. \quad (49)$$

Similarly, at $x=a$, $V_2=V_3$, so

$$-4\pi C_1[a-d]=-\frac{4\pi}{K_{11}}\left[-\frac{P_0s}{n\pi}\sin\frac{n\pi a}{s}+C_2a+C_2'\right]. \quad (50)$$

Adding Eqs. (47) and (50) yields

$$C_2'=0. \quad (51)$$

Hence from Eq. (50) we obtain

$$-4\pi C_1[a-d]=-\frac{4\pi}{K_{11}}\left[-\frac{P_0s}{n\pi}\sin\frac{n\pi a}{s}+C_1a\right], \quad (52)$$

so

$$E^0=4\pi C_1=(8\pi P_0s/n\pi w)\sin(n\pi a/s), \quad (53)$$

where

$$w\equiv 2[a+K_{11}(d-a)]. \quad (54)$$

This differs from Cady's solution of the problem by a factor $\sin n\pi a/s$.

Inserting the value for the external electric field in the boundary conditions, we have at $x=\pm a$,

$$\sum_\alpha c^*_{1j\alpha 1}\frac{\partial u_\alpha{}^r}{\partial x_1}=\frac{8e_{1j1}}{wK_{11}}\sin\frac{n\pi a}{s_r}\sum_\alpha e_{\alpha 11}A_\alpha{}^r, \quad (55)$$

in which we have again inserted the index r. Multiplying each equation by $A_j{}^r$, adding and taking cognizance of Eq. (20), we have for the corresponding boundary conditions on ξ_r at $x=\pm a$:

$$\frac{n\pi\kappa_r{}^2}{s_r}\xi_r{}^0\cos\frac{n\pi a}{s_r}=\frac{8\pi}{wK_{11}}[\textstyle\sum_\alpha e_{\alpha 11}A_\alpha{}^r]^2\sin\frac{n\pi a}{s_r}, \quad (56)$$

or

$$\cos\frac{n\pi a}{s_r}=\frac{8s_re_r{}'^2}{nw\kappa_r{}^0K_{11}}\sin\frac{n\pi a}{s_r}, \quad (57)$$

where

$$e_r{}'^2\equiv[\textstyle\sum_\alpha e_{\alpha 11}A_\alpha{}^r]^2/[\sum_\alpha A_\alpha{}^r]^2. \quad (58)$$

In Eq. (58) it is not necessary to know the absolute value of the A_α^r to determine $e_r'^2$ but only the ratio $A_1^r : A_2^r : A_3^r$ which is determined by Eq. (18) for a given κ_r^2.

Since $\cos n\pi a/s_r = \cos -n\pi a/s_r$ it is apparent that our solution $\xi_r = \xi_r^0 \sin n\pi x_1/s_r \exp i\omega_r t$ will satisfy both boundary conditions provided s_r is the solution of the transcendental Eq. (57). This completes the formal solution of the problem for n odd.

It should be noted, however, that in general s_r is not equal to the thickness of the plate. Physically, this means that in virtue of the electric field arising from the charge distribution caused by the strain, neither the stress nor the strain vanish at the surface of the plate. This is an important qualitative difference between this solution and that of Cady, who assumed that there was a node of strain at the boundary of the plate and then calculated the external electric field and found it to be finite. Thus, his result is fundamentally inconsistent with his initial assumption, which, however, is an excellent approximation owing to the small difference between l and s_r. Indeed, the difference is so small that it is worthy of mention only for the sake of clarity of interpretation.

The foregoing state of affairs is somewhat altered when n is even. In this case we must write

$$V_1 = -4\pi(C_1 x + C_1'), \tag{59}$$

$$V_2 = -(4\pi/K_{11})[-(P_0 s/n\pi)\cos(n\pi x_1/s) + C_2 x_1 + C_2'], \tag{60}$$

$$V_3 = -4\pi[C_3 x + C_3']. \tag{61}$$

From $V=0$ at $x=\pm d$, we obtain

$$V_1 = -4\pi C_1(x_1+d), \tag{62}$$

and

$$V_3 = -4\pi C_3(x_1-d). \tag{63}$$

From continuity of potential we have, at $x=+a$,

$$C_3[-4\pi(a-d)] = -(4\pi/K_{11})[-(P_0 s/n\pi)\cos(n\pi a/s) + C_2 a + C_2'], \tag{64}$$

and, at $x=-a$

$$C_1[-4\pi(-a+d)] = -(4\pi/K_{11})[-(P_0 s/n\pi)\cos(-n\pi a/s) - C_2 a + C_2']. \tag{65}$$

From continuity of electric displacement, we have, at $x=+a$,

$$-4\pi C_3 + 4\pi[P_0 \sin(n\pi a/s) + C_2] = 4\pi P_0 \sin(n\pi a/s), \tag{66}$$

and, at $x=-a$

$$-4\pi C_1 + 4\pi[P_0 \sin(-n\pi a/s) + C_2] = 4\pi P_0 \sin(-n\pi a/s), \tag{67}$$

whence $C_1 = C_2 = C_3$. Adding Eqs. (64) and (65) we find

$$C_2' = (P_0 s/n\pi)\cos(n\pi a/s). \tag{68}$$

Subtracting the same equations we find

$$C_1 = C_2 = C_3 = 0. \tag{69}$$

So, for even harmonics, we conclude that the external field vanishes. Consequently,

$$\xi_r = \xi_r^0 \cos n\pi x_1/l,$$

where l is the thickness of the plate. The faces of the plate are nodes of displacement for the even harmonics and consequently cannot be excited by a uniform electric field applied perpendicular to the plate.

Now by returning to Eq. (57) and realizing from a physical standpoint that $s_r \cong l$, we are in a position to obtain a sufficiently accurate, explicit approximation for the value of s_r and hence of f_r, the frequency of free vibration when n is odd.

First, we demonstrate that $s_r > l$ for n odd. In Eq. (57), if $s_r \cong l$, we must have $\sin n\pi a/s_r$ and $\cos n\pi a/s_r$ with the same sign, since $8e_r'^2 s_r/\kappa_r^2 n w K_{11}$ is essentially positive. This is only possible if $s_r > 2a = l$.

Next we show that Cady's result for an X-cut crystal vibrating in its fundamental thickness mode is the quantitatively correct first approximation. Now Cady defined a quantity

$$c_r' = 4\rho f_r^2 l^2, \tag{70}$$

and found

$$c_{11}' = c_{11}^* - (32 e_{11}^2 l/\pi w K_{11}), \quad n=1. \tag{71}$$

To achieve this result we return to Eq. (57) and shift the origin from $x_1=0$ to $x_1=-\frac{1}{2}s$ and thus obtain

$$\tan \Delta l_r n\pi/s_r = 8 s_r e_r'^2/c_r^* n w K_{11}, \tag{72}$$

where

$$2\Delta l_r \equiv s_r - l, \tag{73}$$

and

$$c_r^* \equiv \kappa_r^2. \tag{74}$$

From Eq. (72), we obtain as the first approximation for Δl_r:

$$\Delta l_r = 8e_r'^2 l^2/n^2\pi w K_{11} c_r^*. \tag{75}$$

From Eqs. (19) and (73) we have

$$4\rho^2(f_r^2/n^2)(l^2+4\Delta l_r l) = c_r^*, \tag{76}$$

which with Eq. (75) yields

$$4\rho\frac{f_r^2}{n^2}l^2\left(1+\frac{32e_r'^2 l}{\pi w K_{11} c_r^* n^2}\right) = c_r^*, \tag{77}$$

or

$$c_r' = c_r^* - 32e_r'^2 l/\pi n w K_{11}. \tag{78}$$

For an X-cut crystal this expression reduces to that of Cady. It is further evident that the effect of the gap on the frequency vanishes when the gap is infinite, and decreases as the square of the harmonic number for a finite gap.

Finally, this theory should be capable of explaining the observed dependence of frequency on gap. According to Cady, the frequency should be related to the reciprocal of the equivalent electrical gap w by a linear relation. Actually, Dye[4] and Cady observed a slight curvature to the relation. The second approximation for Δl_r should yield the sign of this curvature. We may write

$$f_r/n = v_r/2s_r = y_r \tfrac{1}{2} v_r, \tag{79}$$

where

$$v_r \equiv (\kappa_r^2/\rho)^{\frac{1}{2}}, \tag{80}$$

and

$$y_r \equiv 1/s_r. \tag{81}$$

Then the second approximation for s_r yields

$$l y_r^2 - y_r + D_r = 0, \tag{82}$$

where

$$D_r \equiv 16e_r'^2/\kappa_r^2 n^2 w K_{11}\pi, \tag{83}$$

so to the second approximation

$$y_r = \frac{1}{l} - D_r - lD_r^2. \tag{84}$$

If Δf_r is the increment in the frequency as the gap is decreased from an infinite value, for which the frequency is f_r^0, we have

$$\Delta f_r/f_r^0 = -(lD_r + l^2 D_r^2). \tag{85}$$

The frequency therefore drops more rapidly than linearly. This is qualitatively in agreement with experiment, although experiment would indicate that this drop is somewhat more rapid than the theory predicts. This quantitative discrepancy is possibly due to the lack of a uniform field and the fact that the experiments were conducted on the fundamental mode of vibration where the edge effects are more important than for higher modes. This is because the frequencies of vibration of a finite plate will only be equal to those of an infinite plate as the wave-length of the sound waves approaches zero.

In summary, we state the main result of our considerations. The frequencies of free vibration of a piezoelectric crystal in the form of an infinite plate inserted between two grounded electrodes are given by

$$f_r = \frac{n}{2s_r}\left(\frac{c_r^*}{\rho}\right)^{\frac{1}{2}},$$

where c_r^* are the roots of the secular determinant (22) and s_r is the root of the transcendental equation $\cot n\pi a/s_r = 8s_r e_r'^2/nwc_r^* K_{11}$, for n odd; and $s_r = l$, for n even where the various quantities have the connotations ascribed in the text.

It has been pointed out elsewhere[5] that this theory is capable of explaining the discrepancies in the elastic constants of quartz calculated by Atanasoff and Hart[6] on the basis of a somewhat less rigorous theory. The agreement between this theory and the careful results of Atanasoff and Hart is very satisfactory. It is worthy of emphasis that the effective elastic constants of a piezoelectric plate, the so-called c^*, do not obey the same symmetry relations as those obeyed by the ordinary elastic constants.

The author is indebted to Professor W. G. Cady and Professor J. V. Atanasoff for stimulating conversations and correspondence, and considerable constructive criticism.

[4] D. W. Dye, Proc. Phys. Soc. London **38**, 399 (1926).

[5] A. W. Lawson, Phys. Rev. **59**, 838 (1941).

[6] J. V. Atanasoff and P. J. Hart, Phys. Rev. **59**, 85 (1941).

Habit and Orientation in Electron Diffraction

R. P. JOHNSON AND W. R. GRAMS
Research Laboratory, General Electric Company, Schenectady, New York

(Received April 11, 1942)

Electron diffraction patterns of etched tungsten surfaces apparently indicate a preferred orientation of the crystallites, with [100] ⊥ surface. Actually, the etching leaves, on grains of a certain orientation, a structure exceptionally favorable for diffraction, and these selected grains dominate in the scattering. Analogous examples of weighted sampling, rather than random sampling, appear in studies of clays and of graphite. We suggest that crystal habit may frequently replace preferred crystal orientation as the cause of arcing in reflection patterns.

1. ETCHED METAL SURFACES

IN the course of studying electron diffraction by metal surfaces treated in various ways we examined a block of polycrystalline tungsten cut from a rolled strip 3 mm thick. One flat side was polished and then etched for 1 min. in 3 percent H_2O_2 solution, boiling. The semicircles of the reflection pattern had diameters appropriate for the body-centered cubic tungsten lattice, but were broken into well-defined arcs, indicating a preferred orientation of the surface crystallites involved in the diffraction. These crystallites, according to the pattern, have a [100] axis preferentially normal to the surface, and grains deviating from this orientation by more than 25° contribute only negligibly to the scattering. The arc pattern remained entirely unchanged as the sample was rotated in its own plane. We had to conclude that the surface crystallites concerned in the pattern have only the single fiber axis, [100] ⊥ surface, and are turned at random angles about the surface normal.

Rolling a metal commonly orients its crystallites in two directions: one crystallographic axis turns preferentially with respect to the direction of rolling and another turns preferentially with respect to the plane of rolling. We should have found a strong preference for [110] in the rolling direction and a less pronounced preference for [100] perpendicular to the plane of rolling.[1] The discrepancy between this expectation, based on x-ray studies of bulk samples, and our finding that only the surface normal appears as a fiber axis, made us suspect that the surface crystallites involved in the diffraction are not a true sample of the metal grains. To test this proposition we cut a 1-cm cube from a piece of wrought tungsten, polished three mutually perpendicular faces, etched for 1 min. in the boiling H_2O_2 solution, and made patterns of the three surfaces; again, we prepared in a similar way a cube from a block of tungsten sintered but not wrought, and made patterns of three mutually perpendicular faces. These six patterns were indistinguishable and were indistinguishable from the first-mentioned patterns of etched rolled stock. Finally, we made a pattern of the polished and etched end of a drawn tungsten rod in which the crystallites have, as a result of the drawing, a preferred orientation, [110] along the rod axis.[2] Still the pattern showed [100] ⊥ surface. Evidently the preferred orientation indicated by the diffraction patterns is not noticeably influenced by preferred orientation that may be present in the bulk sample.

Three explanations suggest themselves. The first is that the polishing may break up the surface crystallites and reorient the fragments, the rearranged layer persisting through the etching. Simple microscopic examination is sufficient to discount this surmise. The etching reveals the original grains of the bulk sample, producing a serrated structure that varies in tilt and course from one grain to another—in short, the diffraction samples, microscopically, are typical etched polycrystalline surfaces. A second hypothesis, so implausible as to require no discussion, is that the etchant somehow leaves submicroscopic ad-crystals on the surface, and

[1] Clark, *Applied X-Rays* (McGraw-Hill, New York, 1932), second edition, p. 379.

[2] M. Ettisch, M. Polanyi, and K. Weissenberg, Zeits. f. physik. Chemie **99**, 332 (1921).

that the lattice orientation of these ad-crystals is determined relative to the mean surface normal.

The correct explanation, we believe, is that diffracted electrons reach the photographic plate dominantly from those surface crystallites which after the etching display relatively long, sharp peaks emerging nearly perpendicular to the mean surface. Such grains will hide their more bluntly etched neighbors from the beam, and moreover the electrons will penetrate the tips of thin peaks more easily than the broader summits of flatter promontories.

It may, of course, be held simply that any etching which attacks the various crystal surfaces at different rates will leave only grains of a certain orientation projecting above the mean surface level and accessible to the electron beam. We cannot strictly insist that the difference between thin peaks and blunt summits is essential, though our experience with the preparation of metal samples to yield electron diffraction patterns suggests strongly that the details of surface structure within a grain determine the quality of the pattern, and even determine whether or not a crystalline pattern appears.

It remains to prove whether etching of a tungsten crystal in boiling H_2O_2 solution will produce a habit of the postulated sort. We had at hand a single-crystal tungsten wire 0.015 cm in diameter, made by the Pintsch process. When this had been etched in the solution long enough to reduce its cross section by some 50 percent the original circular boundary had given way to a rhombus of acute angle $76°\pm2°$, with slightly bulging sides. A back-reflection Laue pattern of the etched wire, made by Mr. Eric Asp of this Laboratory, identified the long diagonal of the rhombus as [100], the short diagonal as $[01\bar{1}]$, and the wire axis as [011]; the bulging faces are approximately of the (111) type. This result with the single-crystal wire indicates that the etching of a polycrystalline sample will produce on each grain an array of pyramids bounded by approximate (111)-type faces. It follows immediately that the most salient pyramids will indeed occur on grains that have a [100] axis most nearly perpendicular to the sample surface.

Boiling H_2O_2 is not the only etchant which produces on tungsten a surface yielding the pseudo-orientation patterns. We found the same effect after etching with the conventional $HF+HNO_3+H_2O$ mixture. When the single-crystal wire was etched in this solution its cross section again tended toward a bulged rhombus with diagonals in the [100] and the [110] directions. Electrolytic etching of tungsten in NaOH solution produces, under certain conditions, a matte finish, and such a surface also gives a diffraction pattern quite like that of the H_2O_2-etched samples. In fact, in every case where we have obtained a good pattern of bulk polycrystalline tungsten the same apparent preferred orientation, with approximately the same spread about the mean, has appeared.

Molybdenum, also, when etched in boiling H_2O_2 and quickly plunged into cold water to prevent formation of a colored film, yields a similar pattern, again indicating a fiber axis, [100] $\perp$ surface. We have not tested Mo so thoroughly as W, but the few patterns we have made are alike in this respect.

2. SETTLED CLAY SAMPLES

Another case of pseudo-orientation effects has appeared incidentally in some current studies of clay minerals. A drop of a thin water suspension of montmorillonite, of a certain range of particle size, is dried down onto a Formvar pellicle and the resulting sample is examined by transmission, at various angles relative to the electron beam. The diffraction patterns show beyond question that most of the particles, which have a platy habit, lie nearly flat on the Formvar film.[3] When a similar sample, made by drying down a drop of the same suspension on a polished metal block, is examined by reflection, the pattern contrastingly indicates that the flakes are standing preferentially edge-up on the surface, and moreover are preferentially perpendicular to the beam, no matter what the azimuth of the beam with respect to the settled deposit. All these conclusions cannot plausibly be maintained. The difficulty is resolved by assuming that the beam cannot get through the lamellar particles except nearly along the direction in

[3] S. B. Hendricks and C. S. Ross, Zeits. f. Krist. **100**, 251 (1938–39).

which they are thinnest. In the reflection case, flakes which happen to stand nearly edge-up and nearly perpendicular to the beam then dominate in the diffraction, though these particles are by no means representative of the settled aggregate. This explanation is entirely consistent with the known approximate dimensions of the flakes and the known approximate penetration range of the electron beam. When similar samples are made from a monodisperse fraction of montmorillonite, separated centrifugally and known to have a mean particle diameter in the neighborhood of 100A, the reflection pattern agrees with the transmission patterns in showing that the platelets lie preferentially flat on the surface. Diffraction features corresponding to lattice planes parallel to the plate faces now appear prominently in the reflection pattern, though these features were entirely absent from the reflection pattern of the larger particles.

3. GRAPHITE

Flake graphite, such as is used for lubricating small machine bearings, gives patterns analogous to those of the larger clay particles. Transmission patterns of a sample settled from air suspension onto a Formvar film prove that the flakes are predominantly flat on the surface, while a reflection pattern of a similar sample settled onto a polished metal block indicates that the flakes stand preferentially on edge. The discrepancy is again to be explained on the view that the beam can easily penetrate only those flakes that it strikes nearly perpendicularly; such flakes therefore have a weight in the reflection pattern far out of proportion to their frequency of occurrence in the sample.

A fine-grained block of graphitized petroleum coke after smoothing on No. 0 emery paper gives a reflection pattern indicating a preferred orientation of graphite lamellae normal to the surface and to the beam; this indication certainly does not agree with any reasonable picture of the actual surface condition. When, however, the same specimen is polished by rubbing on glass (which quickly coats with an adherent film of graphite) its pattern is that of flakes lying flat on the surface. The polishing, we must say, levels the surface and reduces the exposed flakes to a penetrable diameter. White and Germer,[4] studying carbon black deposits in which the pseudo-graphitic flakes are so small that the electrons can easily traverse them in any direction, get reflection patterns showing prominent $(00\cdot l)$ features and transmission patterns in which $(hk\cdot 0)$ rings are dominant. With graphitic carbon, as with the montmorillonite clay, when the particles are sufficiently small, transmission and reflection patterns tell consistent stories about the preferred orientation.

4. REMARKS

Our results with clays and with graphite are not without precedent: several investigators have remarked upon the absence or extreme weakness of reflections from the basal planes of layer-lattice materials and have attributed this anomaly, as we do, to a lamellar shape of the crystals in the sample.[5] It has not previously been noticed, so far as we know, that peculiarities of crystal habit even in materials of the cubic system can give rise to pseudo-orientation patterns.

We venture to wonder whether weighted sampling of crystallites, in place of random sampling, may not occur rather generally in the diffraction of electrons by surface layers. For example, the thin oxide films formed on polished metals by heating in air often give reflection patterns indicating a preferred orientation with respect to the surface normal. We suggest, in view of the observations described here, that such patterns may need to be interpreted cautiously.

---

[4] A. H. White and L. H. Germer, J. Chem. Phys. 9, 492 (1941).

[5] See L. H. Germer and K. H. Storks, Ind. Eng. Chem., Anal. Ed. 11, 583 (1939) and references given in discussion on p. 588.

Letters to the Editor

PROMPT publication of brief reports of important discoveries in physics may be secured by addressing them to this department. The closing date for this department is the third of the month. Because of the late closing date for the section no proof can be shown to authors. The Board of Editors does not hold itself responsible for the opinions expressed by the correspondents. Communications should not in general exceed 600 words in length.

The Yield of Neutrons from Deuterons on Carbon

CARL L. BAILEY, MELBA PHILLIPS, AND JOHN H. WILLIAMS
University of Minnesota, Minneapolis, Minnesota
May 19, 1942

THE efficiency of the reaction

$$D^2+C^{12}\rightarrow(N^{14})^*\rightarrow N^{13}+n^1$$

as a function of the energy of the deuterons has been investigated by Bonner, Hudspeth, and Bennett[1] in the voltage range from 0.60 to 1.95 Mev. They found that the excitation curve exhibited broad resonances at 0.92, 1.16, 1.30, and 1.82 Mev superimposed on a slowly rising background.

Figure 1 shows the results of a study of this reaction in

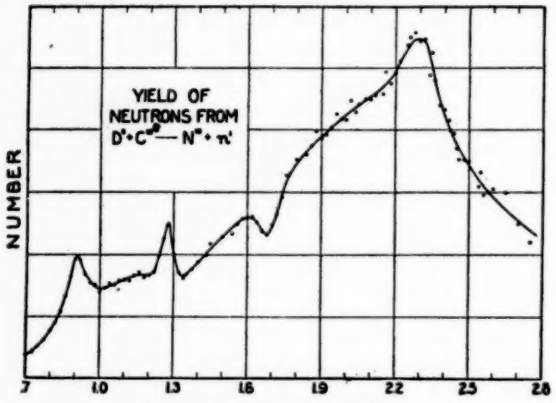

FIG. 1. Deuteron energy in Mev.

the energy range from 0.70 to 2.75 Mev. The energy of the deuterons, accelerated by our pressure electrostatic generator,[2] was controlled to within one percent. Magnetic resolution of the ion beam through small diaphragms, combined with paraffin and cadmium shielding, served to localize the source of neutrons entering a BF_3 chamber. Thin soot targets on heated tantalum backings and bare tantalum backings could be rotated into the ion beam in order to obtain the net yield from carbon.

It is evident that resonances exist in this reaction and that the two most prominent resonances found by Bonner, Hudspeth, and Bennett are in essential agreement with our values of 0.91 and 1.28 Mev. Furthermore, the half-widths of these peaks are of the same order of magnitude, 60 and 50 kev, respectively. The less prominent resonance at 1.16 Mev and the broad resonance at 1.82 Mev found by the Rice Institute group are not resolved in our experiments. On the other hand, the resonance at 1.6 Mev shown in Fig. 1 does not appear in the previous work. If one accounts for the form of the background in the manner suggested below one must conclude that a prominent resonance exists at 2.3 Mev. Only qualitative arguments can be made for the shape of the theoretical excitation function for a nucleus as light as C^{12}, but we should expect the resonances to be superposed on a smooth background representing the increasing penetration factor for incident deuterons. The total yield from all competing processes should thus rise with bombarding energy throughout the range of energies studied here. The observed resonances could all belong to the "first excited configuration" of N^{14}, and be reasonably sharp because of the dearth of levels lying lower.

In view of these considerations a noteworthy feature of the excitation curve for neutron emission is the sharp decrease beyond the 2.3-Mev resonance.

The yield of protons from the reaction

$$D^2+C^{12}\rightarrow(N^{14})^*\rightarrow C^{13}+p^1+Q$$

is at least as great as that for the neutrons reported above for the first two resonances of the excitation curve.[3] Proton emission is not a less probable process, even for low energies because $Q=+2.7$ Mev for this reaction, and hence there is very little barrier effect on the escape of protons from $(N^{14})^*$. It is reasonable that proton emission should gain slowly over neutron emission at high energies, but not sufficiently to account for a decrease in the neutron curve of the observed magnitude. Another competing process, ${}_1D^2+{}_6C^{12}\rightarrow{}_5B^{10}+{}_2He^4$, endothermic by about 1.2 Mev by calculation from the masses and hence energetically possible at these energies, may interfere to cause the large reduction in neutrons. The behavior of the curve is in qualitative agreement with the work of Newson[4] who also attributed the phenomenon to α-particle emission. Unfortunately these α-particles will be too short to be detected experimentally.

[1] Bonner, Hudspeth, and Bennett, Phys. Rev. **58**, 185 (1940).
[2] Williams, Rumbaugh, and Tate, Rev. Sci. Inst. **13**, 202 (1942).
[3] Bennett, Bonner, Hudspeth, Richards, and Watt, Phys. Rev. **59**, 781 (1941).
[4] H. W. Newson, Phys. Rev. **51**, 620 (1937).

Induced Color in Crystals by Deuteron Bombardment

J. M. CORK
University of Michigan, Ann Arbor, Michigan
June 1, 1942

NUMEROUS investigations[1] have been made on the color changes produced in crystals by cathode rays, ultraviolet, x-rays, and the radiations from radium. On bombarding crystals in the cyclotron with deuterons of 10 Mev, color changes are similarly induced. In many crystals the effects are the same as found by the other ionizing radiations, but in some cases they behave differently.

In certain crystals only the bombarded surface actually

traversed by the deuterons exhibits the change in color, while in others a transition occurs throughout the whole crystal, due to the strong gamma-radiation accompanying the bombardment. Often the effect exhibits a reversal; that is, if the intensity of the bombarding beam is too great, the change of color appears at the edges but not at the center of the bombarded area. The color changes produced by deuteron bombardment unlike those due to x-rays show little inclination to fade out, but disappear abruptly if heated through a certain critical temperature.

The following are representative of the induced colors observed for specific crystals:

Alkali halides, NaF—light red; NaCl—amber to black depending on the exposure; NaI—yellow to green; KCl—purple; KBr—deep blue; KI—green. Colors in most cases disappear on heating to about 220°C; glass, a dark amber color, clears on heating to about 300°C.

Fluorite—induced color is a body effect and depends on the original tint varying from green to amethyst.

Quartz—clear crystals show only surface darkening but if originally tinted, as rose quartz, turns to purplish brown throughout.

Beryl—aquamarine and emerald differ only in color, green color not induced in aquamarine by bombardment.

Diamond—inferior amber colored stones assume a green body coloring equivalent to that of the rare natural gems. The change is permanent for ordinary temperatures. On heating to about 900°C the original color returns. The color produced depends somewhat upon the original tint, clear stones showing less change than those with original color. In one case a bluish color was produced.

It is of considerable interest that the metastable states produced by the ejection of electrons by the ionizing radiations can exist at ordinary temperatures indefinitely.

Acknowledgment is made of the kindly interest shown by Professors A. B. Peck and C. B. Slawson of the mineralogy department and to the Horace H. Rackham Fund for financial support.

[1] See, for example, Doelter, *Das Radium und die Farben* (1910); P. S. Bayley, Phys. Rev. **24**, 495 (1924); P. G. N. Nayar, Proc. Ind. Acad. Sci. **14**, 1 (1941).

Anomalous Scattering of Mesons

W. Heitler and H. W. Peng
Dublin Institute for Advanced Studies, Dublin Ireland
May 22, 1942

In two recent papers in this journal Code and Shutt[1] have described measurements of the anomalous scattering of mesons due to their interaction with nuclear particles. The cross section obtained was of the order of magnitude of 0.6×10^{-27} cm² per nuclear particle, for a selected sample of mesons having an average energy of 0.8×10^{9} ev in Code's measurements. The energy was not measured in Shutt's experiment. We wish to point out that these results like previous measurements by Wilson[2] are in reasonable agreement with the meson theory of nuclear forces if we assume a spin 1 or 0 (pseudoscalar mesons) for the meson. We need not make any further *ad hoc* assumptions. The apparent discrepancy of earlier calculations[3] with the experiments is due to the fact that the usual expansion method, under the assumption that the meson-nucleus interaction is small, breaks down at high energies. The reason is that the coupling of the meson with the charge and spin degrees of freedom of the nuclear particles becomes increasingly strong at high energies.[4] It has now been shown by Wilson and by one of us[5] that a more exact quantum mechanical treatment of the scattering problem is possible which differs from the usual expansion method essentially by the inclusion of *damping*. The cross section thus obtained is in units of

$$(\hbar/\mu c)^2=5\times10^{-26}\text{ cm}^2\quad(\mu=\text{meson mass})$$

$$\sigma=4\pi f'^2\frac{G^2p^4}{\epsilon^2(1+\kappa^2)},\quad \kappa=G^2p^3/\epsilon,\quad G^2=g^2+2f^2+f'^2,\qquad(1)$$

where p, ϵ are the momentum and energy of the meson in units of the rest energy μc^2, and g, f, f' are the ordinary coupling constants for longitudinal, transverse, and pseudoscalar mesons, divided by $(\hbar c)^{\frac{1}{2}}$. (The primary meson is assumed to be pseudoscalar.) Some of these constants may be zero, but we believe that the best account of all experimental facts is obtained if they are all different from zero. All three are then of the order of magnitude $g^2\sim f^2\sim f'^2\sim1/10$. For energies of 0.8×10^{9} ev σ becomes of the order of magnitude of 1.8×10^{-27} cm² which—in view of the scanty experimental material and our insufficient knowledge of the constants g, f, f'—may be considered as in reasonable agreement with the measurements quoted above. It must also be remembered that (1) is derived for an infinitely heavy nuclear particle and that the motion of the heavy particle will probably diminish the cross section by a factor 2 or so as ϵ approaches the value Mc^2.

Formula (1) has also been derived recently by Fierz[6] by a semiclassical treatment of the charge degree of freedom. It is also very similar to the cross section for a particle scattered by a classical magnetic dipole field.[7] This is not very surprising in view of the great similarity between the formalisms describing the spin and the charge.

Attempts have previously been made to explain the small experimental value of the anomalous scattering by introducing the hypothesis that the proton-neutron can exist in excited charge and spin states by which the inertia of the charge and spin degrees of freedom would be increased.[8] While this possibility has to be kept in mind we believe now that so far no sufficient foundation for such an hypothesis exists.

The quantum theory of damping can be developed in quite a general way. After the diverging self energies and other similar diverging integrals have purposely and systematically been omitted, a new set of equations can be obtained which is free from any singularities and differs from what is obtained by the usual expansion method by the inclusion of damping. The theory makes no assumption about the strength of the coupling. For a number of examples [compare, for instance, (5)] it can be seen that this damping corresponds to that part of the classical damping which is independent of the size and structure of the particle, but, of course, there is not always a classical analogy. The theory can, without difficulty, also be applied to the multiple processes ("explosions") occurring as a

consequence of the meson theory and the results turn out reasonably in every respect. These questions are dealt with in a paper to appear shortly in the *Proceedings of the Cambridge Philosophical Society.*

[1] F. L. Code, Phys. Rev. **59**, 229 (1941); R. P. Shutt, Phys. Rev. **61**, 6 (1942).
[2] Wilson, Proc. Roy. Soc. **174**, 73 (1940).
[3] Heitler, Proc. Roy. Soc. **166**, 529 (1938).
[4] The case of "strong coupling" has recently been studied by Wentzel [Helv. Phys. Acta. **13**, 269 (1940)] and by J. R. Oppenheimer and J. Schwinger, Phys. Rev. **60**, 150 (1941).
[5] Heitler, Proc. Camb. Phil. Soc. **37**, 291 (1941); Wilson, Proc. Camb. Phil. Soc. **37**, 301 (1941).
[6] Fierz, Helv. Phys. Acta. **14**, 257 (1941).
[7] Bhabha, Nature **145**, 819 (1940); Proc. Ind. Acad. Sci. **11**, 247 (1940); Proc. Roy. Soc. **178**, 314 (1941); Bhabha and Corben, Proc. Roy. Soc. **178**, 273 (1941).
[8] Heitler, Nature **145**, 29 (1940); Bhabha, Proc. Ind. Acad. Sci. **11**, 347 (1940); **13**, 9 (1941); Heitler and Ma, Proc. Roy. Soc. **176**, 368 (1940).

The Effect of Polarized Light on the Absorption Spectrum of the Neodymium Ion in Crystals

E. L. Kinsey and Robert W. Krueger
University of California at Los Angeles, Los Angeles, California
June 11, 1942

IT has been found that the visible absorption spectrum of certain crystals containing neodymium is dependent in a striking manner upon the polarization of the light passing through the crystal. During the last year and a half after we discovered the effect in crystals of neodymium chloride we have examined the absorption spectra, using polarized light, of neodymium nitrate, sulphate, and bromate, and have obtained a quantum mechanical explanation of the effect.

The bromate spectrum has been so fruitful in giving a clue to the nature of the effect that we present in this preliminary note a photograph (Fig. 1) of a small section of it

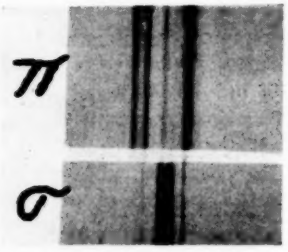

FIG. 1. Absorption of $Nd(BrO_3)_3 \cdot 9H_2O$ near 5750A when polarized light is sent through the crystal perpendicular to optic axis.

taken with the Hilger E1 spectrograph. Fortunately the crystal is uniaxial and has a known structure.[1] The salient feature is the group of five electronic lines spread over a region of 70A near 5750A which is produced by light passing through a crystal plate 0.5 mm thick, cut with the optic axis lying in the surface of the plate. The spectrum marked π is produced by light polarized with the electric vector parallel to the optic axis, and the other marked σ occurs when the electric vector is perpendicular to the axis. When light is sent along the optic axis, only the σ spectrum is observed. The five lines are assumed to correspond to transitions from the lowest component of the ground level $^4I_{9/2}$ of the neodymium ion, which is split by the crystal field, to components of an electrically split upper level.

The levels of the free ion are characterized by values of L and J, the total orbital angular momentum, and total angular momentum quantum numbers, respectively. In a weak crystal field the degeneracy for the free ion caused by the fact that states of different M values (projection of J on the singular axis of the crystal) have the same energy, is partially removed. This effect causes the eigenfunctions of the perturbed levels to be linear combinations of the unperturbed eigenfunctions of the free ion. We have calculated in zero-order approximation, using perturbation and group theory methods, how the unperturbed functions mix to produce the perturbed ones, and have explained the observed polarizations as arising from the particular way in which this mixing occurs. It is found, for example, that the unperturbed functions characterized by the values $\pm\frac{1}{2}$, $\pm 5/2$, $\pm 7/2$ for M enter several perturbed states for $J=9/2$; in fact these values describe the ground state. Those characterized by $M=\pm\frac{3}{2}$ enter others. Transitions from a level of the first type to one of the second involve changes in M of $\Delta M=\pm 1$. Transitions involving $\Delta M=0$ are not present. According to electric dipole selection rules (which we can show operate here) lines corresponding to these transitions are polarized with the electric vector perpendicular to the singular direction of the crystal. On the other hand, transitions between levels of the first type involve changes corresponding to $\Delta M=0$ as well as changes corresponding to $\Delta M=\pm 1$. Lines of this type may be predominantly π lines, or they may be unpolarized. If each one of the six unperturbed eigenfunctions enters the level $M(\pm\frac{1}{2}, \pm\frac{5}{2}, \pm 7/2)$ with equal coefficients, it turns out that the transition produces a predominantly π line. We have accounted in this way for the polarization of most of the lines in four groups throughout the visible region in the bromate spectrum.

The complete work is described in a doctorate thesis written by one of us (R. W. K.) and is being prepared for journal publication.

[1] L. Helmholz, J. Am. Chem. Soc. **61**. 1544 (1939).

On Perturbations Causing Apparent Convergence in the C_2 Spectrum

L. Gerő and R. F. Schmid
Physical Institute, Royal Hungarian University for Technical and Economic Sciences, Budapest, Hungary
January 15, 1942

ON the basis of the rotational analysis of some $^1\Pi-{}^1\Pi$ Deslandres-d'Azambuja and tail bands of the C_2 molecule, carried to moderate rotational quantum numbers only, by Herzberg and Sutton [1] these authors assume a convergence limit about 35,900 cm^{-1} above the lower $^1\Pi$ state of C_2.

In this laboratory an extensive search has been started concerning perturbations in the C_2 spectrum and well-exposed plates of the $^1\Pi-{}^1\Pi$ system disclose that (1) the bands could be followed up to rather high rotational quantum numbers, the involved upper $^1\Pi$ states being several thousand cm^{-1} units higher in energy than 35,900 cm^{-1} above the lower $^1\Pi$ state; and (2) while upper and lower $^1\Pi$ states show numerous local perturbations, which bring in either both or sometimes only the one Λ-type doubling components (Herzberg and Sutton's analysis ends at such

places), the upper $^1\Pi$ states are influenced by an extensive homogeneous perturbation also. It is this latter which causes the appearance of convergency. The rapid decrease of upper state rotational spacing towards higher v values is a general behavior in the perturbation area, if the perturbing state has the smaller rotational constants, and its narrower vibrational structure also causes decrements in the vibrational spacings of the perturbed state. Such phenomena and the usefulness of constructing $[B'-B'']$ curves in detecting perturbations of any kind has been pointed out by Schmid and Gerö.[2]

A detailed report of the perturbations in the C_2 spectrum will be given later. At this time it seems inadvisable to draw conclusions concerning dissociation possibilities of the C_2 molecule, especially not on the basis of any apparent "convergence limit."

[1] G. Herzberg and R. B. Sutton, Can. J. Research **18**, 74 (1940).
[2] R. F. Schmid and L. Gerö, Ann. d. Physik **33**, 70 (1938).

Investigation of the X-Radiation from Te^{121} (125 Days) by Critical Absorption and Fluorescence

R. D. O'Neal and Gertrud Scharff-Goldhaber
Department of Physics, University of Illinois, Urbana, Illinois
June 25, 1942

THE radioactive tellurium isotope Te^{121} (125±5 days) has been investigated by Seaborg, Livingood, and Kennedy,[1] who found that the isotope emits a very complex radiation consisting of electrons and gamma-rays. They considered it probable that Te^{121} decays by K-electron capture to the stable Sb^{121}, but left the possibility open that the radiations are due to an isomeric transition in tellurium. We have now studied the radiations of this isotope in order to find out whether a characteristic x-radiation is emitted. For this purpose we have used the well-known critical absorption method as well as a new "fluorescence method."

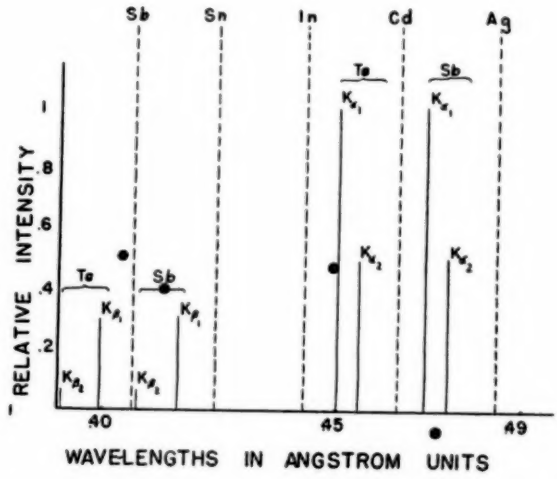

FIG. 1. The diagram shows the K x-ray lines of antimony and tellurium. The intensity of the $K\alpha$ lines is put equal to one. The dashed lines indicate the position of the K-absorption edges of silver, cadmium, indium, tin, and antimony.

The tellurium was separated chemically from a sample of antimony which had been bombarded with deuterons in the 60-inch cyclotron in Berkeley. The radiations from the aged tellurium deposit were detected with a thin walled glass Geiger counter and as absorbers we used thin foils of Ag, Cd, In, and Sn. Figure 1 shows the wave-lengths of the various K x-ray lines of $_{51}$Sb and $_{52}$Te and the K-absorption edges of the neighboring elements for $Z=47-50$[2]. Figure 2

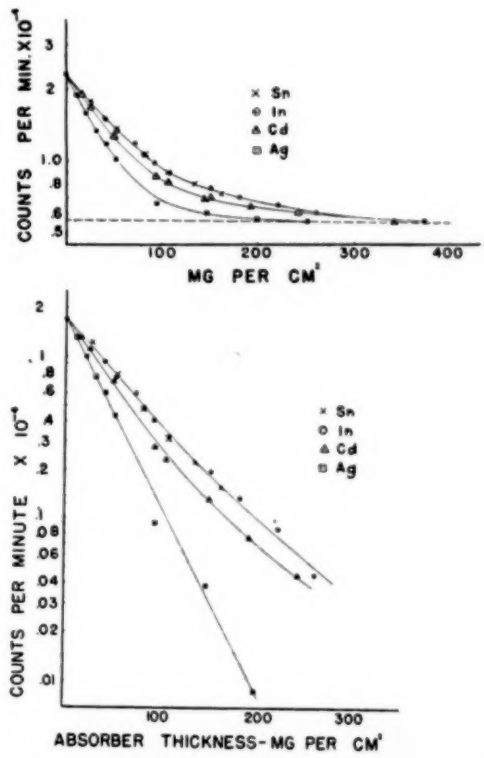

FIG. 2. The upper part of the figure shows the absorption curves of the total radiation from the tellurium sample for tin, indium, cadmium, and silver. The dashed line indicates the contribution of the hard gamma-ray, which was followed up for thicker samples (up to 1 g/cm²) of the four elements. In the lower part, the curves obtained after subtraction of the gamma-ray background are plotted.

shows the absorption curves obtained from the Te sample. The strong absorption in silver indicates that K radiation of antimony is present, but the absorption in cadmium appears to be stronger than might be expected, if no K radiation of tellurium were emitted in addition.

We have therefore investigated the radiation further by a "fluorescence method," which may prove more convenient than the absorption method under certain conditions. For this experiment, the tellurium sample was mounted at a distance of about 5 cm from the counter and a lead wedge was interposed to shield the counter from the direct radiation. Secondary radiation emitted from thin metal foils under an average angle of 100° was recorded by the Geiger counter. The foils, which consisted of the elements Ag, Cd, In, and Sn were of very nearly equal size and weight (~50 mg/cm²). In order to cut out soft electrons an aluminum foil of 21 mg/cm² was wrapped around

the counter. The data confirm the results of the absorption experiments.

The data are: Ag, 290; Cd, 209; In, 160; Sn, 168.

These figures represent counts above the background (212 counts/min.) obtained without the secondary emitters. The errors amount to about 5 percent.

In order to explain why cadmium shows critical absorption for a considerable part of the radiation, one could assume that an isomeric transition in tellurium precedes the K-electron capture whereby an internally converted gamma-ray gives rise to the emission of tellurium K radiation. Therefore, we attempted to separate a Te daughter product by an isomeric separation, making use of the transformation from telluric into tellurous acid.[1] The precipitate was inactive. A daughter product of a half-life $>$ 1 min. and $<$ 1 year would probably have been detected. If no isomeric transition takes place, the x-ray component harder than the Sb $K\alpha$ line which we have observed may be explained in the following way. The capture of the K electron by the Te nucleus and the internal conversion of the succeeding γ-rays in the K shell may follow each other so closely that both K electrons may be missing simultaneously in the antimony nuclei. This would lead to a shift of the $K\alpha$ line towards shorter wave-lengths.

Our thanks are due to Professor E. O. Lawrence and Dr. M. Kamen for the radioactive sample.

[1] G. T. Seaborg, J. J. Livingood, and J. W. Kennedy, Phys. Rev. **57**, 363 (1940).
[2] A. H. Compton and S. K. Allison, *X-Rays in Theory and Experiment* (D. Van Nostrand, New York, 1936).

Information For Contributors

THE Editors of THE PHYSICAL REVIEW would be aided in their task if the following items were used as a guide by all contributors.

MANUSCRIPTS

Send manuscripts to J. W. Buchta, Department of Physics, University of Minnesota, Minneapolis, Minnesota.

Papers must be in English, typewritten double spaced with wide margins on a durable white paper, preferably lettersize. The original copy, not the carbon, should be submitted.

For general style, spellings, abbreviations and form, recent issues of this journal should be consulted.

ABSTRACTS

An abstract must accompany each article. It should be adequate as an *index* and as a *summary*. As an index it should give all subjects, major and minor, concerning which new information is presented. As a summary it should give the conclusions of the article and all numerical results of general interest.

MATHEMATICAL EXPRESSIONS

Make all expressions clear to the typesetter. Identify in the margin of the manuscript Greek letters and unusual symbols.

Use fractional exponents instead of root signs.

Avoid complicated exponents and subscripts. Should it be necessary to repeat a complicated expression a number of times it should be represented by some convenient symbol.

The solidus (/) should be used wherever possible for fractions.

REFERENCES

References should appear as footnotes, numbered consecutively, and arranged thus:

[1] A. B. Smith, Phys. Rev. **41**, 852 (1932).
[2] G. R. Harrison, *Atoms in Action* (William Morrow & Company, New York, 1939), first edition, p. 30.

FIGURES AND TABLES

Legends for figures must accompany manuscript. Each table should have a caption. These in all cases should be complete in themselves so as to make the data intelligible to the reader without reference to the text. Each figure and table should be cited in sequence in the text.

LINE DRAWINGS AND PHOTOGRAPHS

Plan figures for reduction to one third or one fourth the original size. Wherever possible arrange figures so that after reduction they will not be wider than three inches. Lettering must be large enough to be readable (about 3 mm high) after reduction. The figures should be so arranged that the space is used efficiently.

Line drawings must be made with India ink on white paper or tracing cloth. Coordinate paper is not desirable, but if used must be blue-lined and all coordinates to be reproduced drawn with India ink.

Drawings which cannot be used will be returned to the author.

Photographs of drawings seldom are satisfactory. They often do not show clear black and white contrasts and are not suitable for relettering which is sometimes necessary. Photographs of apparatus seldom give as much information as drawings.

Please avoid round or oval photographs.

ALTERATIONS

Take great care that each manuscript is typographically accurate. A limited number of alterations in proof are unavoidable, but the cost of making extensive alterations after the article has been set in type will be charged to the author.

Proof and all correspondence concerning papers in the process of publication should be addressed to the Publications Manager, American Institute of Physics, 175 Fifth Avenue, New York, New York.